THE USE OF ELECTROSPUN SOY PROTEIN ISOLATE/POLYVINYL ALCOHOL NANOFIBERS FOR CONTROLLED DRUG DELIVERY AS WELL AS INVESTIGATION INTO MASS PRODUCTION

A Thesis
Submitted to the Graduate Faculty
of the
North Dakota State University
of Agriculture and Applied Science

By

David Paul Gutschmidt

In Partial Fulfillment of the Requirements
for the Degree of
MASTER OF SCIENCE

Major Department:
Mechanical Engineering

April 2015

Fargo, North Dakota

North Dakota State University
Graduate School

Title

The Use of Electrospun Soy Protein Isolate/Polyvinyl Alcohol Nanofibers for Controlled Drug Delivery as well as Investigation into Mass Production

By

David Gutschmidt

The Supervisory Committee certifies that this ***disquisition*** complies with North Dakota State University's regulations and meets the accepted standards for the degree of

MASTER OF SCIENCE

SUPERVISORY COMMITTEE:

Dr. Long Jiang
Chair

Dr. Xiangfa Wu

Dr. Dennis Wiesenborn

Approved:

4/17/2015
Date

Dr. Alan R. Kallmeyer
Department Chair

ABSTRACT

As the global movement progresses towards environmental awareness, industries are attempting to become less dependent on petroleum based materials. This study investigates the incorporation of Soy Protein Isolate (SPI) into nanofibers and their potential applications. Initially mechanical testing was conducted; it was found that at 1:1 ratio of SPI to polymer (PVA) was optimal. For drug release test, SPI based nanofibers were tested via three formulations including nanoparticle implementation. Results observed that loading the drug onto the nanoparticle showed sustained release, ~67% release at 70 hours. Mathematical models of both diffusion and erosion confirmed experimental findings. SPI based nanofibers were then utilized to deliver the antibacterial substance silver acetate, nanofibers were made from solutions containing various concentrations. Results showed increase in bacterial killing activity as silver concentration increased (0-1.5%). Lastly SPI based nanofibers were mass produced with a needleless electrospinning machine, linking the developed technology to potential industrial application.

ACKNOWLEDGMENTS

I would first like to thank with extreme gratitude my advisor Dr. Long Jiang, for this opportunity and for the continual support and guidance he has given me over my time here at North Dakota State University. Without his help and support this accomplishment would not have been possible.

I would like to thank Dr. Xiangfa Wu and Dr. Dennis Wiesenborn for taking time and being part of my graduate committee. Their support and guidance in this processes has been much appreciated.

I would like to thank the entire research group under Dr. Long Jiang for their support and assistance, especially Xuezhu Xu who has helped assist in many of the experiments. Also Kyle Bunkelman, Xiaoyi Zhou, Andrew Kroll, and Mohammad Sabzi have contributed to help make this research possible. I also must recognize Dr. Liu, in the plant sciences department for guidance and use of laboratory relating to silver acetate studies.

Lastly, I owe a special thanks to the entire Mechanical Engineering Department at NDSU, they have all contributed to making this accomplishment a success.

TABLE OF CONTENTS

LIST OF TABLES

LIST OF FIGURES

LIST OF ABBREVIATIONS

ABS…….Acrylonitrile Butadiene Styrene

Ag……...…….Silver Acetate

D……...……Daltons

E…….……..Elastic Modulus

FEA.....…….Finite Element Analysis

Keto…….….Ketoprofen

Kv……..……kilovolts

LB…….……Luria-Bertani

MPa…….…….Mega Pascal (N/m^2)*10^6

PBS……..Phosphate Buffered Saline

PVA……...……Polyvinyl Alcohol

Rpm…….…….Revolutions Per Minute

SEM…….…….Scanning Electron Microscope

SPI……...…Soy Protein Isolate

TGA…….Thermogravimetric Analysis

USDA……United States Department of Agriculture

UTS…….……..Ultimate Tensile Strength

UV……Ultraviolet

LIST OF APPENDIX TABLES

LIST OF APPENDIX FIGURES

1. INTRODUCTION AND RESEARCH OBJECTIVES

As the global economy make a continuous movement towards being more environmentally conscious, material alternatives for many applications are evaluated. A large movement has been taken to lessen the dependency on petroleum and petroleum based products and instead rely on materials that are either bio-based or renewable. Many countries have put into effect various initiatives and laws to encourage and promote the concept of using these bio-based or renewable resources and becoming more "green." The term "green" is used for a variety of meanings but is usually associated with the idea of becoming more environmentally friendly. The global market has seen a growing tendency to incorporate more natural based products in last 50 years and even more prominently in the last 15 years. As oil prices have steadily risen, companies as well as consumers are searching for ways to avoid petroleum based products. Figure 1-1 shows the oil prices per barrel for the last 25 years (data points taken for average price of oil in January of respective year).

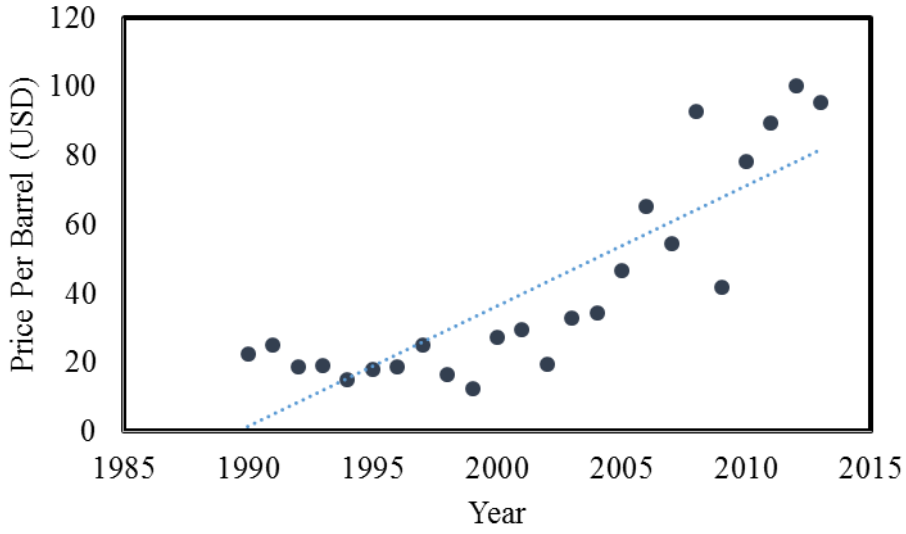

Figure 1-1: Oil prices per barrel since 1990 (USD)

Since 1990 the general trend in price of oil has been an upward one; this had driven companies and industries to investigate ways to become less petroleum dependent. Developing new products, as well as modifying previously engineered product to incorporates materials and/or processes that are less petroleum dependent produces a number of challenges.

Soy beans are an agriculture product that in recent years has become one of the leaders in global production (Cho, et al., 2010). As soy beans have observed an increase in abundance, more devolvement has taken place into areas in which they can be used. While soy bean based products come in many forms, this research focuses on the use of Soy Protein Isolate (SPI) which is one commercially available form of soy protein. By utilizing this readily available resource; not only is petroleum dependency reduced, but another market emerges for an agricultural product produced both locally and abroad. The goal of this research is to accomplish the following:

1. Optimize the soy protein isolate content in nanofibers, then in turn use these nanofibers for successful delivery of a pharmaceutical product
2. Introduce a method of loading a nanoparticle for further controlled and sustained release
3. Develop the incorporation of silver acetate into nanofibers for antibacterial effects
4. Investigate and produce means for mass production of soy based nanofibers

By accomplishing these goals, another use for soy based products is realized while at the same time enhancing the progress of controlled drug delivery systems. Incorporation of the nanoparticle gives flexibly and design ability to the system to accommodate for variables and differing environments. The investigation into mass production is a key aspect that ties this research to future industrial applications. It proves the research viable for large scale production.

2. LITERATURE REVIEW

The literature review for this study addressed four main components: soy-based materials, previous work in both classical and needleless electrospinning, controlled release studies from nanofibers and lastly the use of nanofibers as a vehicle for delivery of the antibacterial substance silver acetate. Previous work in the fields applied to this research are discussed along with their correlation to the work being presented in this study.

2.1. The use of soy based materials

The use of natural products has been a staple of mankind for thousands of years. Since early times people have been using the resources available to them to enhance their quality of living. The use of soy based products in the materials industry is constantly evolving as it progresses further and further each year. Some areas where soy based materials have been used include soy based lubricants, industrial plastics, paintings/coatings, turf management, adhesives and soy based tires. Soy based lubricants have seen increased use due to their bio based nature and strong lubrication performance characteristics. Major factors when considering soy based lubricants include having lower levels of toxicity as well as degrading more rapidly after disposure (Nagendramma, et al., 2012). Industries where soy based lubricants as well as other vegetable based oils are used include but are not limited to: insulating oil, hydraulic oil, metal working fluids, steel cold rolling oils, and gear oils (Nagendramma, et al., 2012) (Fox, et al., 2007). While soy based materials have their advantages, petroleum based oils and lubricants are still king of the industry. Reasons for the trend are numerous and include many factors such as warranty life, longer service life, and lower long term cost. While bio and soy based lubricants may be only one fourth of the cost initially, in some industries over 10 to 20 years the bio based lubricants prove to be more costly when compared to their petroleum counterparts. Industries

where biodegradable soy based lubricants seem to have the most use/potential are chain saw oils, lubricants for compressors, and metal working fluids.

Industrial plastics are another example of an industry where soy based material has been utilized substantially. Currently, many of the plastics in global use are produced with little to no consideration given to their ease of disposal. This is a reason for growing concern as to what will happen to plastics after their intended use is completed. By implementing bio-based products, which in this case is soy based materials, the concern is addressed while at the same time utilizing one of the world's most abundant agricultural products. In most cases, the soy product used are some type of soy protein. Soy protein is commercially available in three different forms; soy protein isolate, soy protein concentrate, and defatted soy flour. The varying factor in the three commercially available forms is the protein content which is highest for SPI, typically above 90%. Soy protein concentrate and defatted soy flower exhibit protein concentrations of around 70% and 53%, respectively (Cho, et al., 2010) (Lusas, et al., 1995). Figure 2-1 shows the break down from one bushel of harvested soybeans.

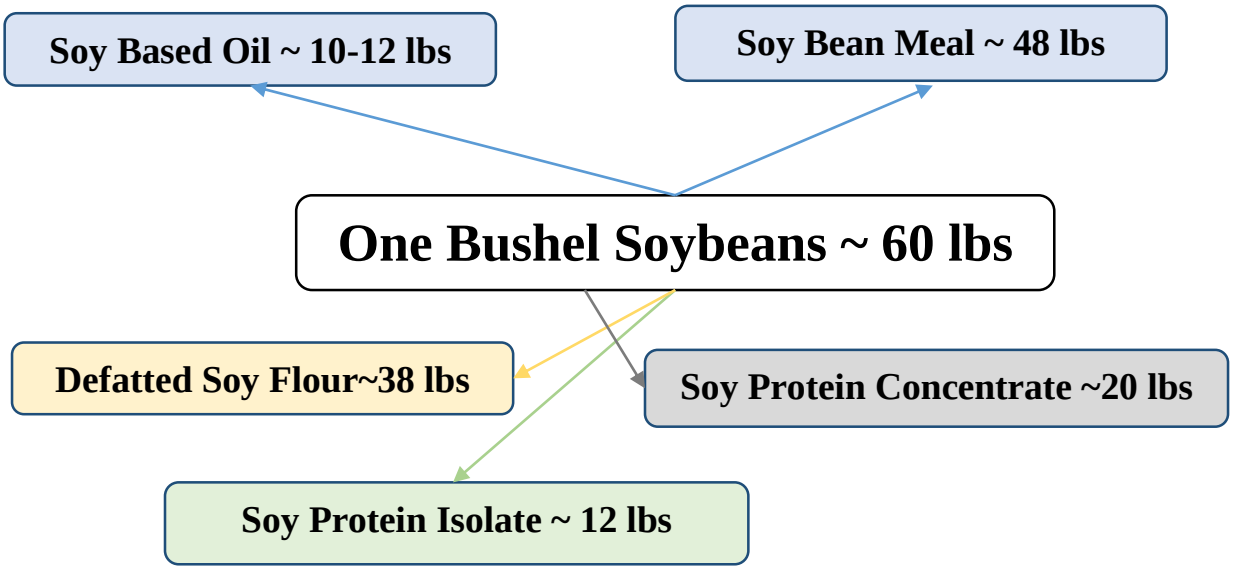

Figure 2-1: Soy bean breakdown from one harvested bushel

As seen in Figure 2-1, SPI produces the least amount of mass from one bushel of harvested soybeans, however it contains the highest soy protein content. The incorporation of SPI into industrial plastics has received an increased amount of investigation over the last 20 years. Industrial plastics made with components of SPI have shown good strength characteristics as well as excellent biocompatibility (Lodha, et al., 2005) (Wang, et al., 1996) (Paetau, et al., 1994) (Swain, et al., 2004). While there are distinct advantages to incorporating soy based material or SPI into plastics, there also are some disadvantages such as an increase in brittleness and sensitivity to water (Lu, et al., 2004) (Paetau, et al., 1994). In the case of the study by Lu in 2004, chitin whiskers were used to reinforce the properties of a SPI based thermoplastic. As the concentration of chitin increased, the greater water resistance demonstrated by the composite. Figure 2-2 shows the results for water uptake from the study.

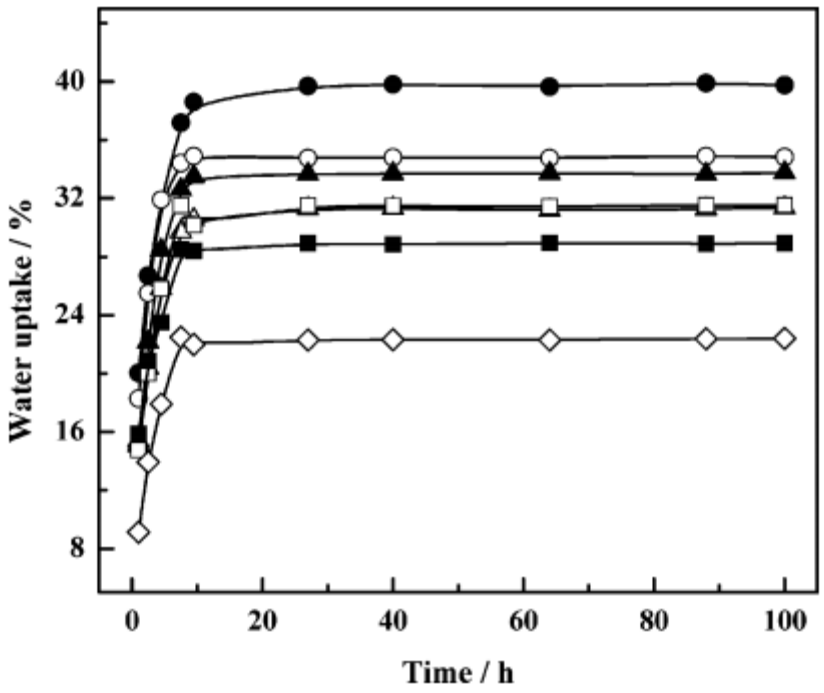

Figure 2-2: Water uptake results from Lu in 2004 (Lu, et al., 2004)

In Figure 2-2 the diamonds represent SPI-30, while the dark squares and light squares represent SPI-25, and SPI-20 respectively. The triangles dark and light show SPI-10 and SPI-15 respectively, and the light circle shows SPI-5 with the dark filled in circle being a GSPI sheet composite. As shown in the figure, as the chitin whisker content increases in the composites there is less water uptake, which is desirable. This demonstrates while there are excellent advantages to using soy based materials, one also must be conscious of the application and potential short comings.

While there have been many areas where the use of soy based material has been investigated, this study in particular focuses on the incorporation of soy based material into nanofibers. For many studies working with nanofibers, SPI is utilized due to the necessity of the high protein content (Cho, et al., 2012) (Xu, et al., 2012) (Vega-Lugo, et al., 2008) (Chen, et al., 2008). SPI in nanofibers is based on the same basic concept as SPI in many other materials; its

properties make it most appealing of the soy based products available. Particularly investigated in one of these studies was the tensile strength of the PVA/SPI fibers as reported in Figure 2-3 (Cho, et al., 2012).

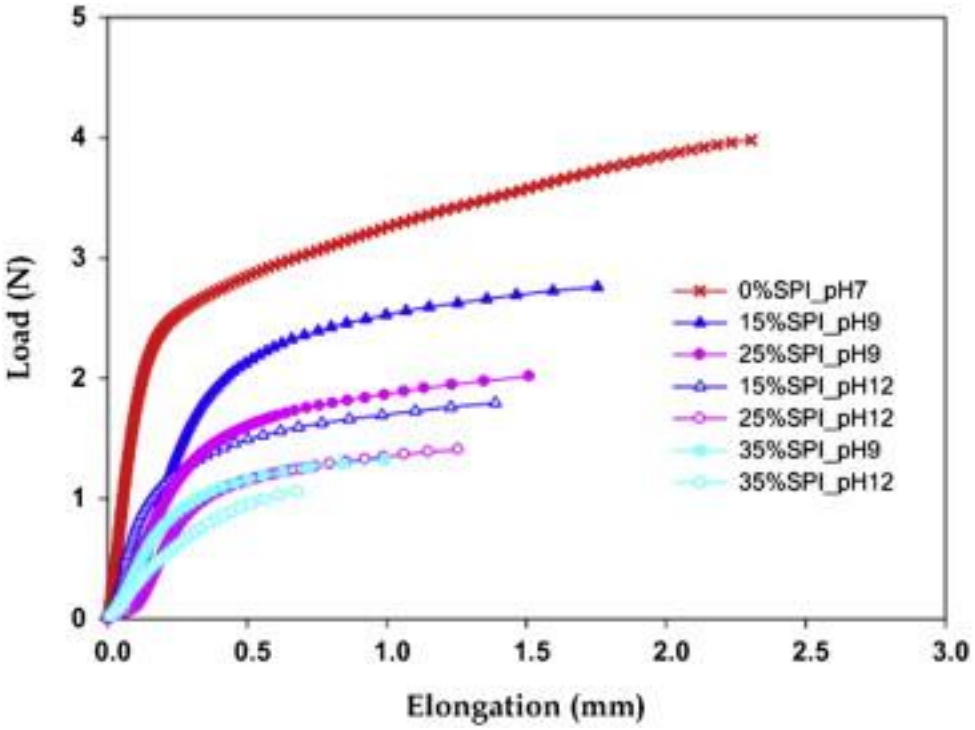

Figure 2-3: Tensile results from PVA/SPI nanofibers from Cho (Cho, et al., 2012)

In Figure 2-3, not only does concentration of SPI effect mechanical properties but also the pH and its correlation on the denaturing of SPI. The composition and properties of the soy proteins are critical to their intended application as different types of proteins exhibit different characteristics in certain environments such as pH precipitation (Kinsella, 1979). The effect and influence of pH on soy proteins and soy protein isolate in particular has been a previous area of research for many studies (Gennadios, et al., 1993) (Renkema, et al., 2000) (Jiang, et al., 2009) (Cho, et al., 2010). A very good visual image demonstrating the effect of pH on the denaturing of SPI and its effect on nanofiber morphology was again investigated by Cho and shown in Figure 2-4 (Cho, et al., 2010).

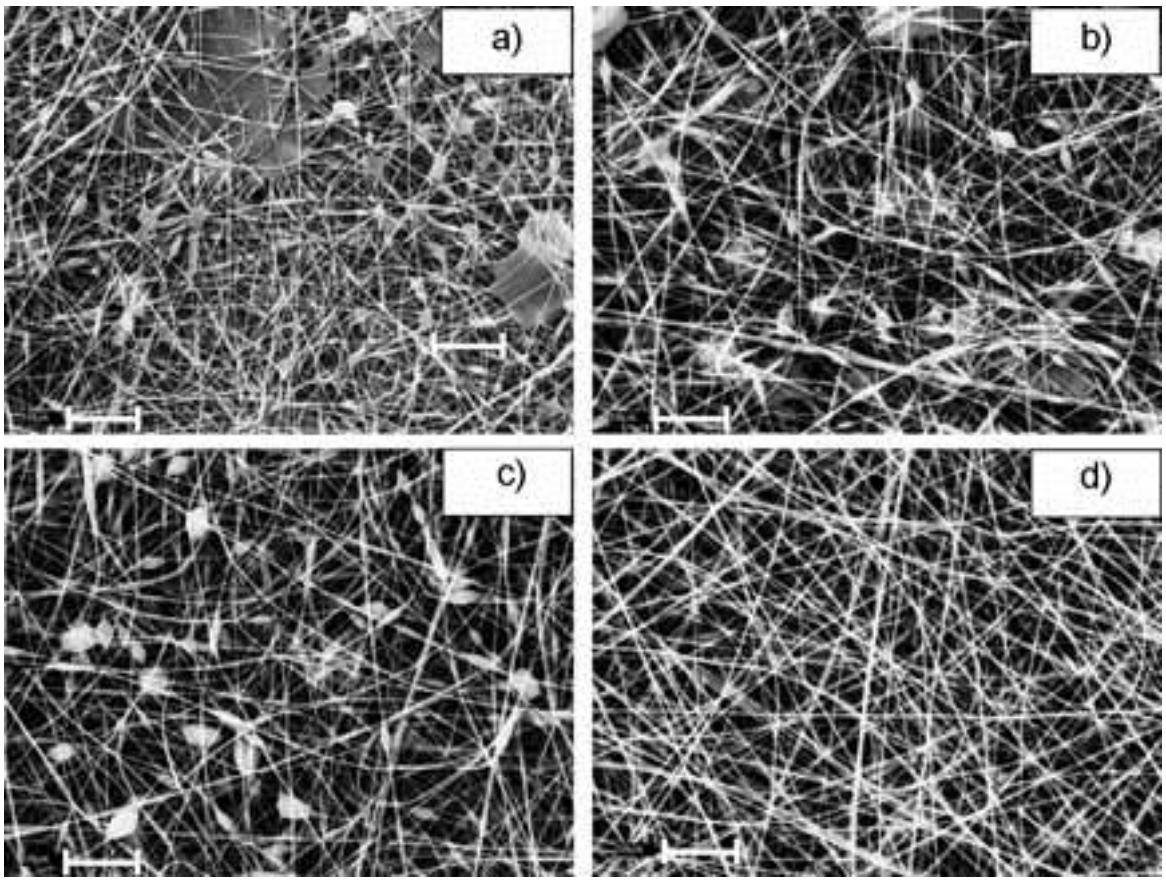

Figure 2-4: Study done by Cho in 2010 demonstrating effect of pH on morphology of PVA/SPI nanofibers; a) pH=7 b) pH=9 c) pH=12, and d) pH=12 plus surfactant (Cho, et al., 2010)

As shown in Figure 2-4, the effect of pH as well as the addition of surfactant has a tremendous effect not only on the reduction of beads but also in decreasing the diameters of the nanofibers which is desired (Cho, et al., 2012).

2.2. Electrospinning and needleless electrospinning

Electrospinning is the process in which an electric field creates a jet from a polymeric solution (Doshi, et al., 1993). In traditional electrospinning processes, as this jet leaves the needle, the solvent begins to evaporate. Once the solvent has evaporated, there remains a charged fiber that can then be collected and/or oriented however it is desired. Figure 2-5 shows a classical electrospinning setup (Ning, et al., 2013).

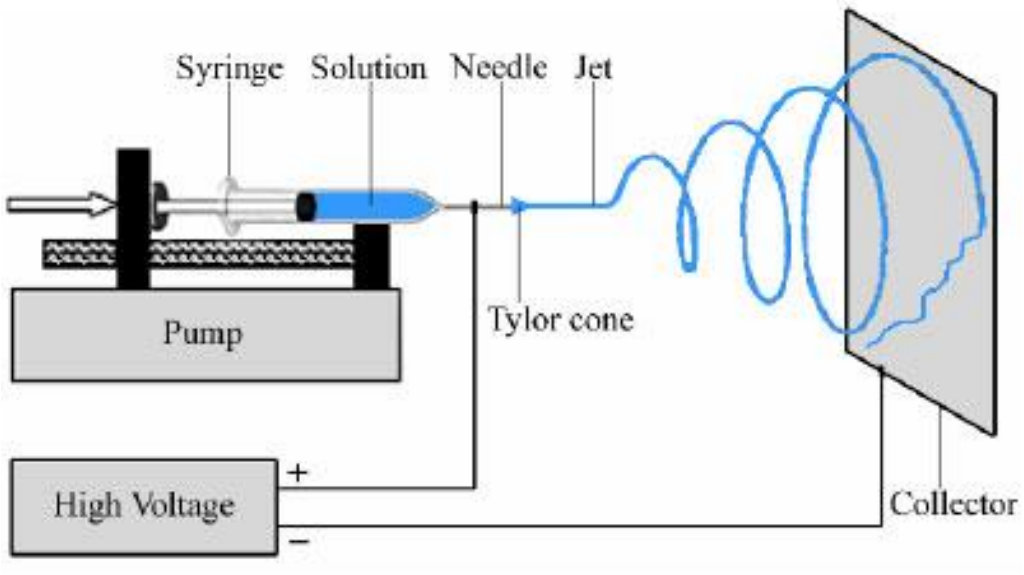

Figure 2-5: Classical electrospinning setup (Ning, et al., 2013)

The polymeric solution is typically dispersed through a syringe and syringe pump, this pump forces solution to the charged needle where the jet can form. Depending on the type of solution being used and the desired outcome there are many variables that can be adjusted in the electrospinning process. The incorporation of soy based material, especially SPI has been previously accomplished and the conditions as well as optimal process parameters have been established for specific scenarios (Xu, et al., 2012) (Cho, et al., 2010) (Cho, et al., 2012) (Vega-Lugo, et al., 2008). One specific case as in the Cho study in 2012, were some of the altercations to the classical electrospinning setup when creating the nanofibers ultimately to be used for the tensile test in which the results are shown in Figure 2-3. In the study, difficulty was found removing samples from the aluminum foil substrate, so a cylindrical bar was used for better removal of samples. This is one specific examples to how slight alterations in the electrospinning process need to sometimes be implemented to accomplish desired outcome.

A specific note in Cho's studies was the implementation of surfactant to reduce the surface tension of the water, which if not addressed can result in bead formations in the fibers,

see Figure 2-4 (Cho, et al., 2012) (Cho, et al., 2010). Introducing the surfactant as well as investigation into the effect of pH on the denaturing of soy improved morphology results greatly. For the research conducted in this study, the electrospinning technique is not one of great importance, the techniques being utilized have been well established and defined for creation of soy based nanofibers in a laboratory setting. However, what will be investigated in much more detail is the potential of mass producing these soy based nanofibers via needleless electrospinning.

Needleless electrospinning is defined as having multiple jets arise from a free surface similar to magnetohydrodynamics, without the use of needles (Yarin, et al., 2004). Other methods have been investigated to enhanced fiber production in needleless electrospinning including utilizing a conical wire coil as the spinneret (Wang, et al., 2009). Another study done in 2009 used a submerged drum for the solution dispersion technique in the needleless electrospinning process (Kostakova, et al., 2009). A diagram of the needleless electrospinning set up that was used in the 2009 study is shown in Figure 2-6.

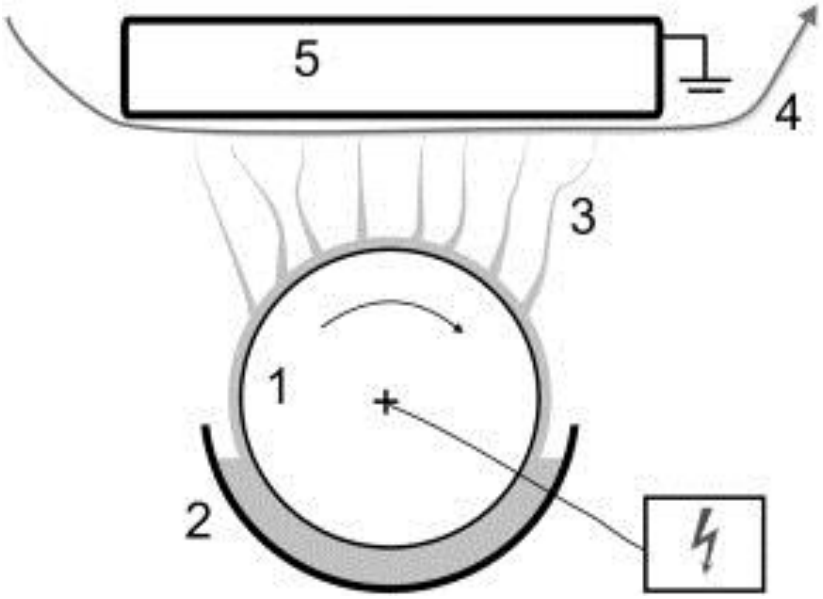

Figure 2-6: Needleless electrospinning mechanism used in 2009 study (Kostakova, et al., 2009)

In Figure 2-6, 1 represents the metal roller to which a positive potential voltage is applied. 2 and 3 represent the reservoir of prepared polymer solution and the direction of fiber formation, respectively. Shown by the number 4 is the substrate to which the fiber collects, while 5 represents the collector plate to which a ground voltage is applied. In other similar studies the ground plate is sometimes applied a slightly negative potential (just like in classical electrospinning). This basic concept with some additions provided the basis for the design of the needleless electrospinning machine constructed to spin soy based nanofibers; an area that has not yet received sufficient investigation.

2.3. Controlled drug release mechanisms

While nanofibers and soy based nanofibers have many different uses and applications as discussed previously; this study in specific focuses on their incorporation as a vehicle for drug delivery. Drug delivery refers to the transport of a pharmaceutical product in specific manner so that a desired therapeutic effect is achieved. The intended use for the soy based nanofibers studied in this paper are not for oral consumption but rather as a type of wound dressing, or medical patch. Potential benefits for using the described methods for drug delivery instead of classical oral consumption are numerous and include more reliable delivery, faster acting, less amount of drug needed, and the ability to target specific areas (Langer, 1998). A specific example would be if an elderly person has a deficiency in a certain vitamin. Instead of taking an oral pill once a day for the remainder of his or her life, the potential to have a patch of drug delivering nanofibers release the correct dosage of drug at the correct time would be tremendously advantageous. The first clear advantage would be that of said elderly patient not having to worry about taking these pills every day. From a pharmaceutical stand point, by entrusting the patient to take the pills, the risk is there that the patient may forget which would

lead to no drug entering the system. By using controlled release fibers that risk is eliminated as the fibers are exposed to blood stream guaranteeing release of the drug. These nanofibers also can be further tailored to control release rates and profiles of drug delivery systems.

The discussion of "sustained" or "delayed" drug release can best be described visually. Figure 2-7 shows the results from a drug release study that demonstrates sustained release (Wang, et al., 2012).

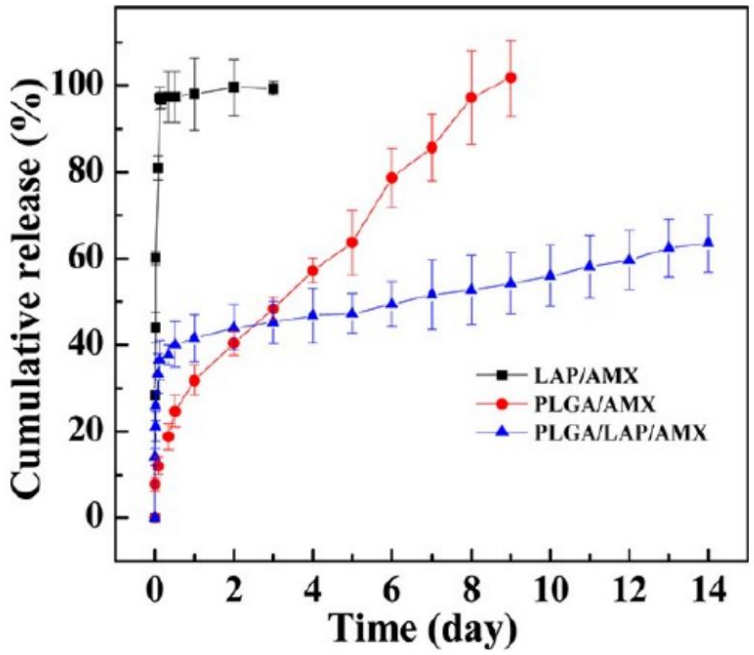

Figure 2-7: Release results show how sustained release prolongs drug delivery (Wang, et al., 2012)

In the case of this study, amoxicillin was the drug being delivered; note how different formulations of the drug delivery vehicle, in this case nanofibers, influenced the release time. The "LAP/AMX" reached ~95% release in less than 12 hours, while the other formulations only observed ~45% release after a time period of 4 day or 96 hours. The "LAP/AMX" formulation demonstrates a classical "burst" effect, which is trying to be eliminated by the recent trend in

sustained release studies. As aforementioned, it is much more desirable to have a slow constant release of the designated drug. Figure 2-8 shows an early drug delivery study from 2003 where no burst effect was observed (Zeng, et al., 2003), while Figure 2-9 shows the results from a 2011 study with PLGA nanofibers (Meng, et al., 2011).

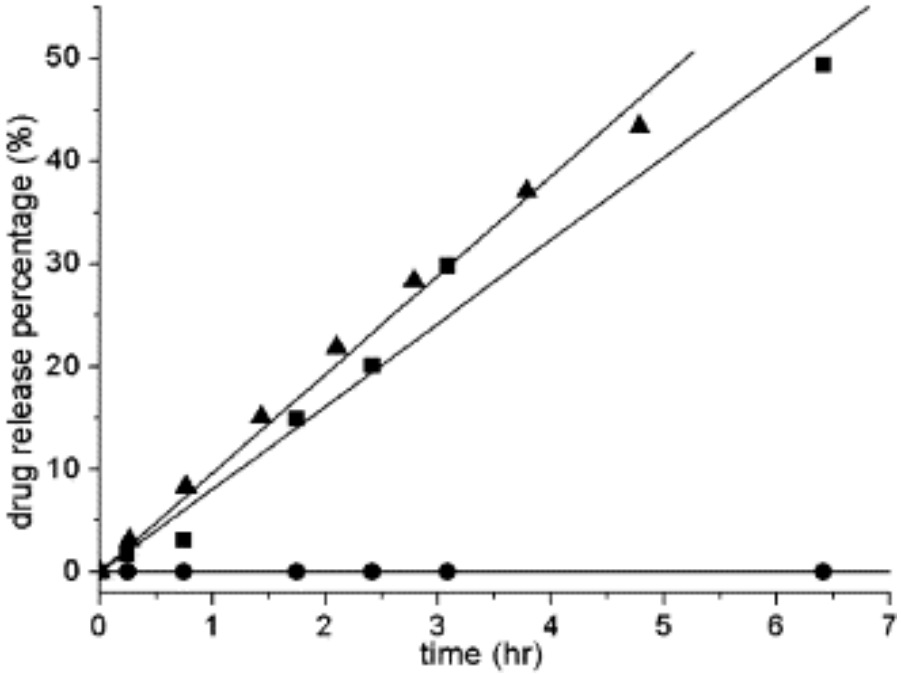

Figure 2-8: Early study showing beginning stages of release from biodegradable electrospun fibers (Zeng, et al., 2003)

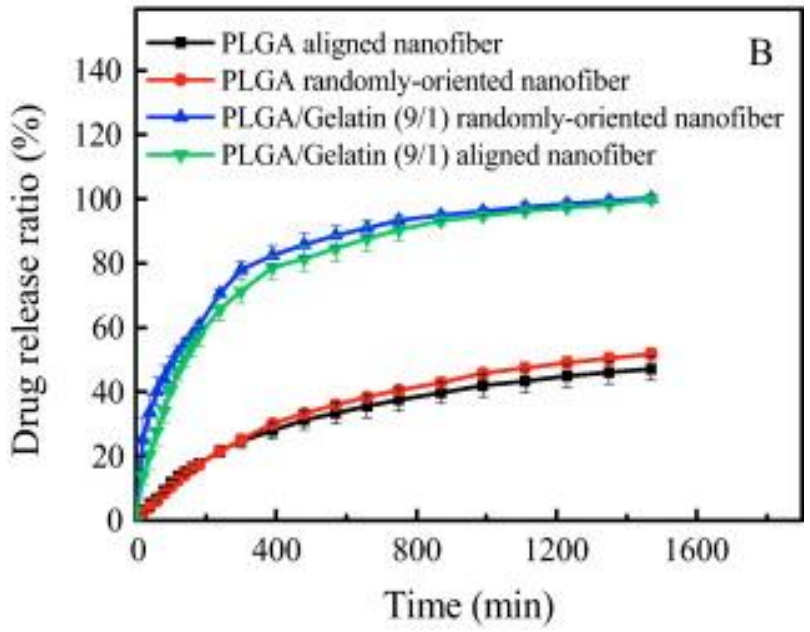

Figure 2-9: Drug release results from 2011 study (Meng, et al., 2011)

In both Figure 2-8 and Figure 2-9 drug release is much more rapid than when compared to some of the various formulations in Figure 2-7 (minutes versus days for release times). Since different studies are being compared no solid correlation can be drawn; however it should be observed and noted that in different studies "sustained" release can have different meanings.

In certain cases, the use of nanofibers alone is not enough to delay the release for a long enough period of time, in these instances, a nanoparticle is sometimes introduced to further retard the drug delivery rate. A nanoparticle is defined commonly as geometry with one dimension between 1 and 100 nm (Auffan, et al., 2009). While nanoparticles and nanomaterials have many advantageous properties; in the case of controlled drug delivery, their primary advantages are small size and large surface area. In previous studies, many researchers have experimented with nanoparticles and their effect on drug release (Brannon-Peppas, 1995) (Wang, et al., 2012) (Singh, et al., 2009) (Peetla, et al., 2015) (Jain, 2014). Essentially in controlled release drug studies, the nanoparticle is used to further retard the drug delivery rate. When

referring pack to Figure 2-7, the reason for the "PLGA/LAP/AMX" slow release profile is that the LAP nanodisks are encapsulated by the PLGA fibers.

For this particular study the nanoclay sepiolite was chosen as the nanomaterial to further control drug release rates. Sepiolite is a naturally occurring fibrous chain-structure mineral found in clays around the world; the porous nature made sepiolite a suitable drug carrier (González-Pradas, 2005) (Inagaki, et al., 1995). Sepiolite contains a unit cell formula of $[(Si_{12})(Mg_8)(O_{30})(OH)_4(OH)_2 \cdot 8H_20]$ and is comprised of alternating block and tunnel like structures that grow in the oriented fiber direction. The nature of these blocks includes a structure of a single magnesia sheet enclosed by two tetrahedral silica sheets. The silica sheets are non-continuous, and the discontinuities and inversions are the culprit for the tunnel like structure (Özcan, et al., 2006) (Rytwo, et al., 2002) (Chen, 2007). The specific structure of sepiolite makes it a suitable vehicle for drug delivery due to its high retention capabilities and swelling characteristics (Chen, 2007) (Xie, et al., 2010). A schematic of sepiolite projected onto the (0 0 1) plane is shown in Figure 2-10 (Tartaglione, et al., 2008).

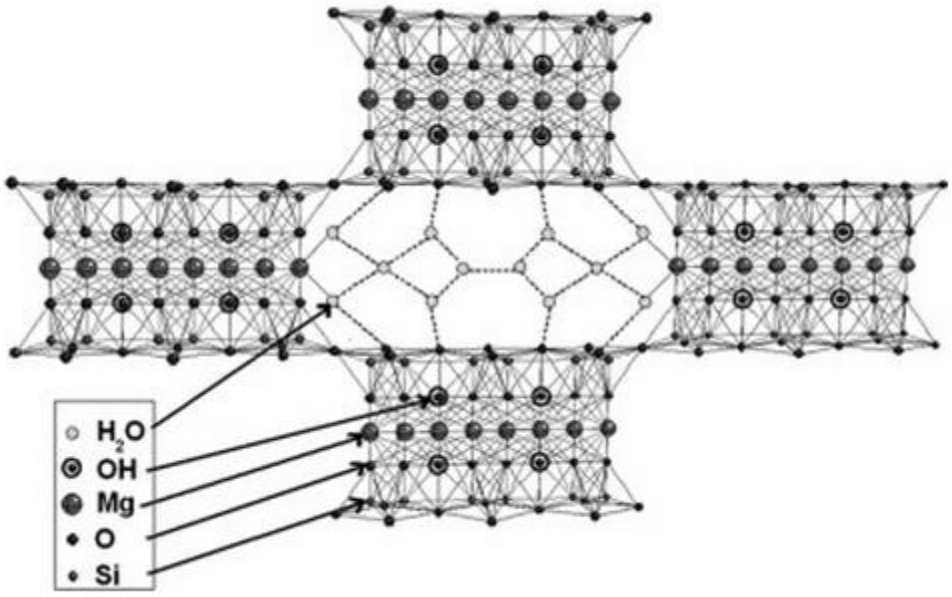

Figure 2-10: Structure of sepiolite, projection onto the (0 0 1) plane (Tartaglione, et al., 2008)

The structure of sepiolite makes it an excellent choice as the nanoparticle to include in the controlled delivery process; not only does it have the ability to retard drug release capabilities, it is also a naturally occurring material to coincide with the "green" approach taken by this research.

In conclusion of controlled drug release mechanism studies, two important trends come to surface. The first, is that encapsulation said drug inside of an electrospun nanofibers is one avenue in which release rate is controlled. This alone however is sometimes not enough to control drug delivery by the amount required; in these cases, a nanoparticle is introduced. The novelty of this research is using soy-based nanofibers for the drug delivery process. The combination of soy protein isolate nanofibers along with naturally occurring sepiolite has not yet been reported for a controlled drug delivery mechanism.

2.4. Antibacterial studies as related to nanofibers

Nanofibers have seen previous success as use in vehicles for drug delivery as discussed in the previous sections; however, another area where nanofibers have been utilized is in the delivery of antibacterial substances. Essentially the concept is very similar but instead of release

of a pharmaceutical product, an antibacterial product is released. Previous studies have shown successful release of antibacterial components from nanofibers. The component of these studies focused on for this research will be the release of silver acetate (Kong, et al., 2008) (Hong, et al., 2006) (Bonan, et al., 2015) (Abdelgawad, et al., 2014).

The bacteria killing ability or antibacterial nature of the nanofibers is measured by determining the zone of inhibition, or essentially the effective region where the sample restricts bacteria growth. A petri dish with and bacterial substance (often e-coli) is used to show this effect. Figure 2-11 demonstrates an example of this from a study done in 2008 (Kong, et al., 2008).

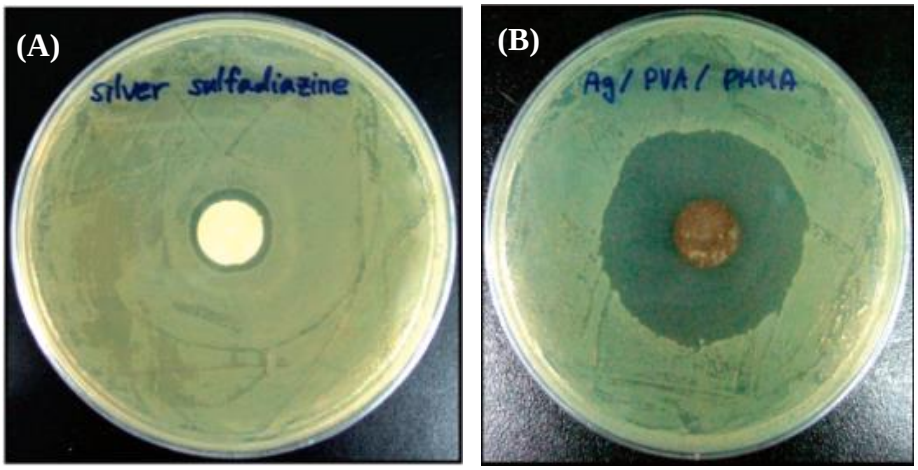

Figure 2-11: Antibacterial experiment containing silver acetate performed in 2008 (Kong, et al., 2008)

Notice how in Figure 2-11 that there seems to be a "ring" around the sample, this is especially noticeable in sample B. Essentially, sample B in this experiment was silver/PMMA nanofibers and displayed a larger zone of inhibition when compared to the silver sulfadiazine (sample A). The use of silver acetate for antibacterial studies is a topic that has received much attention in past years. The current study conducted hopes to expand on this by delivering the silver acetate via electrospun soy protein based nanofibers.

3. INVESTIGATION AND PREPERATION INTO THE ELECTROSPINNING OF SOY BASED NANOFIBERS

This chapter discusses the methods and experimental procedures for the controlled release study utilizing soy based nanofibers. This includes overview of materials, solution formulation, electrospinning parameters, as well as experimental design. Procedure for loading the nanoparticle with drug and description of in-vitro testing are also stated.

3.1. Experimental procedure and design

Overall objectives for this study included both optimizing the soy protein isolate content in nanofibers, then in turn use these nanofibers for successful delivery of a pharmaceutical product as well as introduce a method of loading a nanoparticle for further controlled and sustained release. In order to achieve these objectives the approach taken was to first determine the critical content of soy protein isolate needed in the nanofibers. The nanofibers formed in this experiment were primarily made from two types of material, soy protein isolate (SPI) and polyvinyl alcohol (PVA). By varying the solid weight percentages of these two materials, mechanical properties differed accordingly. Once an optimal amount of weight percentage soy was determined, experimental studies were conducted for the in-vitro drug release experiments.

The controlled drug release experiments consisted of a few different stages, firstly a baseline was established for the drug, which in this case was selected to be ketoprofen or (RS)2-(3-benzoylphenyl)-propionic acid. In order to test the amount of ketoprofen in the phosphate buffered saline, a UV-vis spectrophotometer was utilized. The drug was analyzed against phosphate buffered saline as it is used in a majority of in-vitro experiments to simulate the desired body fluid (Yoo, et al., 2009) (Loh, et al., 2010) (Thakur, et al., 2008). The in-vitro experiments will be explained in full in the controlled release experimental setup section.

As discussed in the literature review, it has been seen in drug release studies that the introduction of a nanoparticle has the potential to further sustain the release of said drug. In the case of this study, sepiolite was introduced for this purpose. In order to see the desired results the decision was made to attempt to "load" the drug onto and into the sepiolite so that its release rate is more tailored for a slower delivery. This loading process as well as the testing procedure for loading efficiency is gone into in detail in the drug loading technique and efficiency section.

An overview of material is listed as follows: Poly (Vinyl-Alcohol) (M_w = 125,000g /mol), powdered Sepiolite, Triton X-100 Laboratory Grade, and Silver Acetate (99% pure, M_w= 166.91 g/mol) were obtained from Sigma-Aldrich. Sodium Hydroxide (NaOH) was obtained from ACROS Orgainics. Ketoprofen or (RS)2-(3-benzoylphenyl)-propionic acid (99% pure, M_w= 254.28 g/mol) was received from Ark Pharm, Inc. Soy protein isolate (PRO-FAM 974) was acquired from Archer Daniels Midland Company. Its content included (90%), fat (4%), ash (5%), and some carbohydrates (<1%). Chemicals and substances were used as received. Distilled water was used in all experiments.

3.2. Optimization of soy content in nanofibers and electrospinning parameters

For optimization, soy protein isolate content in the nanofibers wanted to be maximized without sacrificing mechanical properties. Mechanical properties are important for these nanofibers as the intended application involves their use as a type of wound covering. For simplicity this can be compared to Band-Aid, the Band-Aid needs to be tough to stand up to everyday activities. Based on literature and electrospinning techniques being utilized in this research it was decided to test 6 different formulations of PVA/SPI to determine the optimal ratio of weight percentage PVA to SPI. To determine this optimal ratio, mechanical properties were investigated of nanofibers containing various amounts of weight percentage SPI. The six

formulations tested were as follows; Neat PVA, 70wt%PVA/30wt%SPI, 60wt%PVA/40wt%SPI, 55wt%PVA/45wt%SPI, 50wt%PVA/50wt%SPI, and 50wt%PVA/50wt%SPI with Sepiolite. Abbreviations for the above formulations are denoted as Neat P, 70P30S, 60P40S, 55P45S, 50P50S, and 50P50S-S, respectively. The samples were prepared as follows.

PVA solution was prepared by combining 0.5% wt. Triton X-100 and 14% weight PVA in an aqueous solution and allowing said solution to mix for 4 hours at 95° C with a magnetic stirrer. SPI solution was prepared by combing 6.3% weight SPI powder in an aqueous solution, and allowing it to mix for 10 minutes at room temperature. Then the pH of the SPI solution was adjusted to 11 by adding Sodium Hydroxide (NaOH) pellets at room temperature. SPI solution was then mixed 30 minutes at 80° C. PVA and SPI solutions were combined at the desired ratio of weight based on the formulation being mixed. New combined solution was then mixed for 45 minutes at 60° C.

The electrospinning setup consisted of a horizontally mounted syringe with a circular rotating collecting plate which measured 350 mm in diameter. Ambient conditions were used to carry out the electrospinning. For the experiment, a horizontal electrospinning set-up was utilized as shown in Figure 3-1 (Ning, et al., 2013).

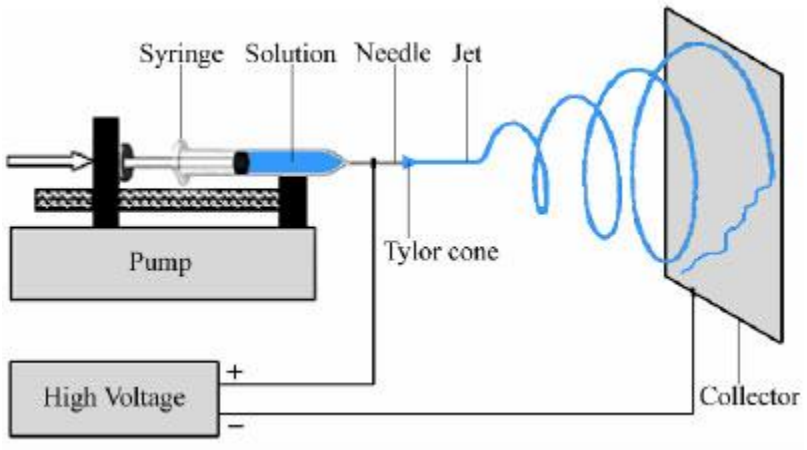

Figure 3-1: Horizontal electrospinning setup used to spin PVA/SPI nanofibers, image from (Ning, et al., 2013)

As noted the collector plate used in the experiments was rotating as a slow speed (56 rpm) to ensure fibrous mat had even dispersion of randomly oriented fibers. Formulations were electrospun to achieve continuous beadless fibers. The formulations were loaded into a 10 mL disposable syringe that dispersed the solution through a 22 gauge, 1" long needle. The solution was fed at the determined feed rate by a Fisher Scientific model no. 78-0100I syringe pump. Gap distance was maintained at 30 cm with the following voltages and feed rates for the corresponding PVA/SPI weight percentage. Neat P- 19 kV and 1.2 mL/h, 70P30S- 19 kV and 1.2 mL/h, 60P40S- 20kV and 1.21 mL/h, 55P45S- 19 kV and 1.17 mL/h, 50P50S-22 kV and 1.22 mL/h and 50P50S-S- 23 kV and 1.25mL/h. Sample were electrospun until enough fibers were collected for a tangible sample to be removed, this was typically ~8 hours. After being electrospun, fibers were dried in a vacuum oven for 24 hours at 15inHg and 105°C to remove remaining moisture and residue from electrospinning process.

Testing of PVA/SPI samples consisted of a tensile test with straight bar nanofiber samples. Specimens were cut into 5 mm by 25.4 mm bar samples and thickness of samples was then determined by a ratcheting micrometer. In order to ensure samples were not destroyed or

damaged during pretest handling, paper gigs were made to reduce likely hood of damage. Figure 3-2 shows an example of a test paper jig without a nanofiber sample (A), with a nanofiber sample (B), and after the sides of the jig have been cut (C). Samples were tested using an Instron testing machine with a 100 N load cell, tensile tests were conducted at a rate of 3mm/min until failure of the specimen occurred.

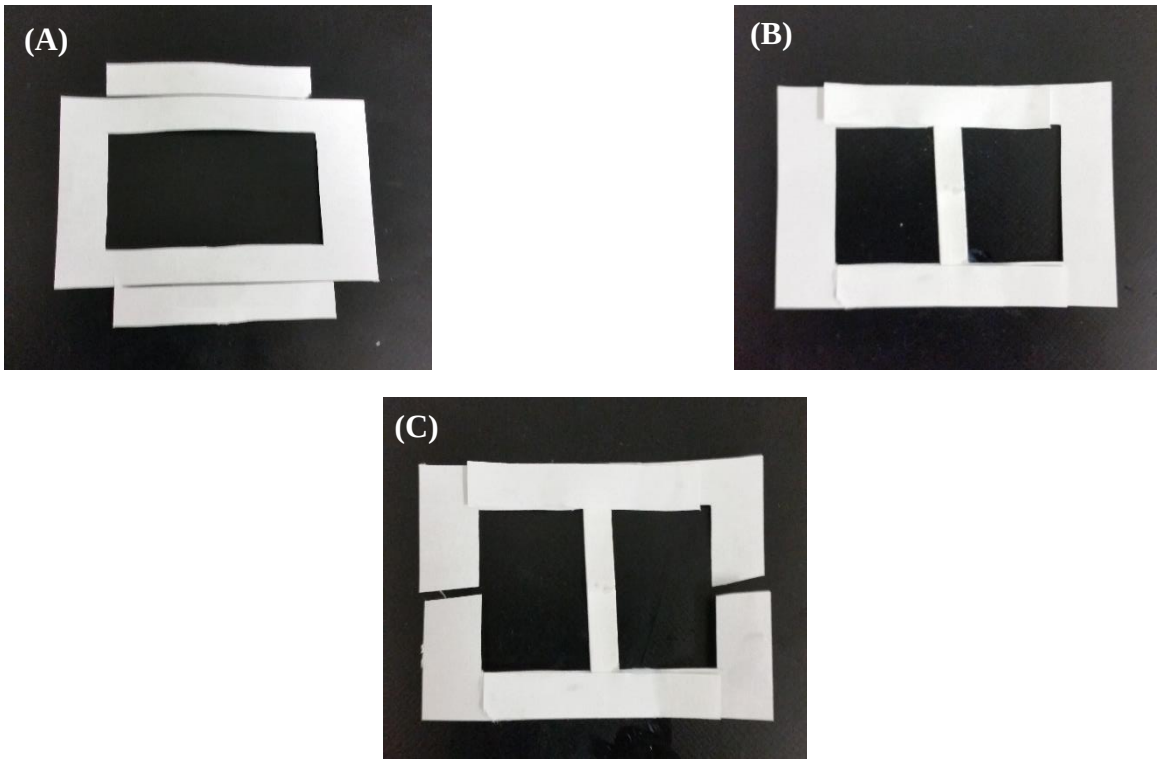

Figure 3-2: Images of PVA/SPI nanofibers and paper jigs before testing: test paper jig without nanofiber sample (A), with nanofiber sample (B), and after the sides of the jig have been cut (C)

3.3. Drug loading technique and efficiency

Drug loading technique and efficiency ultimately applies to loading the drug ketoprofen onto and into the naturally occurring nanoparticle sepiolite. Not only was loading of the drug into the nanoparticle a critical step in the study, but also determining the amount of drug that was loaded (efficiency) was necessary to determine future concentration calculations. The following is the procedure used to load the drug ketoprofen onto and into the sepiolite.

First, sepiolite and ketoprofen should be combined at a 1:1 solid weight ratio and then added to an aqueous solution. The aqueous solution was mixed for 48 hours at 50° C with a magnetic stirrer at 600 rpm. Upon completion of mixing, the solution was then centrifuged at 8,000 rpm for ten minutes to separate the sepiolite from the aqueous ketoprofen solution. The centrifuge process is essential to separate the now "loaded" sepiolite from the remaining aqueous ketoprofen solution. Upon separation, sample were dried in vacuum over for 24 hours at 111° C, 15 inHg in remove any remaining moisture. Thermo gravimetric analysis (TGA) was then conducted on the drug loaded sepiolite to determine the loading efficiency. When utilizing the TGA, baselines were first established for ketoprofen and sepiolite alone, and then the analysis was conducted on the combined or loaded sepiolite to determine what mass percentage belonged to which material. Amount of ketoprofen loaded on the sepiolite was determined from mass loss between 100° and 850° C. The drug load efficiency was calculated by shown below in Equation 3.1

$$Loading\ Efficiency = \frac{D_R}{D_O} \times 100\% \qquad 3.1$$

where D_R and D_O represent the mass of the loaded ketoprofen on the sepiolite, and the initial total ketoprofen used, respectively. The amount of drug loaded sepiolite was eventually added to the PVA/SPI solution so that a percent by mass ratio of ketoprofen was maintained.

3.4. Controlled release experimental setup

The controlled release experiment consisted of electrospinning PVA/SPI fibers at weight percentages previously determined by the mechanical testing results from the optimization of soy content in the nanofibers. It was found that a 1:1 ratio of PVA/SPI was optimal for this current study. Three different formulations were tested for the controlled release study including:

PVA/SPI/Keto, PVA/SPI/Keto loaded Sep, and PVA/SPI/Keto mixed Sep were chosen for their ability to be tailored for desired release rates. PVA/SPI/Keto has only the drug ketoprofen encapsulated in the nanofibers, mechanism for release involve both diffusion and erosion. PVA/SPI/Keto loaded Sep is shown in Figure 3-3, the drug loaded sepiolite is encapsulated inside of the PVA/SPI nanofibers. There are two mechanisms in the release, the release from the nanofibers by erosion and diffusion, and thereafter the release of the drug from the nanoparticle. PVA/SPI/Keto mixed Sep contains drug and sepiolite in the fiber with no preloading; therefore release is primarily a function of diffusion/erosion of fiber, rather than nanoparticle interaction.

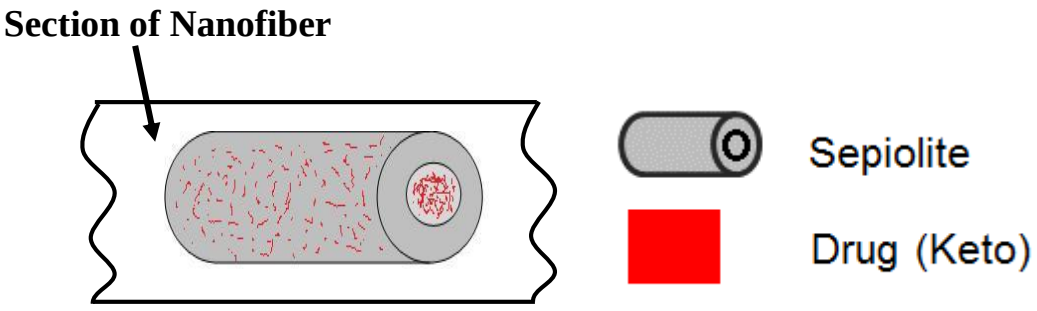

Figure 3-3: Diagram of a nanofiber containing PVA/SPI/Keto loaded Sepiolite, the nanofiber provides an encapsulation for the nanomaterial (sepiolite) and the drug (ketoprofen)

The procedure to produce the said three formulations was done as described previous in mechanical testing section. Upon completion of mixing, either ketoprofen, ketoprofen loaded sepiolite, or ketoprofen mixed with sepiolite was added to the solution in solid form and homogenized for five minutes with a mechanical mixer at 3200 rpms to ensure even dispersion before electrospinning. Conditions for electrospinning were again chosen so that continuous, beadless nanofibers were being produced. Electrospinning conditions were optimized for each of the drug/drug carrier combinations. For the PVA/SPI/Keto an electric potential of ~22 kV was used, a distance between the tip of the needle and the collecting plate was set to 30 cm.

When electrospinning had concluded, fibers were dried at least 18 hours at 15 inHg at 105° C to remove moisture and residue. For the drug loaded sepiolite, a ~23 kV potential was used with a feed rate of 1.25 mL/h, otherwise all other conditions remained constant. The PVA/SPI/Keto mixed Sepiolite was optimized with the following conditions; a ~21 kV potential with a feed rate of 1.25 mL/h, again a 22 gauge needle with a 1" length was used and the gap was set to 30 cm. Figure 3-4 shows a schematic of the three formulations in their respective electrospun nanofiber forms.

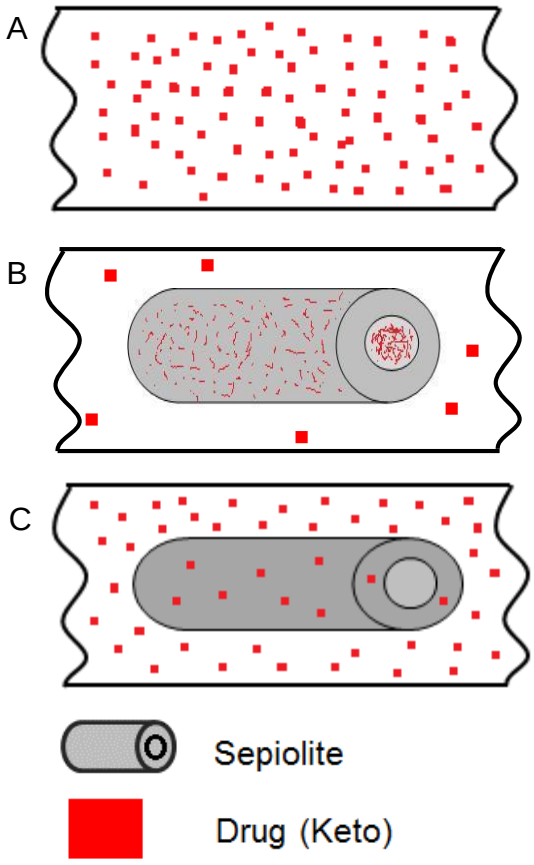

Figure 3-4: A) PVA/SPI/Keto; B) PVA/SPI/Keto loaded Sepiolite; C) PVA/SPI/Keto mixed Sepiolite

UV-vis spectroscopy was used to study the in vitro release kinetics from PVA/SPI/Keto, PVA/SPI/Keto loaded Sepiolite, and PVA/SPI/Keto mixed Sepiolite. Amount of fiber used was determined by the ketoprofen content of the fibers so that 1.26 grams of ketoprofen was used. The measured amount of fibers were then dispersed into 5 mL Phosphate Buffered Saline (PBS) solution (pH=7.4) and placed in a dialysis bag with a molecular weight cutoff of 12,000 Daltons and submerged in a buffer of 80 mL of PBS. Solution was heated to 37.2° C and stirred magnetically at 120 rpm. At specified time intervals, 5 mL of PBS solution was removed and replaced with 5 mL pure PBS. Removed samples were then analyzed using a Cary 500 UV-vis spectrophotometer at 260 nanometers. Known amounts of ketoprofen were first analyzed against PBS using UV- Vis to establish a calibration line for specific drug concentrations in the PBS solution. Results for PBS calibration line are shown in Figure 3-5. Determination of calibration line was done based on previous controlled release studies (Kim, et al., 2006) (Wang, et al., 2012) (Chung, et al., 1999). Five sample were used in the calibration to ensure sufficient precision in the measurement process.

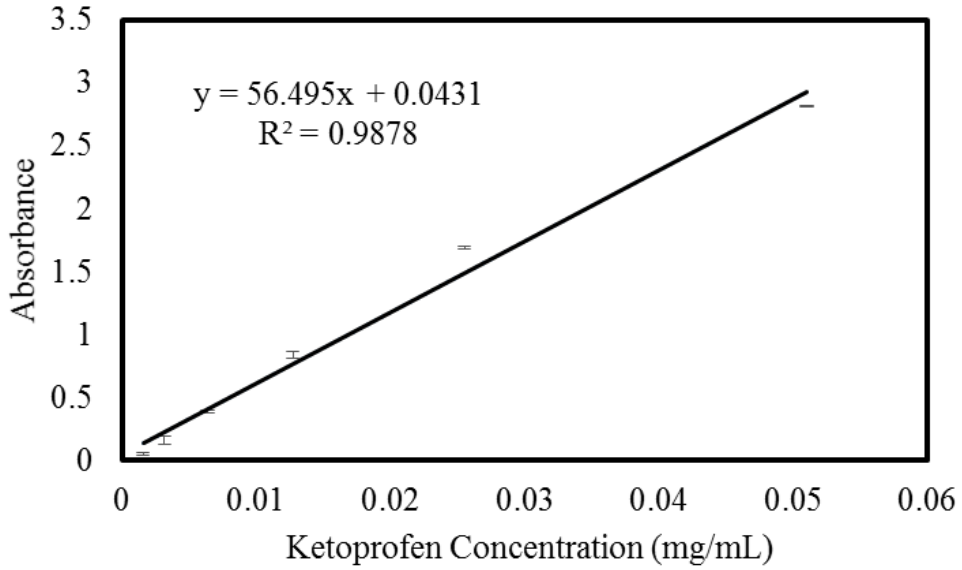

Figure 3-5: Calibration line for ketoprofen generated by using ketoprofen in phosphate buffered saline ranging from 0.00159mg/mL to 0.051 mg/mL

This relationship provides an avenue to relate a measured absorbance to a specific concentration of ketoprofen in PBS. As samples were removed, they were tested resulting in an absorbance value found by using the UV-vis spectrophotometer. This absorbance was then used to back calculate the ketoprofen concentration in the specific sample. Note it was critical that the dialysis bag was used in the experimental method. This ensured that as samples were taken to determine the concentration of ketoprofen, no nanofibers were accidentally removed. The drug released from the nanofibers and was allowed to pass through the dialysis bag into the surrounding PBS, while the dialysis bag protected the fibers against removal for further release analysis. Three samples were analyzed for each type of nanofibers formulation so that a statistical analysis could be conducted. A schematic of the drug release experiment using the dialysis bag is shown in Figure 3-6.

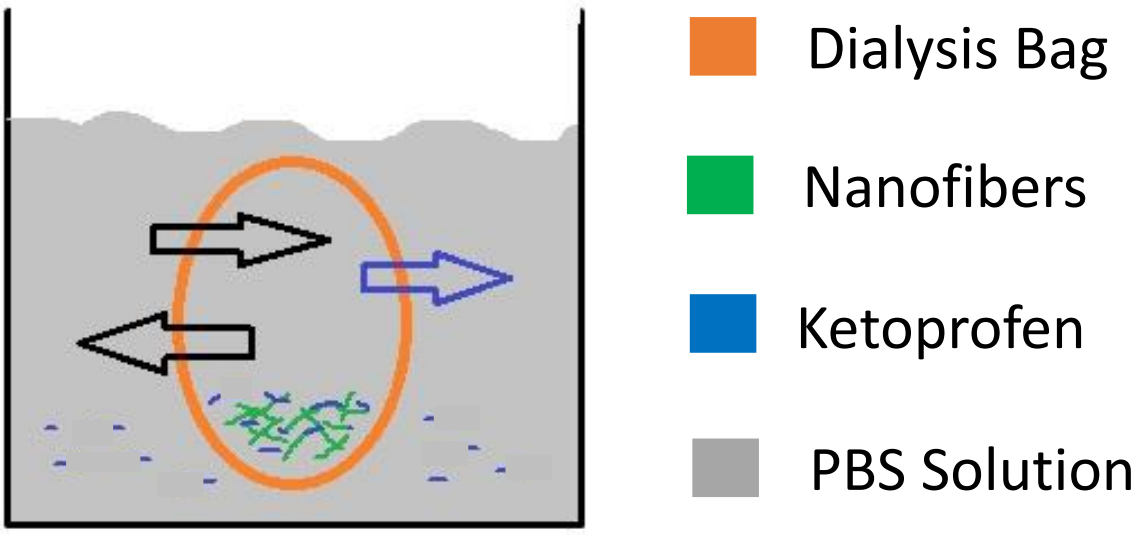

Figure 3-6: Schematic of in-vitro drug release experiment

The dialysis bag acts a type of filter, allowing the drug to pass through while retaining the nanofibers, this ensures that only drug already released from the nanofibers is measurable outside the dialysis bag. For this particular experiment, a dialysis bag with an M_w cutoff of 12,000 D was used based on literature (Levy, et al., 1990) (Siepmann, et al., 2004). A schematic of the dialysis bag's mechanism is shown in Figure 3-7. Note how the drug is free to move through the dialysis bad to achieve equilibrium, however drug still encapsulated in the nanofibers is not; only once the drug is released may it pass.

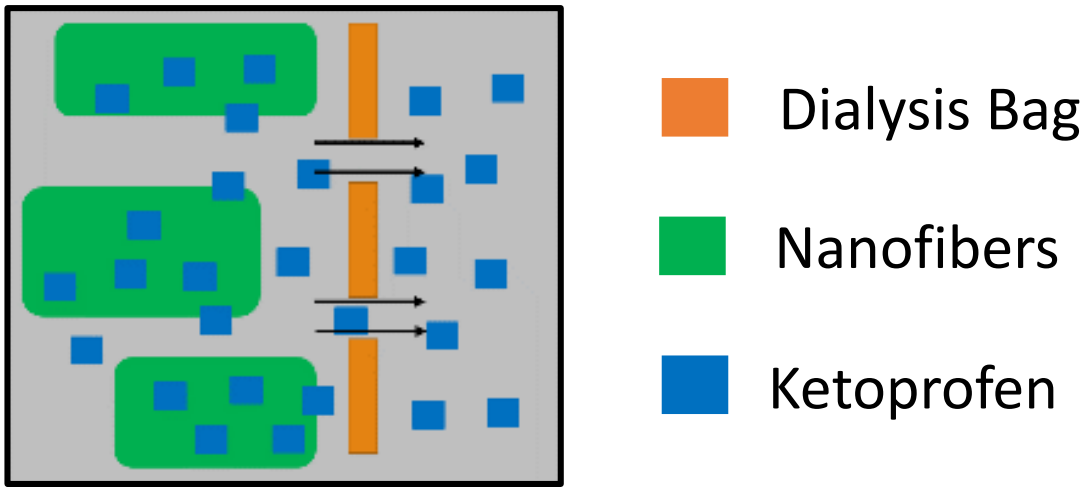

Figure 3-7: Schematic of dialysis bag release, drug releases while retaining nanofibers

Prior to use, dialysis bag were stored as recommended by manufacturer in a refrigerated container inside water containing factory packaging. Upon removal, bags were utilized immediately to maximize efficiency. Time intervals were determined to ensure equilibrium of diffusion had optimal opportunity to take place.

4. INITIAL EXPERIMENTAL RESULTS

The following chapter displays the initial experimental results for the controlled release study. First, mechanical testing results are described to demonstrate why the selection of 50 wt% SPI nanofibers was chosen. Next, loading efficiency of drug to nanoparticle was investigated using TGA showing a 49% efficiency in the loading process. Finally, in-vitro results showed implementation of the drug loaded nanoparticle significantly delayed the release rate. At 70 hours, the nanofibers containing the drug loaded nanoparticles shows ~67% release compared to the other formulations that were all above 90% release at 70 hours. Mathematical modeling was done using both diffusion and erosion models to verify results.

4.1. Mechanical testing results

The desired outcome from the mechanical testing experiment was to determine the optimal amount of soy protein isolate content in the PVA/SPI nanofibers. Results for mechanical testing were analyzed for both elastic modulus (E) and ultimate tensile strength (UTS). Figure 4-1 and Table 4-1 show the results for the various formulations that were tested. Mechanical testing was performed on six different samples; Neat P, 70P30S, 60P40S, 55P45S, 50P50S, and 50P50S-S.

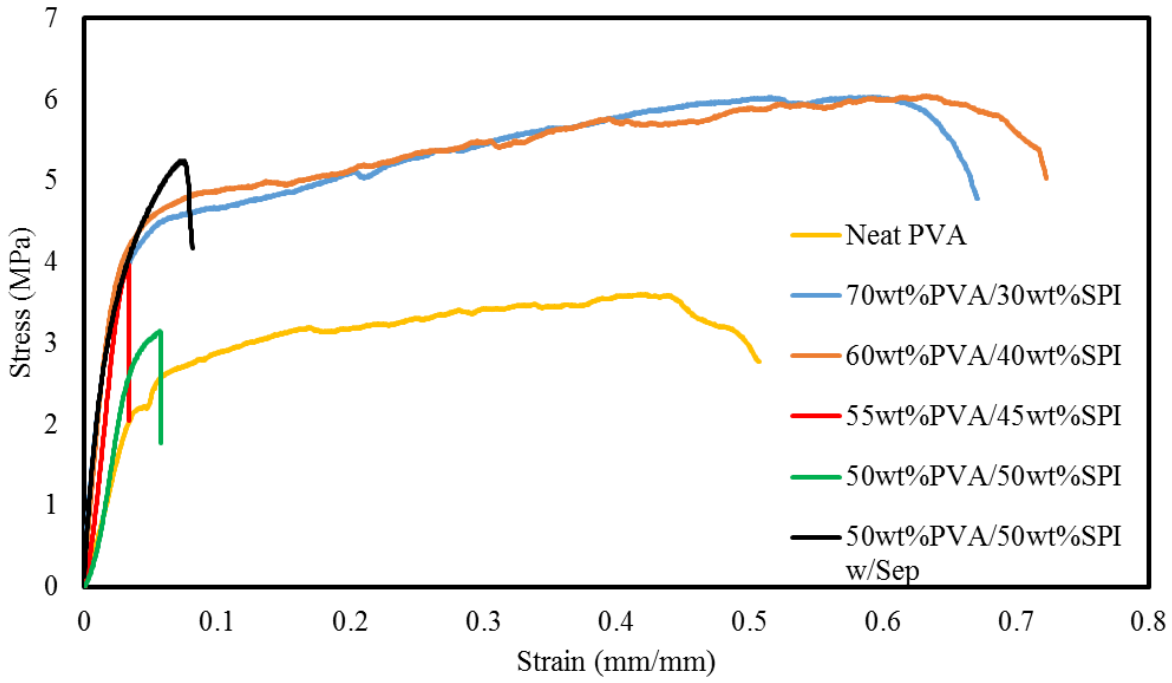

Figure 4-1: Results for tensile testing of varying PVA/SPI nanofiber formulations

Table 4-1: Mechanical testing results of PVA/SPI nanofibers

Material	E (MPa)	STDEV (MPa)	UTS (MPa)	STDEV (MPa)	Stain at Fracture (%)	STDEV (%)
Neat P	81.9	25.9	4.1	0.7	65.9	11.5
70P30S	179.3	22.5	6.5	0.5	74.5	13.7
60P40S	179.5	16.9	6.3	0.3	69.4	1.8
55P45S	114.9	35.4	3.5	0.4	3.4	0.3
50P50S	105.3	31.1	3.3	0.1	5.2	0.6
50P50S-S	208.9	8.3	4.9	0.8	9.0	1.5

Initially the addition of SPI to the PVA nanofibers resulted in an increase in both modulus and UTS. For Neat P modulus and UTS values were 81.1 MPa and 4.1 MPa, respectively. As the amount of SPI was increase to 30wt% and 40wt%, both modulus and UTS increased as well, values were measured to be 179 MPa and ~6.3 MPa respectively. At 50P50S, properties fell but values were relatively close to that of Neat P. The 50P50S-S sample showed

the highest modulus of all samples tested (208.9 MPa) and demonstrated an UTS 4.9 MPa. These properties are sustainably better than that of 50P50S which did not contain sepiolite. Results from mechanical testing are important as they show that 50wt% SPI is the maximum allowable SPI concentration for the electrospinning set-up used in this study, as well as the addition of sepiolite at 50wt% SPI shows an increase in modulus and UTS, when compared to without sepiolite. From these results it is clear why 50wt%PVA/50wt%SPI (1:1) was chosen as the weight ratio for the drug release study. It maximizes SPI content in nanofibers while showing little to no decrease in mechanical properties compared to Neat PVA. Figure 4-2 shows a specimen after fracture, all samples used in calculations were selected based on desired fracture as shown. Some samples displayed fracture that was less desired and these sample were omitted.

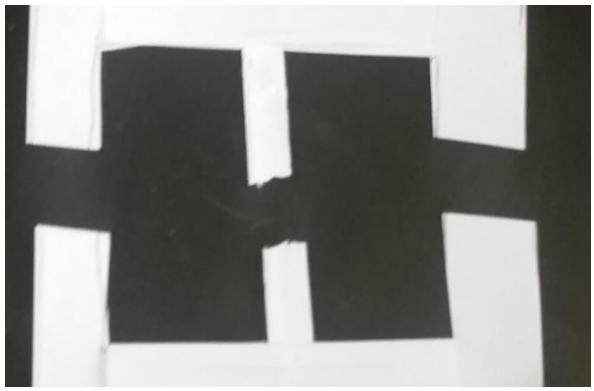

Figure 4-2: PVA/SPI specimen after fracture post tensile test

4.2. Loading efficiency

The experiment was done in triplicate and results from TGA are shown in Figure 4-3. Samples of ketoprofen, sepiolite, and ketoprofen loaded sepiolite were analyzed. To determine the percent weight, sample weight loss was analyzed between 100° C and 850° C. Results showed that the ketoprofen loaded sepiolite was initially 67% by weight sepiolite and 33% by weight ketoprofen. The slope for the ketoprofen loaded sepiolite is greater than that of the

sepiolite; showing continued weight loss due to the addition of ketoprofen. Also plotted is the derivative curve shown in Figure 4-4.

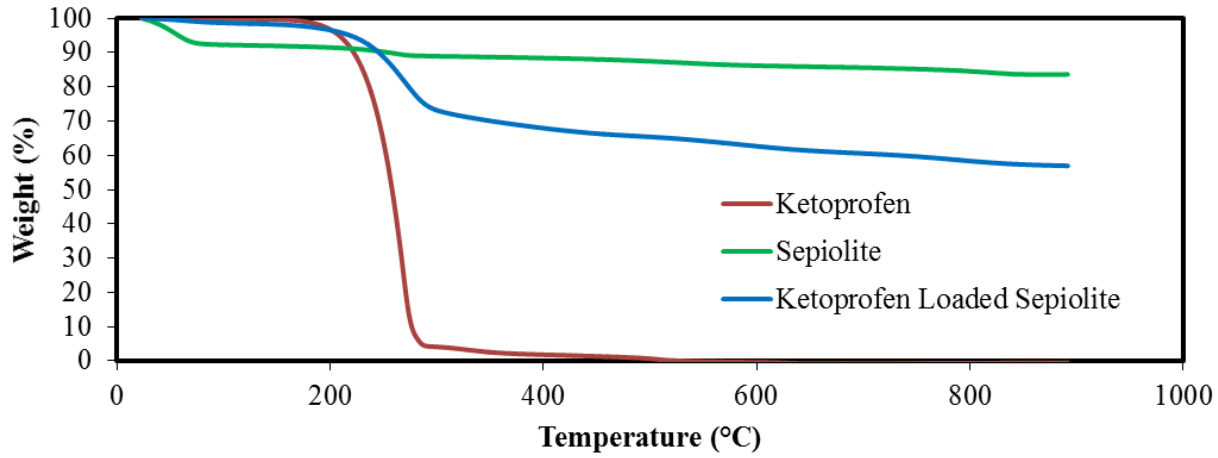

Figure 4-3: Results from TGA analysis show that ketoprofen loaded sepiolite contained initially 67 wt. % sepiolite and 33 wt. % ketoprofen

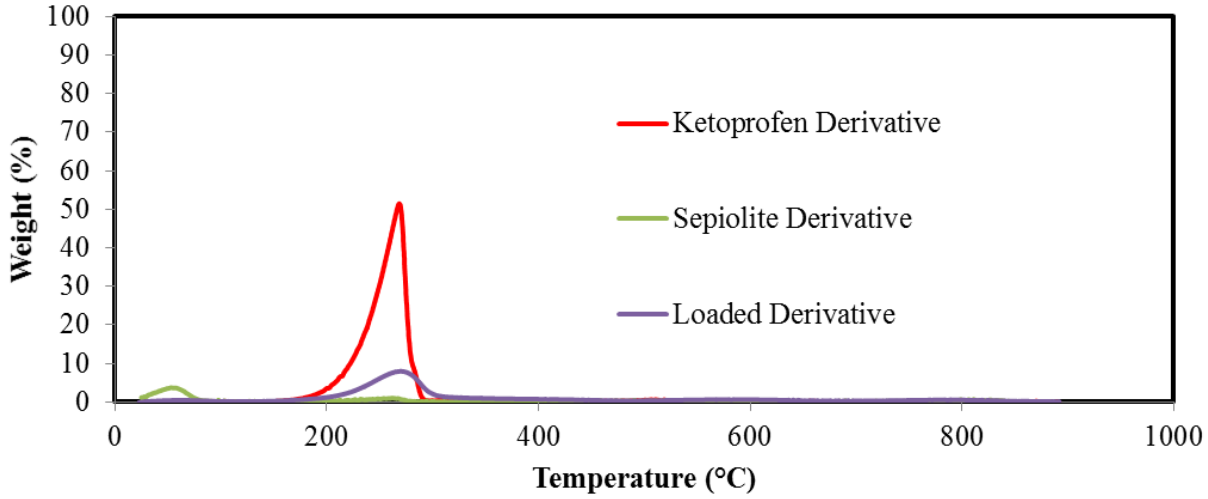

Figure 4-4: Derivative results from TGA analysis showing weight loss rate

Upon determination that the loaded sepiolite was initially loaded with 33wt% ketoprofen (calculated from Figure 4-3), loading efficacy was calculated by Equation 3.1. Initially ketoprofen and sepiolite were combined at a 1:1 weight ratio, however the loaded sepiolite was 33wt% ketoprofen, this results in a loading efficiency of 49% for the process used to load the

ketoprofen on the sepiolite. Loading efficiency was calculated based on amount of ketoprofen that was loaded onto the sepiolite compared to the amount of ketoprofen initially combined with the sepiolite as described by Equation 3.1. SEM images of loaded vs unloaded sepiolite were taken for visual verification and fiber diameter analysis. Figure 4-5 shows the collection of images. In Figure 4-5 (B) the sepiolite appears swelled due to the loading of ketoprofen in the tubular structure and attachment of drug on the porous exterior. Diameter of the sepiolite used in the two samples was analyzed (50 nanoparticles) and shown in Table 4-2.

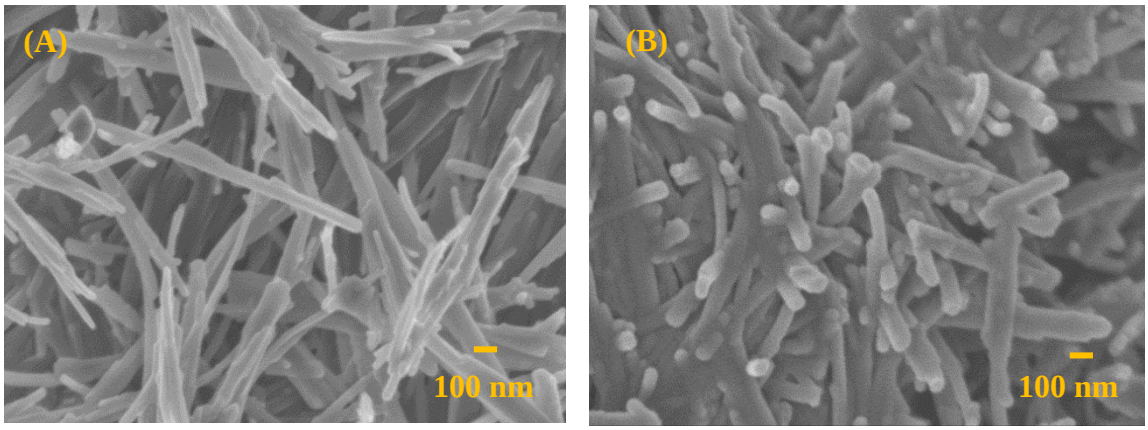

Figure 4-5: SEM imaging shows (A) sepiolite as received, (B) drug loaded sepiolite; particle diameter analysis showed that addition of loading drug increased sepiolite diameter ~50%

Table 4-2 shows the distribution of the sepiolite diameters, 50 nanoparticles were measured for the analysis.

Table 4-2: Fiber diameter analysis of sepiolite versus ketoprofen loaded sepiolite

Nanoparticle Type	Mean (nm)	Standard Deviation	Minimum (nm)	Maximum (nm)
Sepiolite	59.8	22.4	27.7	107.9
Keto Loaded Sepiolite	89.7	25.6	46.4	145.9

The ketoprofen loaded sepiolite showed an increase in diameter of 50% over the received the sepiolite, I propose this increase or swelling in diameter is a result of two phenomena. Firstly and most prominently the sepiolite's porous microstructure was coated with the drug. As the drug attaches itself to the outside of the sepiolite, the diameter increases simply due to the attachment. Note how the attached drug gives a more "smooth" look to the particles in Figure 4-5 (B) compared to the non-loaded sepiolite in Figure 4-5 (A). Secondly, some amount of drug actually enters the tubular sepiolite which results in the swelling or expansion of the tube. This phenomena may also contribute to the increase in diameter however it is believed the primary factor for increasing diameter is due to the drug attachment on sepiolite's exterior surface.

4.3. Morphology studies

The morphology of the nanofibers becomes an important aspect in understating the behavior of the drug release results. As discussed previously, there are many parameters in electrospinning that directly correlate to the structure and characteristics of the fibers, such as fiber diameter. These characteristics have direct results on the release profiles demonstrated by the three different formulations investigated in this study. Images were captured using Scanning Electron Microscopy (SEM) conducted at the USDA building on the campus of North Dakota State University. Figure 4-6 shows images of the three different samples used in the drug delivery experiment. In Figure 4-6 (A) and (A') represent PVA/SPI/Keto at 10,000x and 30,000x magnification, respectively. (B) and (C) correspond to the formulations of PVA/SPI/Keto loaded Sepiolite and PVA/SPI/Keto mixed Sepiolite, respectively. In Table 4-3 is a summary of the fiber diameters.

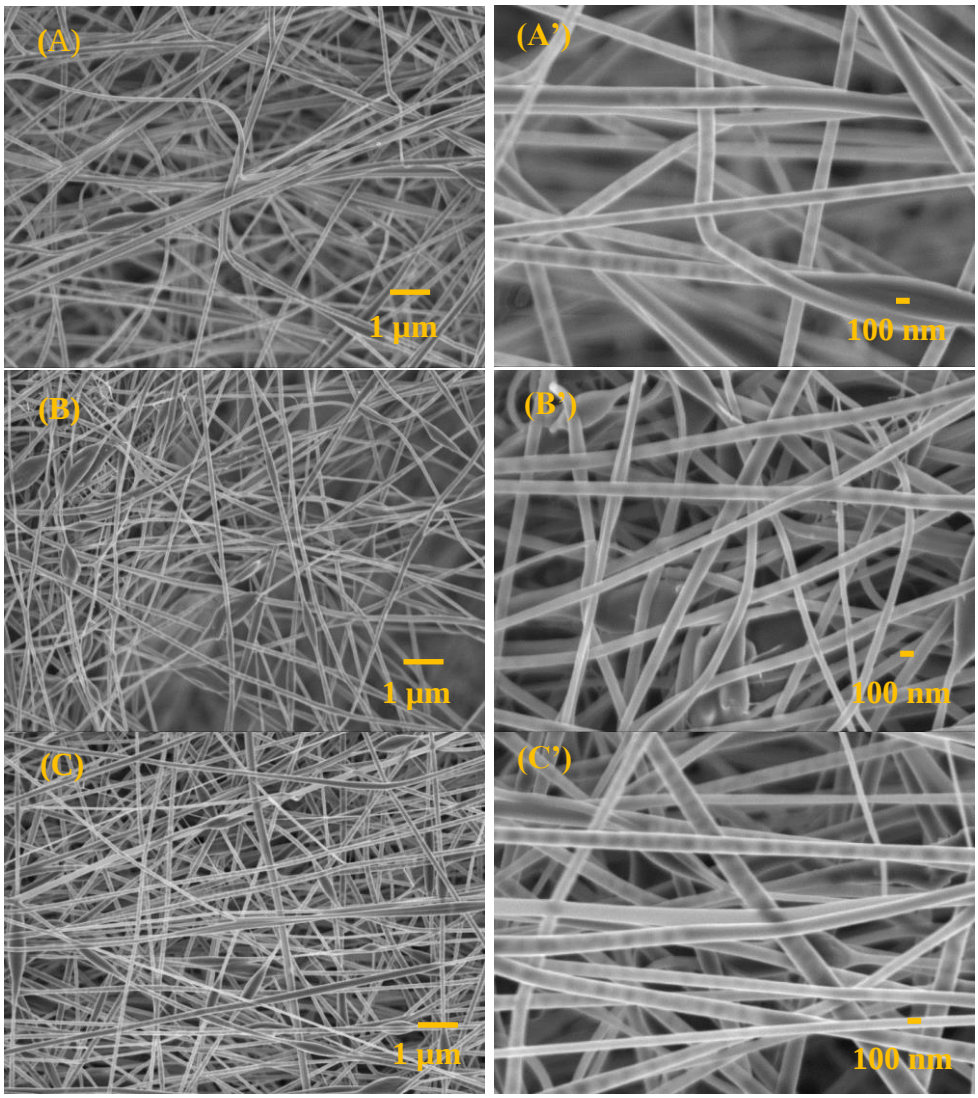

Figure 4-6: SEM images of samples, (A-A') PVA/SPI/Keto; (B-B') PVA/SPI/Keto loaded Sepiolite; (C-C') PVA/SPI/Keto mixed Sepiolite. A,B,C show 10,000x; A',B',C' show 30,000x

Table 4-3: Fiber diameter, analyzed from SEM images (50 fibers)

Fiber type	**Mean (nm)**	**Standard Deviation**	**Minimum (nm)**	**Maximum (nm)**
PVA/SPI/Keto	137.0	23.9	96.2	197.7
PVA/SPI/Keto Loaded Sepiolite	117.0	29.7	56.5	224.5
PVA/SPI/Keto mixed Sepiolite	129.2	33.0	78.8	215.3

4.4. In-vitro release profiles

Release profiles of the various formulations of nanofibers were tested in PBS solution (pH = 7.4) at 37.2 °C. The ketoprofen release profile was compared for three solutions: PVA/SPI/Keto, PVA/SPI/Keto loaded Sepiolite and PVA/SPI/Keto mixed sepiolite with the same drug content by weight. Results of the release profiles are shown in Figure 4-7. After 70 hours, PVA/SPI/Keto loaded sepiolite had released ~67% of the drug initially loaded in the nanofibers. This was substantially less than both PVA/SPI/Keto and PVA/SPI/Keto mixed sepiolite that both displayed over 90% drug release after 70 hours. The primary reason a more sustained release is observed in the PVA/SPI/loaded sepiolite is the effect of loading the ketoprofen into and onto the tubular sepiolite. As the fiber erodes/experiences diffusion, there is a two stage release of the drug, the first is the release of the ketoprofen encapsulated in the fiber, and the second is the ketoprofen loaded onto/into the sepiolite. In Figure 4-7, for PVA/SPI/Keto loaded Sepiolite, after the initial release, it is shown that the slope begins to level out until around 120 hours where the release rate again increases. Figure 4-8 shows the release results for the first 16 hours of release, note that even at this stage the PVA/SPI/Keto loaded sepiolite has the slowest release profile. It is postulated that this again is due to loading, because some of the drug is loaded into/onto the sepiolite, the amount of drug available for release is less when compared to fibers where loading was not implemented. Experiments were done in triplicate to provide sufficient data for statistical analysis.

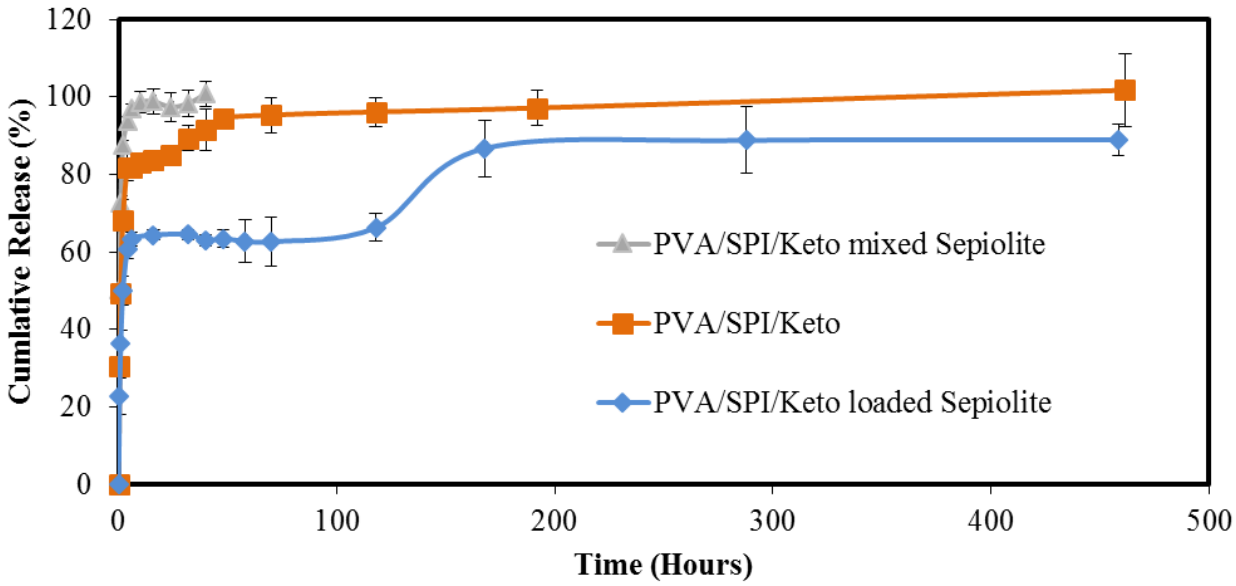

Figure 4-7: Release profiles for PVA/SPI/Keto, PVA/SPI/Keto loaded sepiolite and PVA/SPI/Keto mixed sepiolite. PVA/SPI/Keto loaded sepiolite showed the most sustained release as a result of loading the drug into the sepiolite

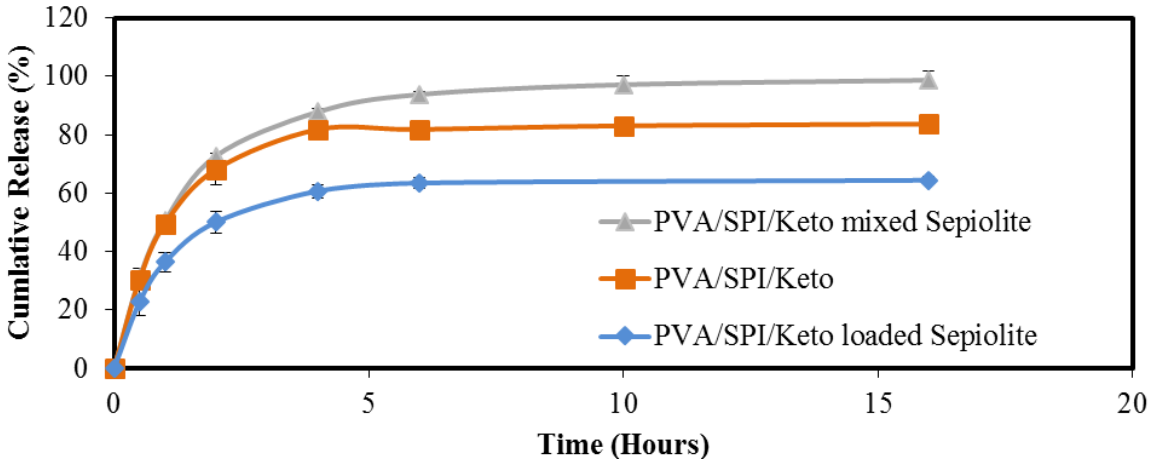

Figure 4-8: Release profiles for PVA/SPI/Keto, PVA/SPI/Keto loaded sepiolite and PVA/SPI/Keto mixed sepiolite after the first 16 hours

When correlating the release results in terms of fiber diameter an interesting trend is observed. From a diffusion or erosion standpoint, with all factor remaining constant, fibers with the smallest diameter should release the drug at the fastest rate. The holds true for the case of PVA/SPI/Keto (~137 nm) versus PVA/SPI/Keto mixed sepiolite (~129 nm). While the

nanomaterial sepiolite is present in the PVA/SPI/Keto mixed sepiolite, it is not loaded with the drug, so release profile was expected to be similar to that of PVA/SPI/Keto. Results showed that PVA/SPI/Keto mixed sepiolite actually released the drug faster than PVA/SPI/Keto, hence the smaller diameter fibers release drug at a more rapid rate given there is no loading of drug into nanoparticle. The PVA/SPI/Keto loaded Sepiolite had the smallest fiber diameter (~117 nm) however it still displayed the most sustained release profile. Another issue presented is that in the PVA/SPI/Keto mixed Sepiolite, the addition of the sepiolite took up a significant amount of volume in the fibers. Previous fiber analysis showed that mean sepiolite diameter was 59.8 nm, while the PVA/SPI/Keto mixed Sepiolite nanofibers exhibited a mean fiber diameter of 129.2 nm. Therefore the sepiolite, containing no preloaded drug took up a significant amount of volume in the fiber; thus leaving the drug particles a smaller volume to distribute in. Figure 4-9 shows a diagram of the three types of nanofibers tested, as shown, the fiber containing sepiolite mixed with ketoprofen (C) has a large amount of drug near the surface of the fiber. As diffusion or erosion occurs, drug more near to the surface of the fiber is released at a more rapid rate than the drug encapsulated near the center of the fiber. This phenomena explains why the release profile for PVA/SPI/Keto mixed Sepiolite is the most rapid when compared to the other nanofibers.

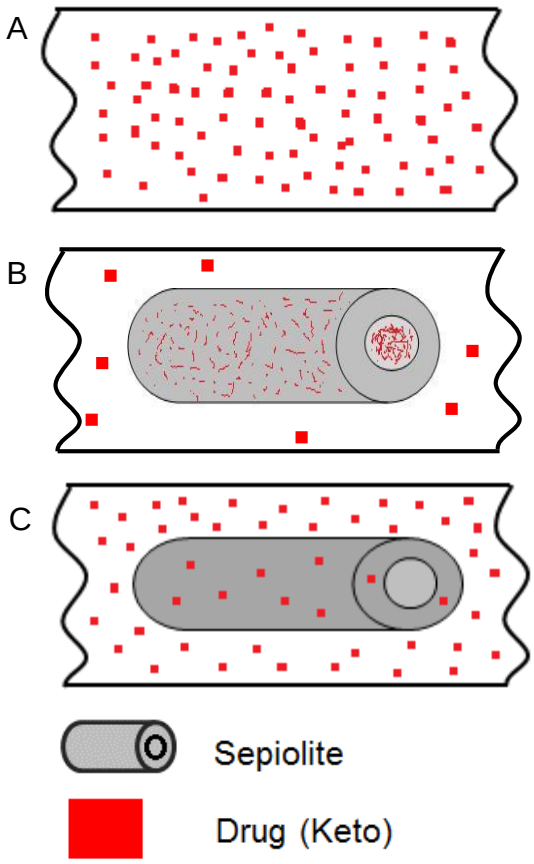

Figure 4-9: A) PVA/SPI/Keto; B) PVA/SPI/Keto loaded Sepiolite; C) PVA/SPI/Keto mixed Sepiolite

With all other factors remaining constant, the sustained release was a result of loading the drug into the nanoparticle. Not only does this result in a much more sustained release rate, it also makes the delivery rate much more controllable as loading efficiency and fiber diameter are both controllable variables in the release process.

4.5. Mathematical modeling results

The simple semi empirical erosion based mathematical model purposed first by (Hopfenberg, 1976) assumed that release rate of drug is proportional to the surface area of the device (fiber) that is changing with time in respect to the surface area of the device. The total

mass transfer process is assumed to add up to a single order zero order process (this is characterized by the rate constant k_o) (Hopfenberg, 1976). While the zero-order process may correspond to a single phenomenon, it would also be the result from the super position of multiple processes; swelling, dissolution, and/or cleavage of polymer chains. The model can be applied to surface eroding polymer systems where a zero-order surface attachment of the drug is the rate limiting release step. Hopfenberg derived the following Equation 4.1 shown in its general form which is valid for spheres, cylinders, and slabs.

$$\frac{M_T}{M_\infty} = 1 - \left(1 - \frac{k_o \times t}{c_o \times a}\right)^n \qquad 4.1$$

Where M_t represents the amount of drug released at a specified time and M_∞ is the amount of drug released at an infinite amount of time. C_o and t represent the initial drug concentration within the system and time (corresponding to M_t), respectively. Since the study involves nanofibers which have a cylindrical geometry, *a* represents the radius of the cylinder and *n* represents the shape factor for which cylinder is 2. The model proposed by Hopfenberg does not take into account the edge and end effect on the cylinder.

Another model often implemented in drug release studies is the diffusion based swelling model proposed by Peppas which states that upon contact with biological fluids, the polymer portion of nanofiber begin to swell creating two phases (Peppas, et al., 2000). The drug molecules are allowed to diffuse from the swollen rubbery phase that is created. This diffusion was proposed by Peppas described by Equation 4.2 and is modeled as follows

$$\frac{M_T}{M_\infty} = kt^n \qquad 4.2$$

Where M_t represents the amount of drug released at a specified time and M_∞ is the amount of drug released at an infinite amount of time. In the equation k is a proportionality

constant, while t represents time and n is the diffusion exponent (Peppas, et al., 2000). In the case of cylinders, n is taken as 0.45 for a diffusion controlled delivery system (Siepmann, et al., 2012). Cylinder was chosen because this is the geometrical shape of nanofibers. Equation 4.2 only applies to the initial 60% of the release as defined by Peppas (Peppas, et al., 2000). Implementation of both the erosion and diffusion model are to determine release constants (k_o and k) for the varying formulation of nanofibers. Calculation of k_o and k allows quantification of release profiles to compare the different formulations tested.

The erosion model was investigated first, the erosion model or Equation 4.1 was applied to the formulations of PVA/SPI/Keto, PVA/SPI/Keto loaded sepiolite and PVA/SPI/Keto mixed sepiolite. Due to the nature of the release profiles, the erosion model was applied for the longest time allowable, after which curve fitting was utilized for prediction of values after which the erosion model is applicable (typically ~60% release). The first formulation investigated was that of PVA/SPI/Keto (see Figure 4-9 for nanofibers schematic), Figure 4-10 shows the calculated k_o values based on the observed experimental data and Equation 4.1.

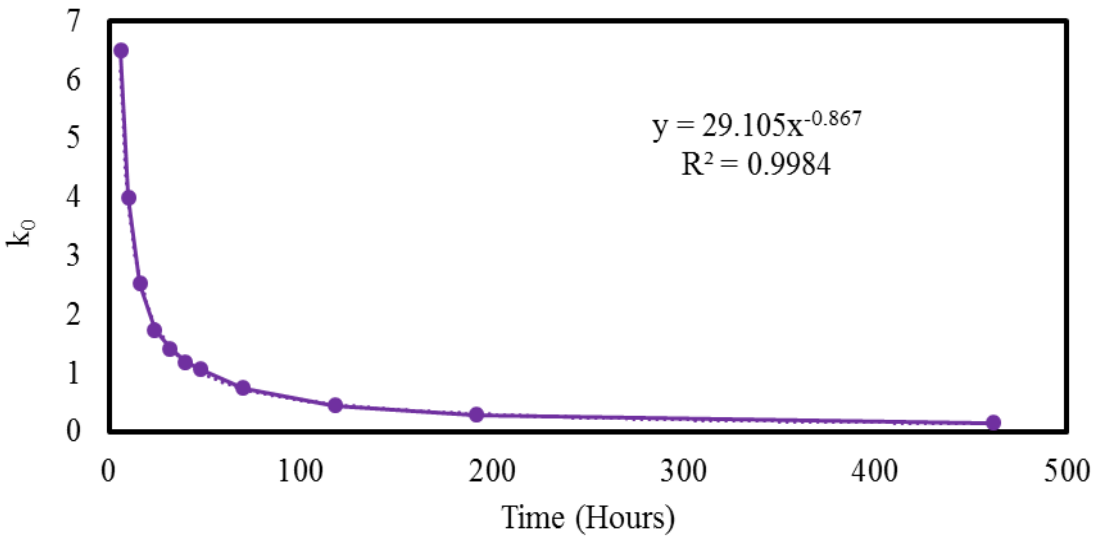

Figure 4-10: PVA/SPI/Keto determined k_o values from erosion model

The higher the k_o value, the higher rate at which the drug is being released from the nanofibers. In this particular case, the erosion model was applied at the time interval from 0 to 2 hours, at 2 hours PVA/SPI/Keto displayed on average 68.1% release, from there the curve fit equation determined from Figure 4-10 was applied. An overlay of the predicted values versus the observed data for PVA/SPI/Keto using the erosion model with k_o =18.4 is shown in Figure 4-11.

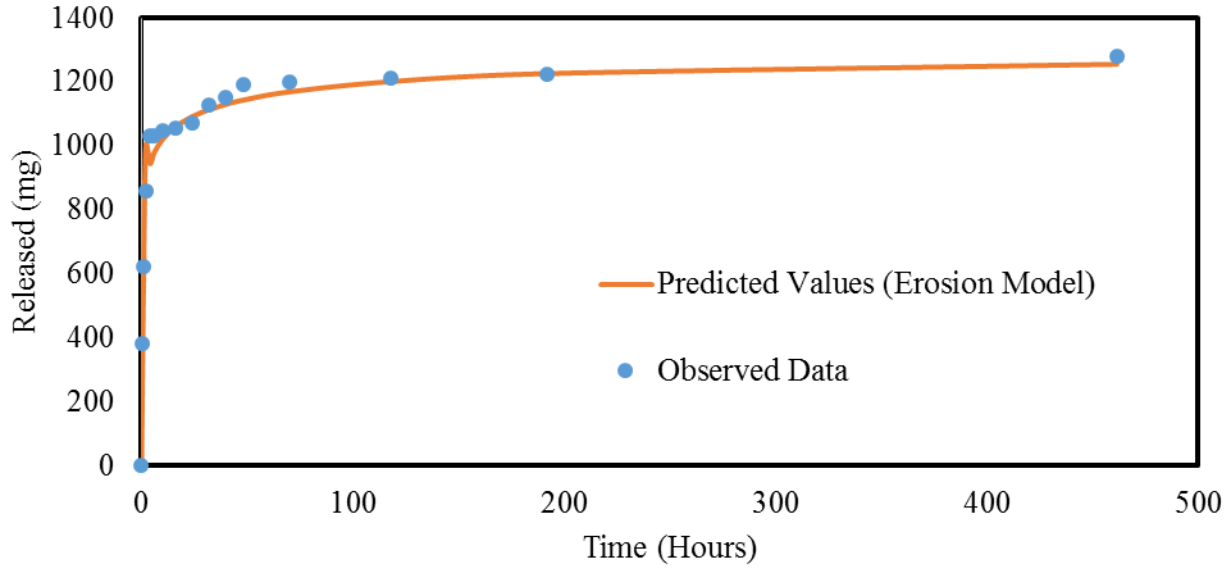

Figure 4-11: PVA/SPI/Keto, observed data plotted in overlay versus predicted values based on erosion model

The second formulation investigated was that of PVA/SPI/Keto mixed Sepiolite (see Figure 4-9 for nanofiber schematic), Figure 4-12 shows the calculated k_o values based on the observed experimental data and Equation 4.1 for PVA/SPI/Keto mixed Sepiolite.

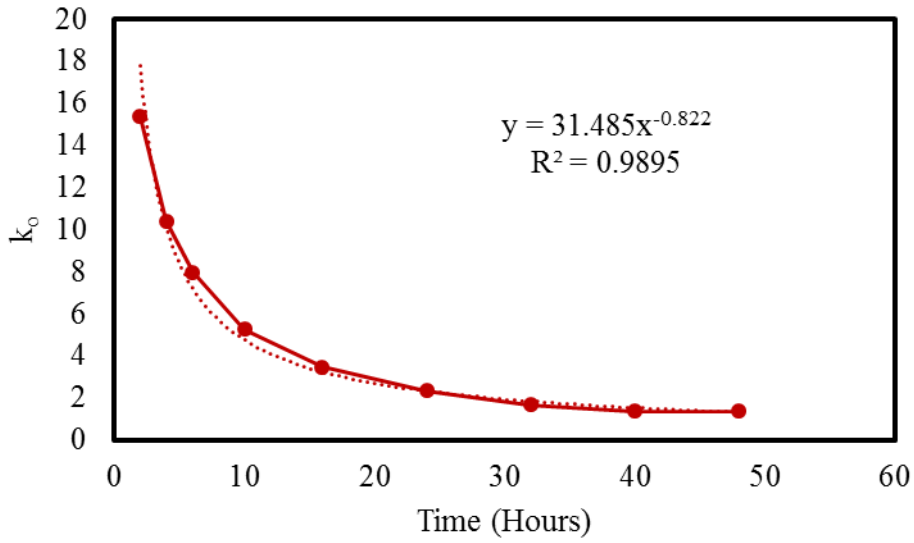

Figure 4-12: PVA/SPI/Keto mixed Sepiolite determined k_o values from erosion model

Again, the erosion model was applied at the time interval from 0 to 2 hours, at 2 hours PVA/SPI/Keto mixed Sepiolite displayed on average 72.7% release, from there the curve fit

equation determined from Figure 4-12 was applied. An overlay of the predicted values versus the observed data for PVA/SPI/Keto mixed Sepiolite using the erosion model with k_o =18.7 is shown in Figure 4-13.

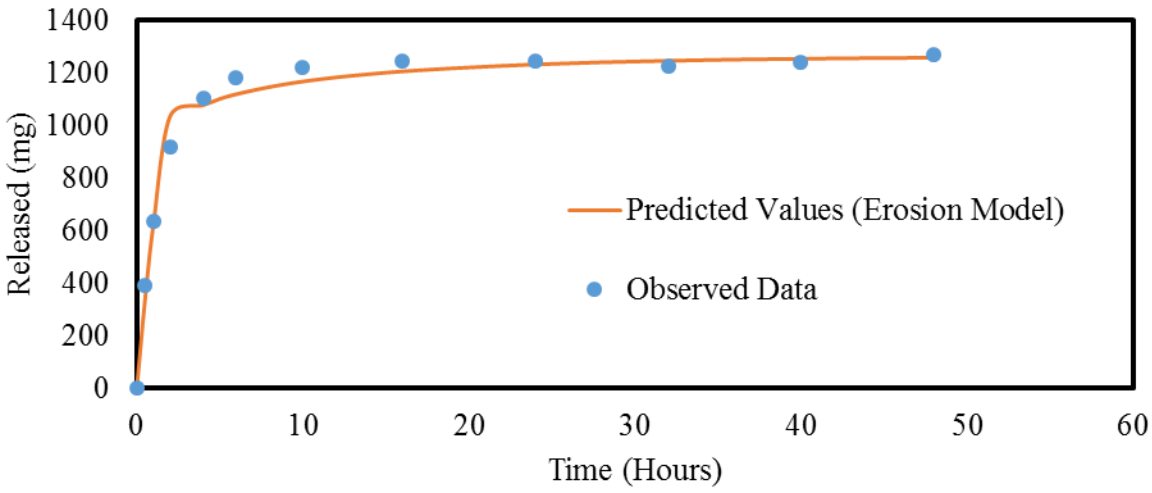

Figure 4-13: PVA/SPI/Keto mixed Sepiolite, observed data plotted in overlay versus predicted values based on erosion model

The third formulation investigated was that of PVA/SPI/Keto loaded Sepiolite (see Figure 4-9 for nanofiber schematic), Figure 4-14, Figure 4-15, and Figure 4-16 show the calculated k_o values based on the observed experimental data and Equation 4.1 for PVA/SPI/Keto loaded Sepiolite at specific time intervals.

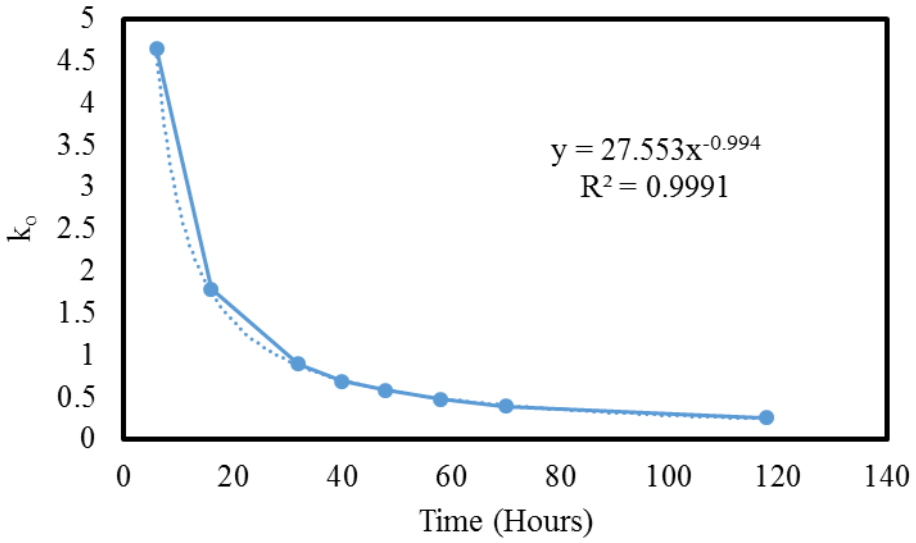

Figure 4-14: PVA/SPI/Keto loaded Sepiolite determined k_o values from erosion model, from 0 < t < 120 hours

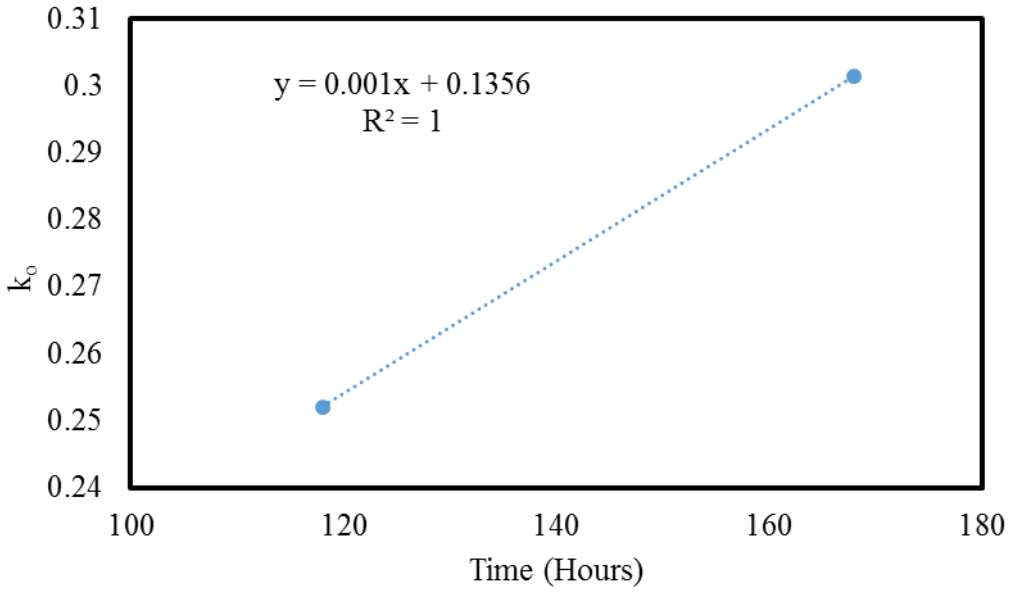

Figure 4-15: PVA/SPI/Keto loaded Sepiolite determined k_o values from erosion model, from 120 < t < 170 hours

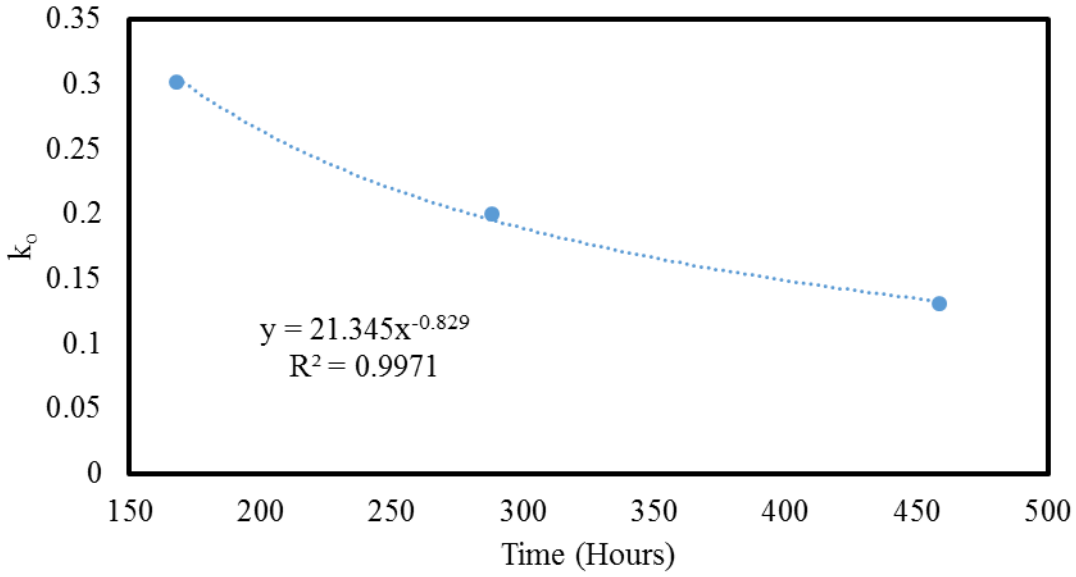

Figure 4-16: PVA/SPI/Keto loaded Sepiolite determined k_o values from erosion model, from 170 < t < 470 hours

For this model, the erosion model was applied at the time interval from 0 to 4 hours, at 4 hours PVA/SPI/Keto loaded Sepiolite displayed on average 60.7% release, from there the three distinct curve equations determined from Figure 4-14, Figure 4-15, and Figure 4-16 were applied. An overlay of the predicted values versus the observed data for PVA/SPI/Keto loaded Sepiolite using the erosion model with k_o =11.8 is shown in Figure 4-17. The equation for Figure 4-14 was applied for 4 to 120 hours, the equation from Figure 4-15 was applied from 120 to 170 hours, and the equation from Figure 4-16 was applied for the remainder of the release (170 to 470 hours).

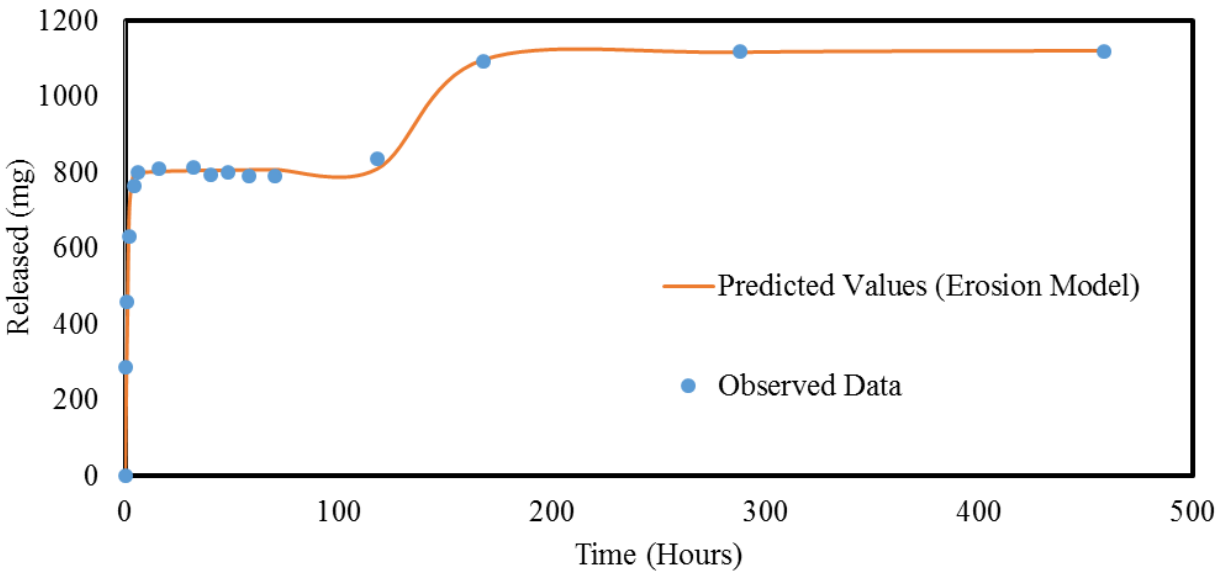

Figure 4-17: PVA/SPI/Keto loaded Sepiolite, observed data plotted in overlay versus predicted values based on erosion model

The diffusion model was also applied to the three formulations, the diffusion model or Equation 4.2 was applied to the formulations of PVA/SPI/Keto, PVA/SPI/Keto loaded Sepiolite and PVA/SPI/Keto mixed Sepiolite. Due to the conditions set forth by Peppas, the diffusion model was applied for approximately 60% of the release, after which curve fitting was utilized for prediction of values after which diffusion model was applicable. If observed data allowed further implementation of diffusion model to release rate percentages above 60%, it was implemented. The first formulation investigated was that of PVA/SPI/Keto (see Figure 4-9 for nanofiber schematic), Figure 4-18 shows the calculated k values based on the observed experimental data and Equation 4.2 for PVA/SPI/Keto.

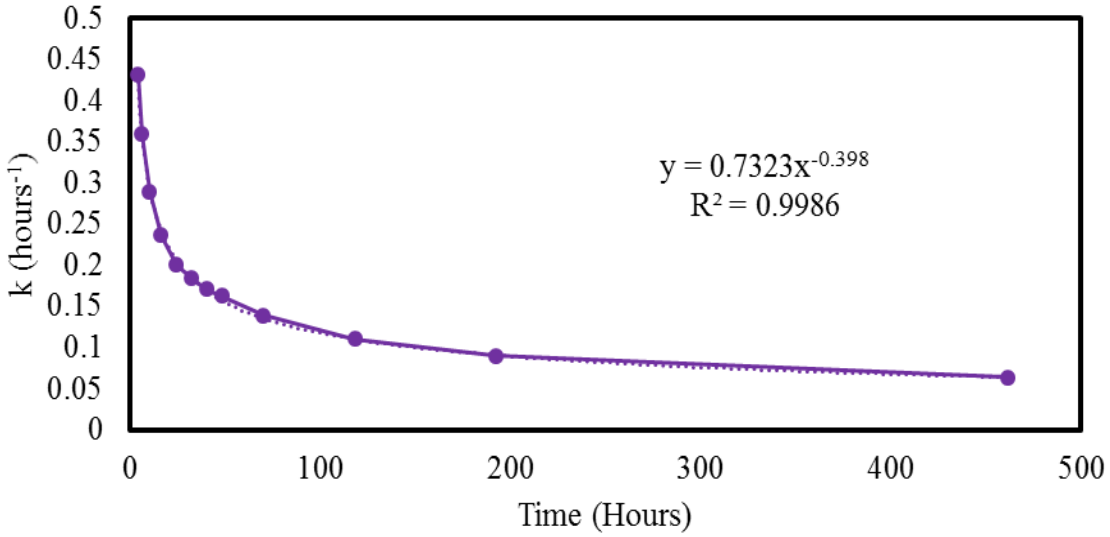

Figure 4-18: PVA/SPI/Keto determined k values from diffusion model

The diffusion model was applied at the time interval from 0 to 4 hours, at 4 hours PVA/SPI/Keto displayed on average 84.7% release, from there the curve fit equation determined from Figure 4-18 was applied. As mentioned typically diffusion models are only used for the initial 60% of the release, however in this case the model applied to over 84% percent of the drug release for this particular formulation. An overlay of the predicted values versus the observed data for PVA/SPI/Keto using the diffusion model with k=4.5 is shown in Figure 4-19.

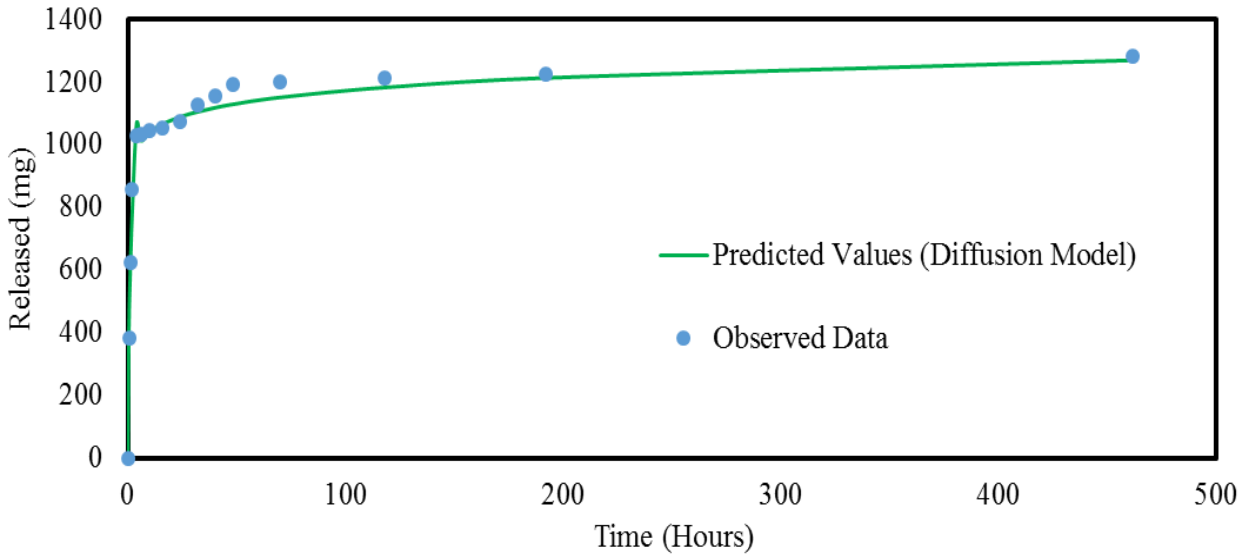

Figure 4-19: PVA/SPI/Keto, observed data plotted in overlay versus predicted values based on diffusion model

PVA/SPI/Keto mixed Sepiolite (see Figure 4-9 for nanofiber schematic), was also modeled by the diffusion Equation 4.2. Figure 4-20 shows the calculated k values based on the observed experimental data and Equation 4.2. Due to the nature of the data observed, the diffusion model was applied from 0 to 6 hours, resulting in a k value of k=4.8. After 6 hours, the equation from Figure 4-20 was implemented. An overlay of the predicted values versus the observed data for PVA/SPI/Keto mixed Sepiolite using the diffusion model with k=4.8 is shown in Figure 4-21.

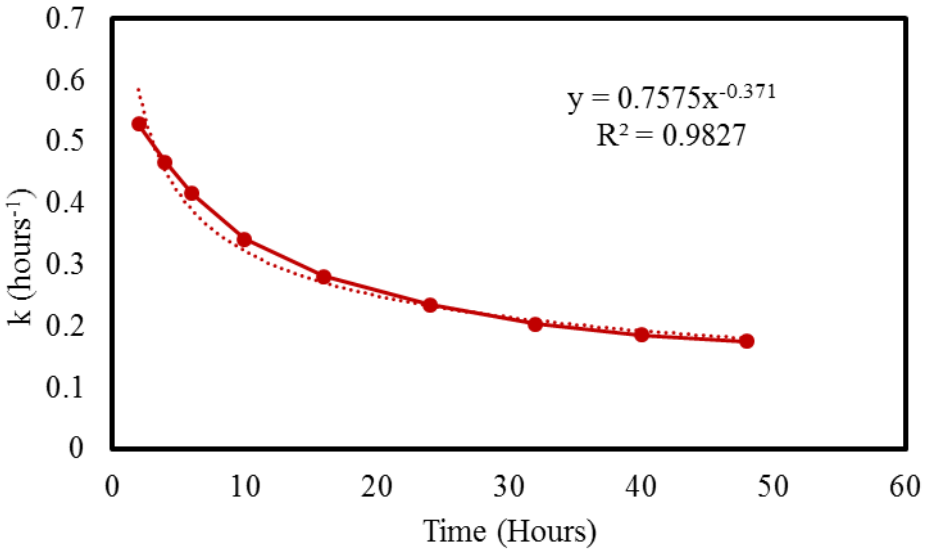

Figure 4-20: PVA/SPI/Keto mixed Sepiolite determined k values from diffusion model

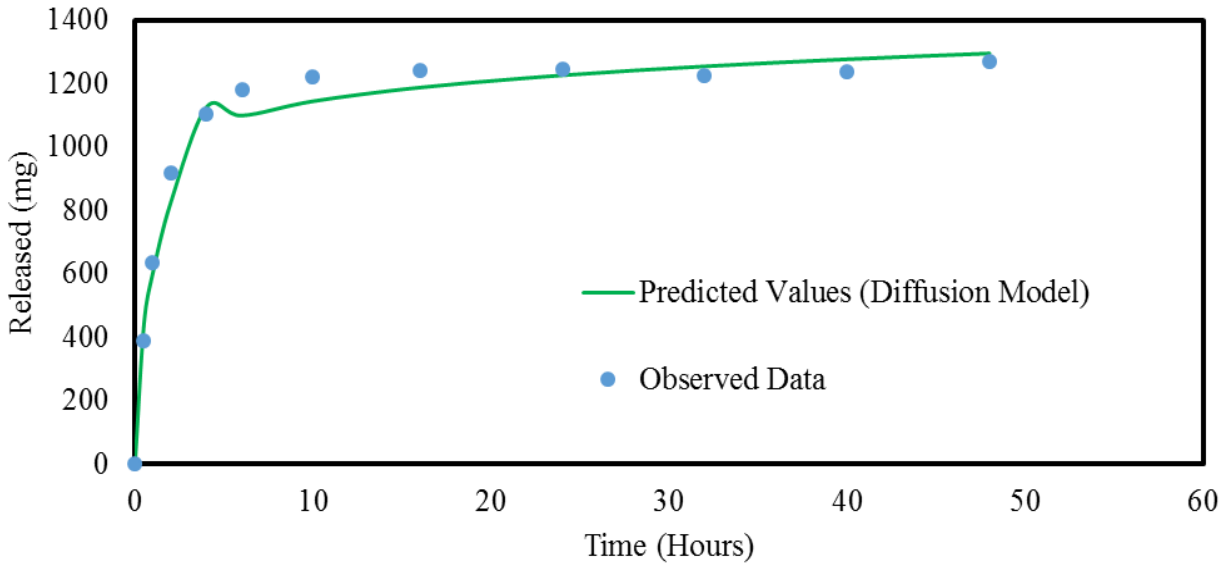

Figure 4-21: PVA/SPI/Keto mixed Sepiolite, observed data plotted in overlay versus predicted values based on diffusion model

Lastly, the diffusion model was applied to PVA/SPI/Keto loaded Sepiolite (see Figure 4-9). Since this nanofiber incoroated the loading of the nanoparticle sepiolite, the release

happened in an almost two stage effect, for this reason the release constant k was modeled at three diffetent time intervals as shown in Figure 4-22, Figure 4-23, and Figure 4-24.

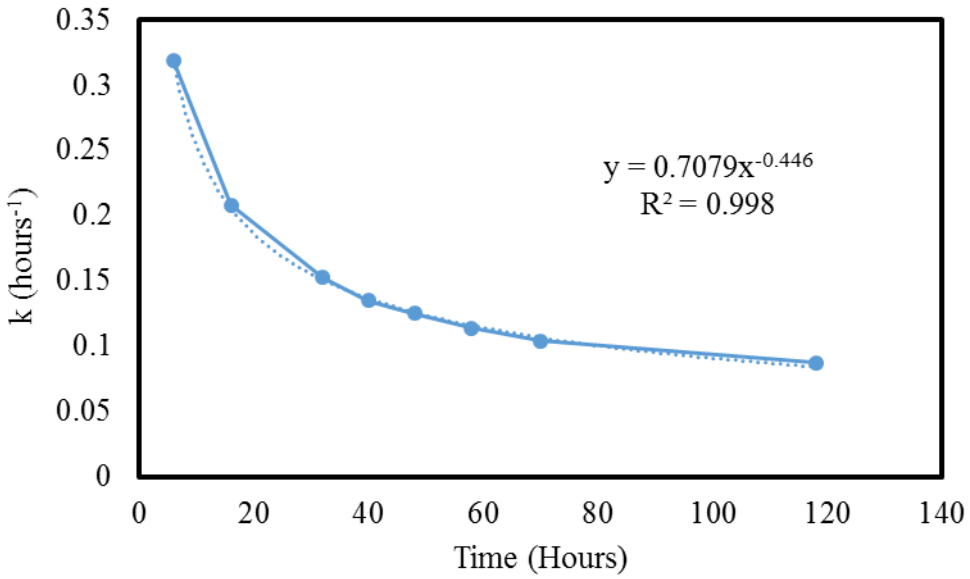

Figure 4-22: PVA/SPI/Keto loaded Sepiolite determined k values from diffusion model, from 0 < t < 120 hours

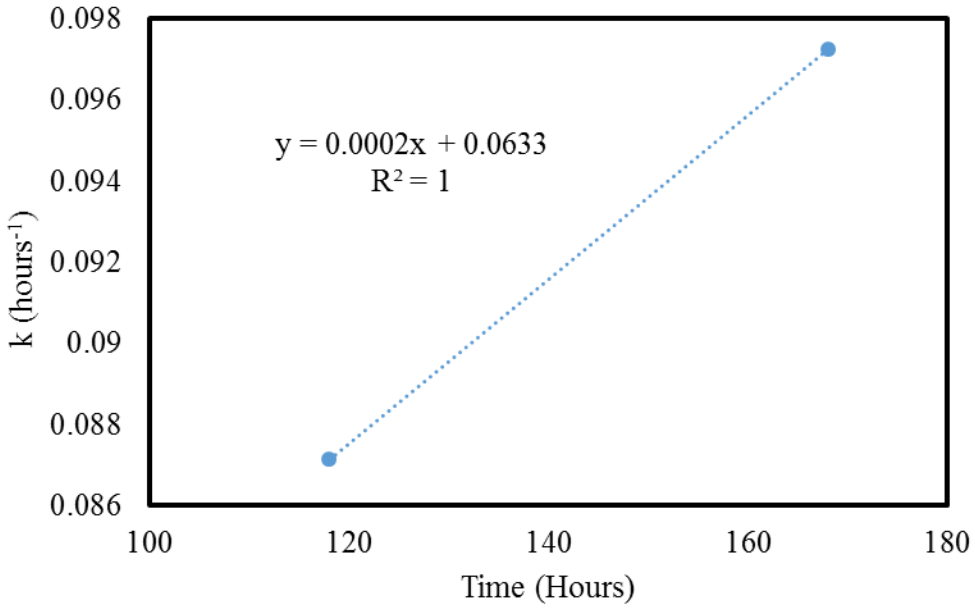

Figure 4-23: PVA/SPI/Keto loaded Sepiolite determined k values from diffusion model, from 120 < t < 170 hours

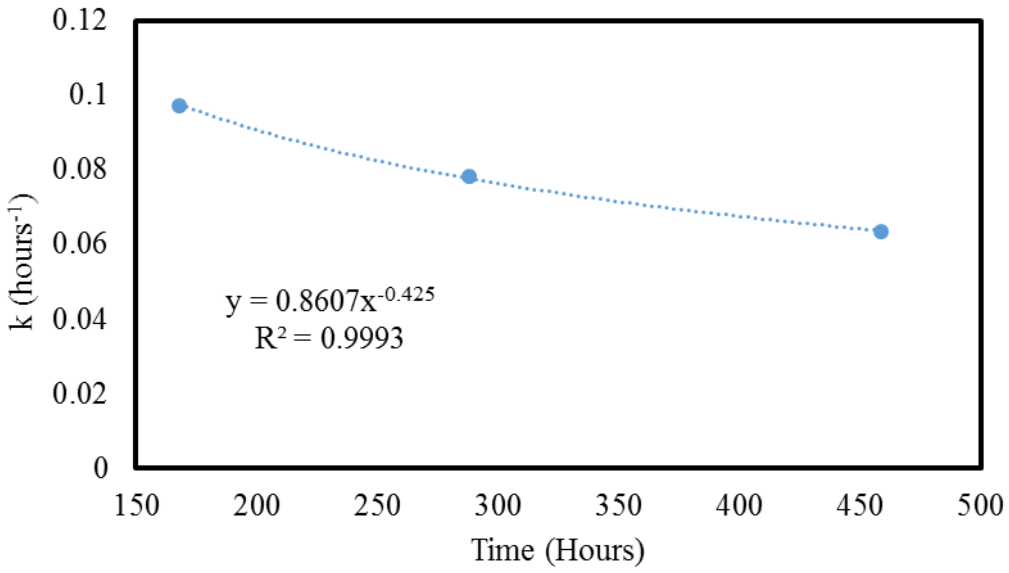

Figure 4-24: PVA/SPI/Keto loaded Sepiolite determined k values from diffusion model, from 170 < t < 470 hours

In the case of the PVA/SPI/Keto loaded Sepiolite, the diffusion model was applied at the time interval from 0 to 4 hours, at 4 hours PVA/SPI/Keto loaded Sepiolite displayed on average 60.7% release, from there the curve fit equations determined from the appropriate time interval were applied. An overlay of the predicted values versus the observed data for PVA/SPI/Keto loaded Sepiolite using the diffusion model with k=3.9 is shown in Figure 4-25.

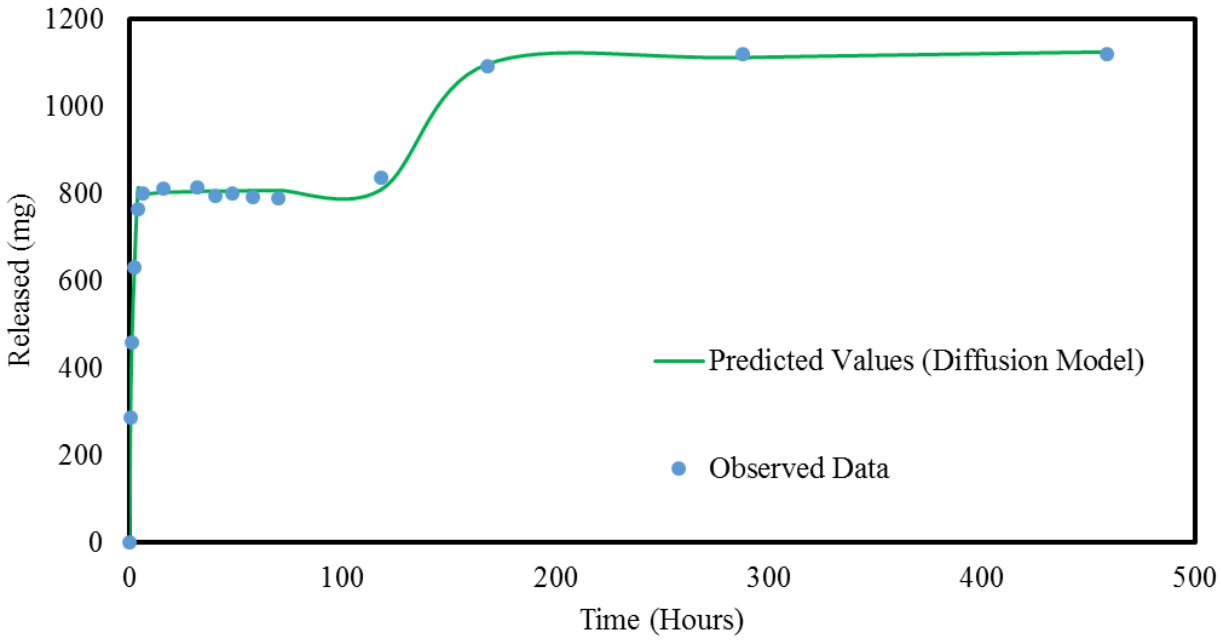

Figure 4-25: PVA/SPI/Keto loaded Sepiolite, observed data plotted in overlay versus predicted values based on diffusion model

In summary, both mathematical models provided numerical constant release values (k_o and k) for the initial stages of release. These release constant values were compiled and displayed in Table 4-4. Both models showed the nanofibers that contained the loaded nanoparticle sepiolite displayed the most sustained release, this takes into account the smaller diameter of nanofibers included in the erosion model. For this reason it is clear the loading of nanoparticle is primary reason for delayed release when compared to the other formulations.

Table 4-4: Summary of rate constants from both erosion and diffusion models

	PVA/SPI/Keto	PVA/SPI/Keto mixed Sepiolite	PVA/SPI/Keto loaded Sepiolite
Erosion Model (k_o)	18.4	18.7	11.8
Diffusion Model (k)	4.4	4.8	3.9

Also to be noted in Table 4-4, is the slightly higher rate constant values for nanofibers containing ketoprofen and sepiolite mixed together versus ketoprofen alone, the reason for this is as discussed earlier. The implantation of the nanoparticle alone with no pre-loading actually

increases release rate as the nanoparticle occupies a large volume inside the fiber. This forces the drug more near the surface of the nanofibers making it more readily available for release.

For initial experimental results, it was found the a 1:1 ratio of SPI/PVA was optimal for drug release studies based on the mechanical testing conducted in section 4.1. The technique used for loading the nanoparticle resulted in 49% efficiency and had a substantial effect on the delaying of release rate in the in-vitro testing. Nanofibers containing the drug loaded sepiolite showed a release rate percentage of 67% at 70 hours while other formulations exhibited over 90% released at the same corresponding time. Mathematical modeling taking fiber diameter into account verified these findings.

5. INTRODUCTION OF SILVER ACETATE AND BACTERIAL KILLING EFFECTS

Soy based nanofibers have been proven to be a viable vehicle for controlled drug release as shown in previous results. The following section demonstrates their versatility by utilizing the nanofibers for delivery of the antibacterial substance silver acetate. The results showed the soy based nanofibers successfully delivered the silver acetate in the concentrations tested. The silver acetate was tested against DH5-alpha E. Coli in petri dishes.

5.1. Implementation of silver acetate into nanofiber composition

To incorporate the bacteria killing silver acetate into the soy based nanofibers, a 70/30 composition of PVA to SPI was chosen due their superior mechanical properties. Fibers were prepared in a similar fashion as previous where PVA solution was prepared by combining 0.5% wt. Triton X-100 and 14% weight PVA in an aqueous solution and allowing said solution to mix for 4 hours at 95° C with a magnetic stirrer. SPI solution was prepared by combing 6.3% weight SPI powder in an aqueous solution, and allowing it to mix for 10 minutes at room temperature. Then the pH of the SPI solution was adjusted to 11 by adding Sodium Hydroxide (NaOH) pellets at room temperature. SPI solution was then mixed 30 minutes at 80° C. PVA and SPI solutions were combined at the determined 70 wt. % PVA to 30 wt. % SPI ratio, and then mixed for 45 minutes at 60° C. The next step involved adding the silver acetate, note that silver acetate is photosensitive, care was taken so that the samples were then not exposed to direct light. Silver acetate powder was added in four different concentrations, 0%Ag (Control), 0.5%Ag, 1%Ag, and 1.5%Ag. These percentages were of the total solid weight including the PVA, SPI, and Ag. From there, samples were mixed 30 minutes at room temperature and then homogenized for 5

minutes with a mechanical shear homogenizer at 3200 rpm to ensure Ag dispersion. Samples were then ready for electrospinning.

The electrospinning setup consisted of a horizontally mounted syringe with a circular rotating collecting plate which measured 350 mm in diameter. Ambient conditions were used to carry out the electrospinning. The collector plate used in the experiments was rotating at a slow speed (56 rpm) to ensure fibrous mat had even dispersion of randomly oriented fibers. Formulations were electrospun to achieve continuous beadless fibers. The formulations were loaded into a 10 mL disposable syringe that dispersed the solution through a 22 gauge, 1" long needle. The solution was fed at the determined feed rate by a Fisher Scientific model no. 78-0100I syringe pump at a rate of 1.5mL/hour. Gap distance was maintained at 27 cm with a positive and negative voltage applied of 17 kv and 1.5 kv respectively. Samples were spun 11 hours and then dried before bacterial killing ability tests were performed.

To test the bacteria killing effectiveness of the varying percent Ag acetate nanofibers samples, round. 12.7 mm disks were punch out of nanofibers mats for analysis. To test the Ag samples, petri dishes we used with Luria-Bertani (LB) Medium and DH5-Aplha E. Coli. Petri dishes were prepared by first preparing the LB medium. Initially, 2.5g Bacto-Tryptone, 1.25g Bacto-Yeast Extract, 2.5g NaCl, and 250 mL distilled water were mixed for ten minutes at room temperature; adjusting the pH to 7.5. Following the mixing, 3.75g Agar was added to the solution for solidification. Solution was the autoclaved for 20 minutes at 121°C and 15 psi, a 20 minute ramp to reach 121°C was used. Upon removal from autoclave, solution was stirred fifteen minutes and the poured into petri dishes so that full surface area coverage occurred. Solution was allowed to solidify an additional fifteen minutes and was then placed in the fridge.

Next, 100 µL of DH5-Alpha was mixed with 900 µL of LB medium in liquid form inside of a capsule. This capsule was then subjected to vigorous mixing before removing 100 µL and applying it on the center of the previously prepared LB medium petri dish. The E. Coli containing solution was then spread until it covered the area of the petri dish, the circular section of nanofibers containing Ag acetate was then placed in the center of the dish, see Figure 5-1. The petri dish containing the sample was placed in an oven at 29°C to allow for bacteria growth. Note that four total petri dishes were used for the following samples, one petri dish per sample, respectively; 0% Ag (Control), 0.5% Ag, 1% Ag, and 1.5% Ag.

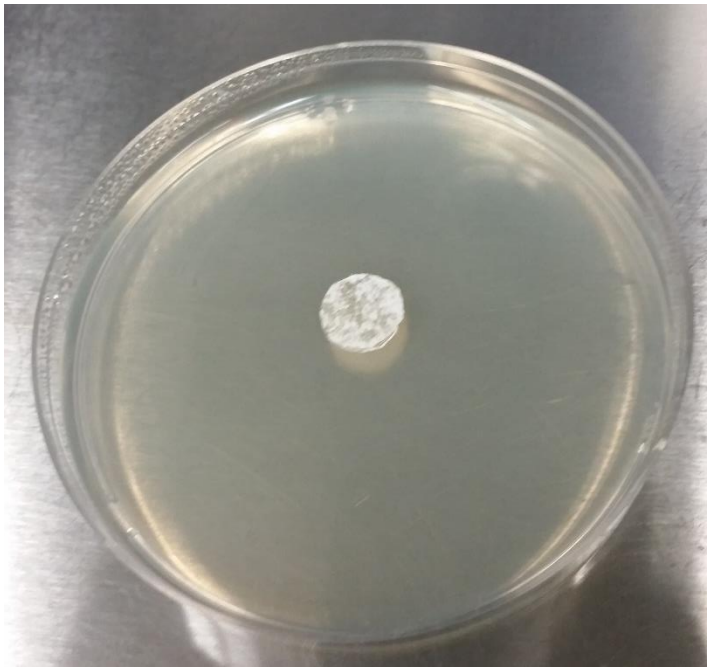

Figure 5-1: Image of nanofibers containing Ag acetate immediately after being placed in DH5-Alpha E. Coli (0 hours)

5.2. Bacterial killing effect results and discussion

The samples were monitored and the bacteria growth was observed. First documentation of growth was recorded at the 48 hour mark. While results could be observed already after 24

hours, the 48 hour images documented the growth more distinctly. Shown in Figure 5-2 are images of the four Ag acetate nanofibers samples after 48 hours.

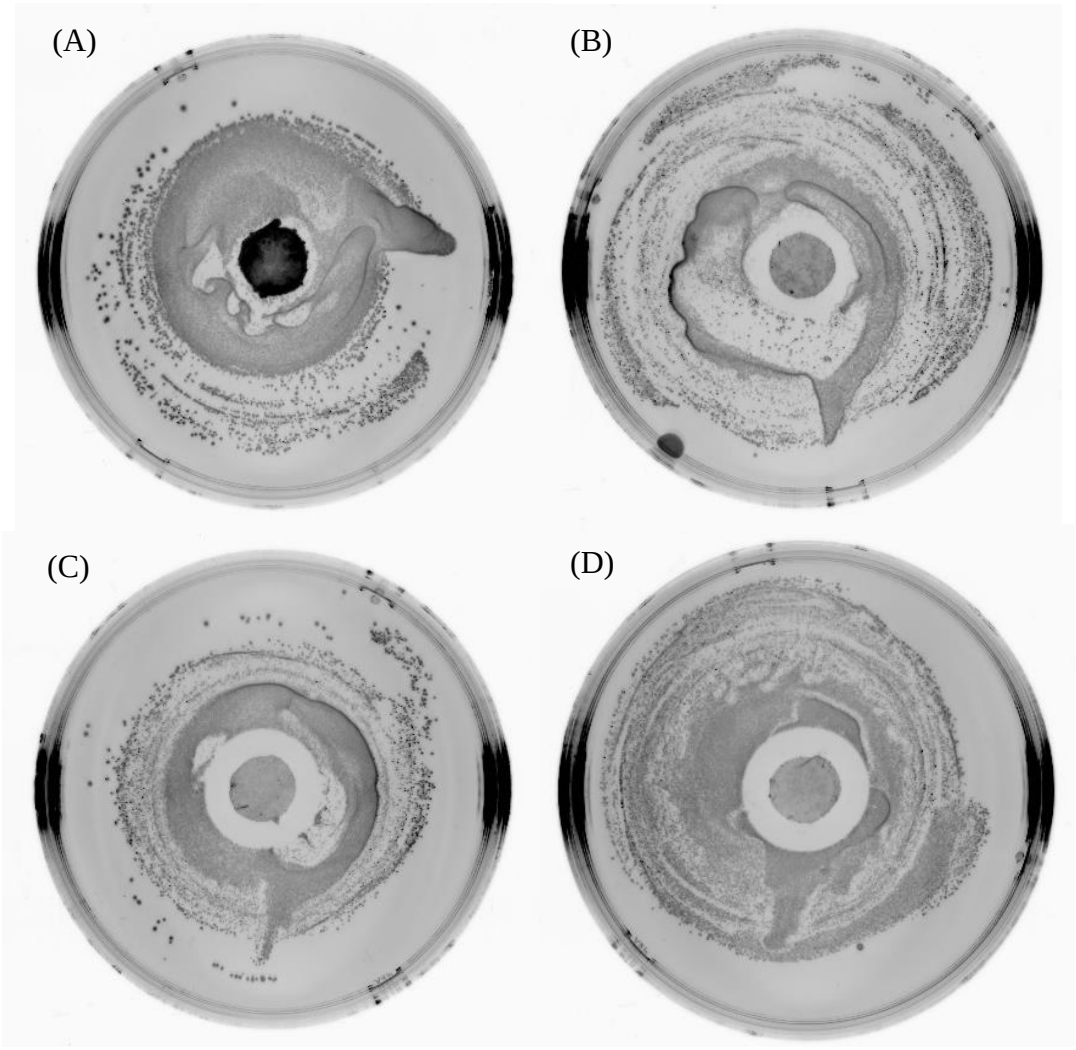

Figure 5-2: SPI based nanofibers containing Ag after 48 hours. (A) 0% Ag, (B) 0.5% Ag, (C) 1% Ag, (D) 1.5% Ag

As can be seen in Figure 5-2, clear antibacterial behavior can be seen in the 0.5% Ag, 1% Ag, and 1.5% Ag when compared to the (A) 0% Ag sample. It is visibly clear that the 1% and 1.5% have a larger kill zone (area where no E. Coli growth is present) than that of the 0.5 % Ag sample. This is to be expected as the increasing concentration of Ag should result in a larger

area of inhibited E. Coli growth. Samples continued to be monitored but results were consistent with those observed at the 48 hour mark, in Figure 5-3 are images captured at 88 hours.

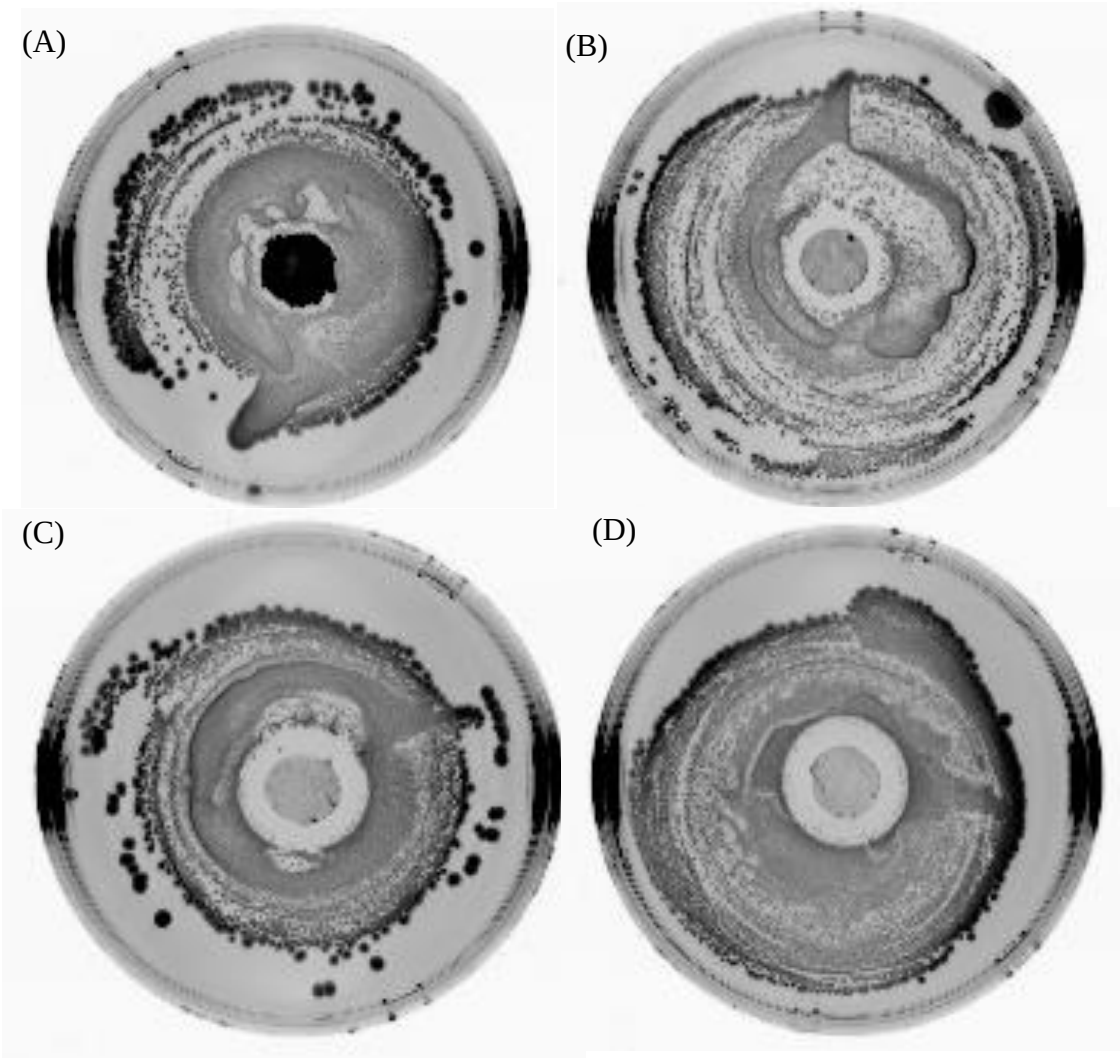

Figure 5-3: SPI based nanofibers containing Ag after 88 hours. (A) 0% Ag, (B) 0.5% Ag, (C) 1% Ag, (D) 1.5% Ag

In the images it is difficult to see the e-coli growth on the 0% Ag or "control" sample, for that reason images in color were taken to see the clear effect of the Ag acetate. The images are shown in Figure 5-4. In Figure 5-4, the control sample containing no contents of Ag acetate is shown on the bottom of each image (A), (B), and (C) respectively. The control sample is then compared to the 0.5% Ag, 1.0% Ag and 1.5% Ag samples in (A), (B) and (C); respectively. The

more “white” color of the control or 0% Ag sample in the three images denotes E. Coli growth as initially all samples looked like the image from Figure 5-1. The images captured in Figure 5-4 were taken after 88 hours of exposure to the E. Coli.

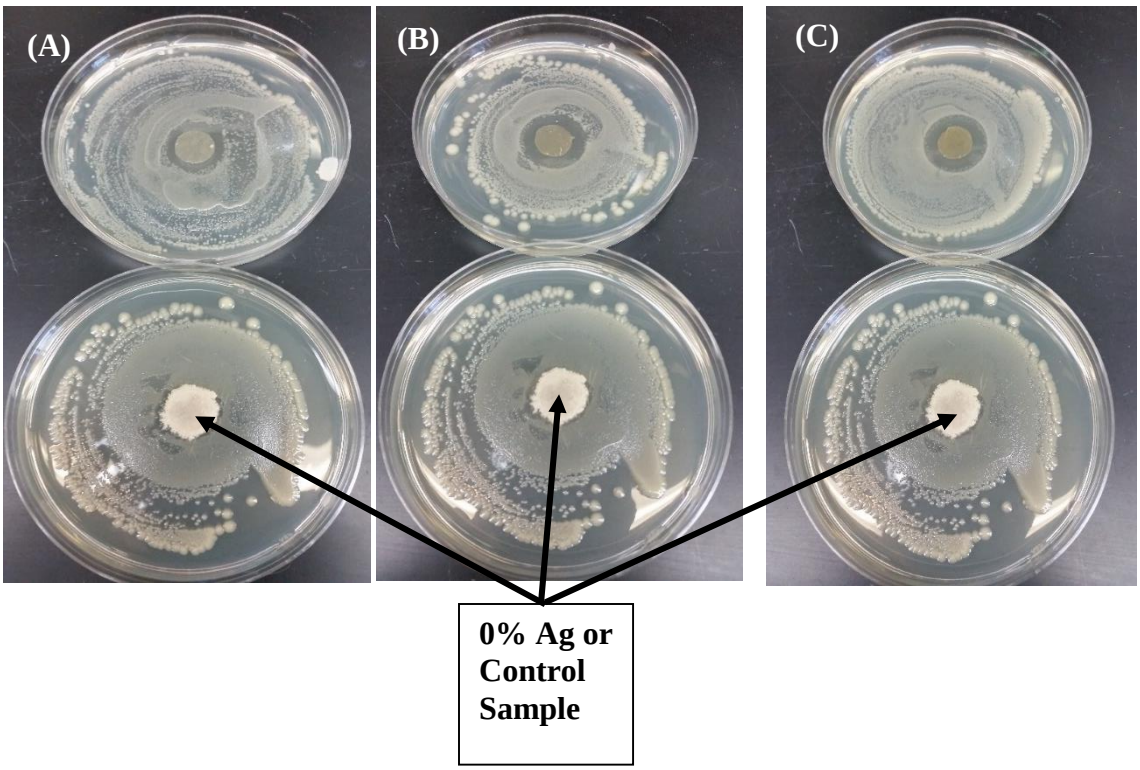

Figure 5-4: Captured images showing: (A) 0% Ag vs. 0.5% Ag, (B) 0% Ag vs. 1.0% Ag, and (C) 0% Ag vs. 1.5% Ag

In order to quantify the effects of the Ag acetate, a plot was made to measure the width of inhibition zone of the individual samples. The initially cut nanofibers samples were 12.7 mm in diameter which translates into a radius of 6.35 mm. The width of inhibition zone was measured from edge of the samples and is plotted in Figure 5-5. As the concentration of Ag acetate increased in the nanofibers, so did the width of inhibition zone in which antibacterial activity was observed. Twenty measurements were taken for each sample, and the distances were measured from the edge of the sample to the first encountered growing e-coli. Note that for the 0% Ag

sample, while there appears to be a small ring of no E. Coli, when magnification is applied small patches of E. Coli are growing. This is again observed more clearly in Figure 5-4 than as seen in Figure 5-2 and Figure 5-3.

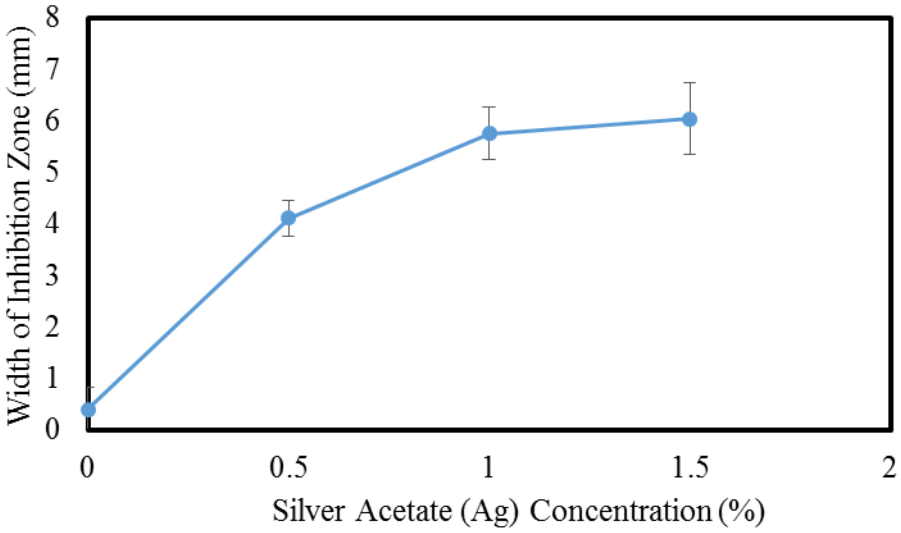

Figure 5-5: Plot of width of inhibition zone of tested Ag acetate nanofiber samples

Overall, implementation of Ag acetate in the soy based nanofibers for antibacterial activity was successful with the methods used. Specifically, using traditional electrospinning techniques with 30wt% SPI resulted in nanofibrous mats that displayed varying amounts of bacterial killing ability based on their concentration of silver acetate.

6. INVESTIGATION INTO MASS PRODUCTION OF SOY BASED NANOFIBERS

In the previous works of this study, soy based nanofibers have been shown to have success both as a vehicle for controlled drug delivery and for delivery of the antibacterial substance silver acetate. This testing was all done in a research setting by means of classical electrospinning. In order to make the next step for industrialization, mass production of the nanofibers had to be accomplished. The design and fabrication of a needleless electrospinning machine was accomplished and described in the next section. Results are presented along with future recommendations.

6.1. Design/testing of needleless electrospinning machine

The objective to investigate and produce means for mass production of soy based nanofibers brought about the fabrication of a needleless electrospinning machine. A needleless electrospinning machine functions much like a classical electrospinning set up except for the fact that a single needle is replaced with a mechanism so that a higher volume of fibers can be produced. Producing a higher volume of nanofibers is the primary reason for development of the needleless electrospinning machine. This project was initially started by Dr. Xiangfa Wu and his senior design group; however, myself under the guidance of Dr. Long Jiang as well as Dr. Xiangfa Wu undertook the completion of the needleless electrospinning machine. A few critical design criteria was needed for successful achievement; firstly, the collection system for collecting the nanofibers had to be completely automated. Secondly, the machine had to be fully adjustable so that it could accommodate a variety of soy based polymeric solutions. A schematic of the proposed initial design is shown in Figure 6-1.

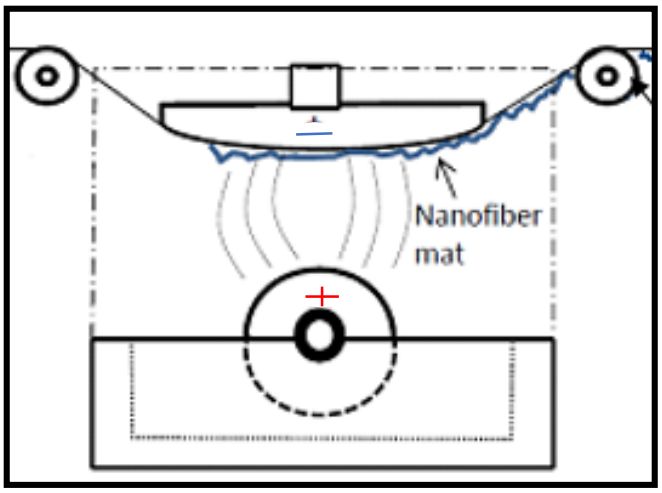

Figure 6-1: Proposed initial design of needleless electrospinning machine

Essentially, instead of dispersing the solution through a syringe and syringe pump as done with classical electrospinning techniques, this design instead utilized a drum partially submerged in the desired soy based solution; similar to the study by Kostakova (Kostakova, et al., 2009). The drum is subjected to a positive applied voltage and is located directly underneath a collecting plate subjected to a slightly negative potential. With the voltages applied, the electro-conductive solution "jumps" across the gap between the submerged drum and the collecting plate to create nanofibers. In the design, the fibers never actually reach the collecting plate; which is where they want to go from a physics standpoint. Instead the fibers are intercepted and collected on a substrate that is being slowly conveyed underneath the collecting plate, see Figure 6-1. This substrate is then collected by a mechanically driven roller.

An immediate challenge that was encountered on the design was controlling the "feed rate" of the material; this would be similar to the rate at which the syringe disperses solution in classical electrospinning. Due to the nature of the rotating drum, the feed rate for the solution is difficult to control; therefore it is addressed from the fiber collection standpoint; which is directly related to the velocity at which the substrate moves. In order to precisely control the rate at

which the substrate moves, a variable speed controller was utilized along the an electric motor geared down at a 71:1 ratio so that rotation of output shaft was at a minimum. To further gear down the rotation speed of the collection roller, a pulley system was used. The pulley further reduced the ratio 10:1, the pulleys used needed to be lightweight and non-conductive due to the nature of the high voltage so the pulleys were 3-D printed from (Acrylonitrile Butadiene Styrene) ABS plastic. Images of the components of the automated substrate collection system are shown in Figure 6-2.

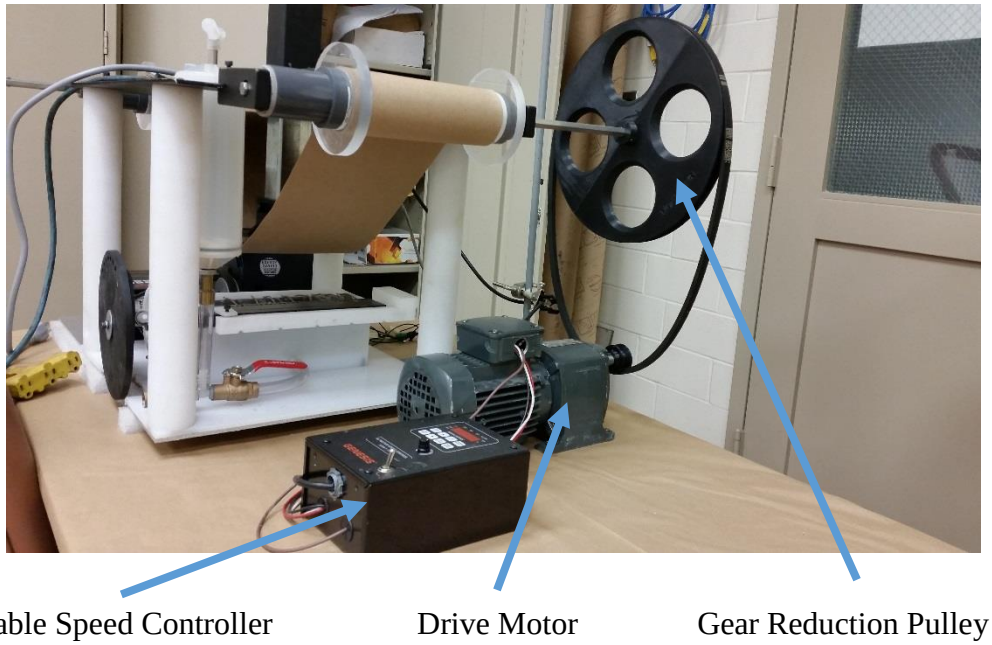

Figure 6-2: Automated collection system for needleless electrospinning machine

Implementing the variable speed controller along with the easily exchangeable pulleys give the needleless electrospinning machine unlimited flexibility to accommodate any soy based solutions desired. The variable speed controller restricts the operational output of the electric motor on a 0 to 100% output basis, due to the extremely low load on the motor; it easily turns the collector roller even at less than 1% output.

The collector plate utilized in the design was specially 3-D printed out of the material ABS for both its low density and low electrical conductivity properties. The collecting plate in the working machine was covered with a negatively charged conductive foil so it was critical for the actual plate to be non-conductive so that no current jumped to other metal components of the machine. Also, the collecting plate required a convex nature so that fibers would constantly be applied at the same location of substrate. In Figure 6-3 is a computer generated image of the collector plate that was 3-D printed and implemented on the device.

Figure 6-3: Collecting plate used on needleless electrospinning machine

In section FEM verification for needleless electrospinning machine design, FEM analysis was conducted to determine the maximum weight that could be supported for the adjustable collecting plate assembly. Results found that a 40 lb force could be supported with less than 0.01 inches deflection and no occurance of yeilding; findings were confirmed with use of coarse, intermediate and fine meshes. A factor of safety of over 4 was exersiced. Upon verfifcation from FEM, that the wieght of collectin plate and translation mechanism would not casue any significant defelection, the machine was ready for testing. To test the needleless

electrospinning machine; PVA solution was prepared by combining 0.5% wt. Triton X-100 and 14% weight PVA in an aqueous solution and allowing said solution to mix for 4 hours at 95° C with a magnetic stirrer. SPI solution was prepared by combing 6.3% weight SPI powder in an aqueous solution, and allowing it to mix for 10 minutes at room temperature. Then the pH of the SPI solution was adjusted to 11 by adding Sodium Hydroxide (NaOH) pellets at room temperature. SPI solution was then mixed 30 minutes at 80° C. PVA and SPI solutions were combined at the desired ratio of weight based on the formulation being mixed; in this case that ratio that was 7:3, PVA to SPI respectively. New combined solution was then mixed for 45 minutes at 60° C and was then ready for needleless electrospinning.

6.2. Results and discussion of mass produced nanofibers

Initially attempts at electrospinning the PVA/SPI solution were un-successful as the solution would not jump the distance from the rotating drum to the collecting plate. By conducting trial and error experimentation, it was found that disruption of the PVA/SPI solution led to much better fiber production. For this reason, a surface disruption device was designed and fabricated. The device utilized the rotational motion already being applied to the submerged drum and converted it into linear motion by way of a rotating cam. The initial design called for the cam to be made out of steel because of the readily available material. The fabricated cam is shown in Figure 6-4.

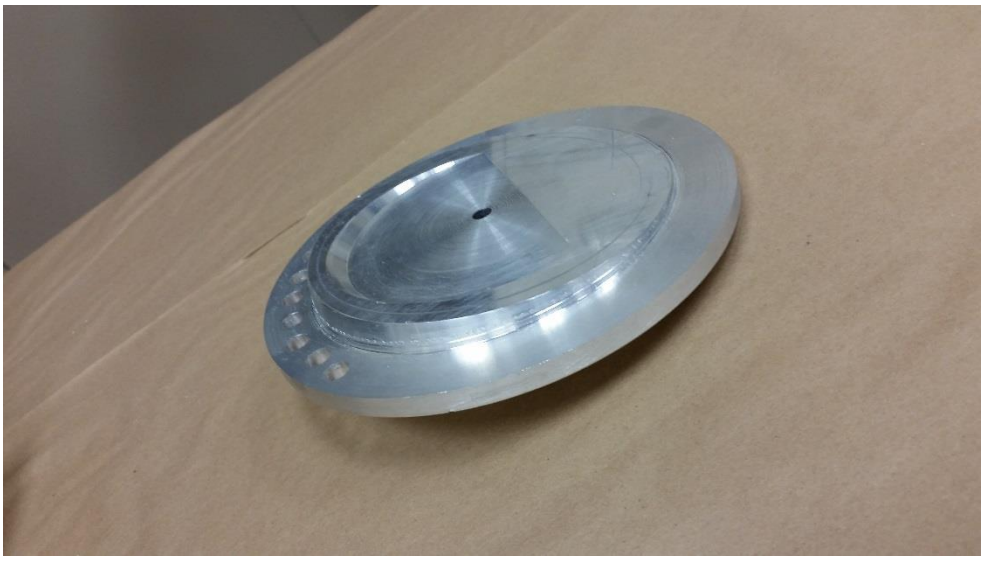

Figure 6-4: Initially designed cam, fabricated from steel

While the geometry of the cam worked out nicely, the material choice was not acceptable as it caused issues due the electorally conductive nature of the steel. Instead, 3-D printed ABS was again utilized and in Figure 6-5 are images of the computer generated (A) and actual model (B), respectively.

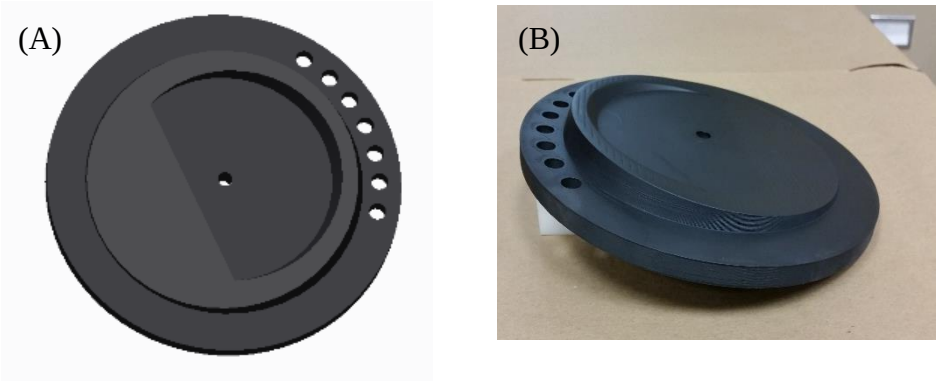

Figure 6-5: Needleless electrospinning cam; (A) computer generated model, (B) actual part via 3-D printing

The cam played an essential role in driving the surface disruption device which was made from copper wires that ran across the drum of the needleless electrospinning machine. As the

cam rotates, it drives the copper wires back and forth across the rotating drum. In Figure 6-6 is an image of the surface disruption device.

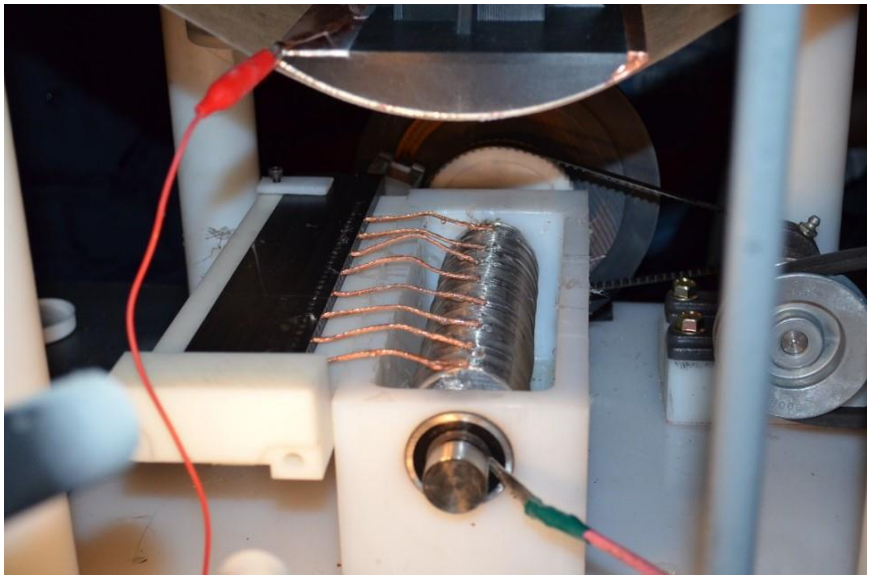

Figure 6-6: The copper wires represent the surface disruption mechanism used to increase volume of nanofiber production

A few other observations that can be noted from Figure 6-6 are the two red wires attached to the rotating drum and to the collecting plate. The top wire is attached to a piece of highly electrically conductive foil that is adhered to the bottom of the collecting plate. This allows the negative voltage to be applied, and in turn allows fibers to be collected onto the substrate. The lower red wire with the green tape is attached to the rotating drum that is partially submerged in the PVA/SPI solution. The wire carries a positive potential of nearly 35 kV which is applied to the drum and in turn to the solution. With both of the voltages being applied, soy based nanofibers can be mass produced successfully as shown in Figure 6-7. Note how the fibers seem to be jumping from the drum right onto the substrate, this demonstrates successful completion of the objective.

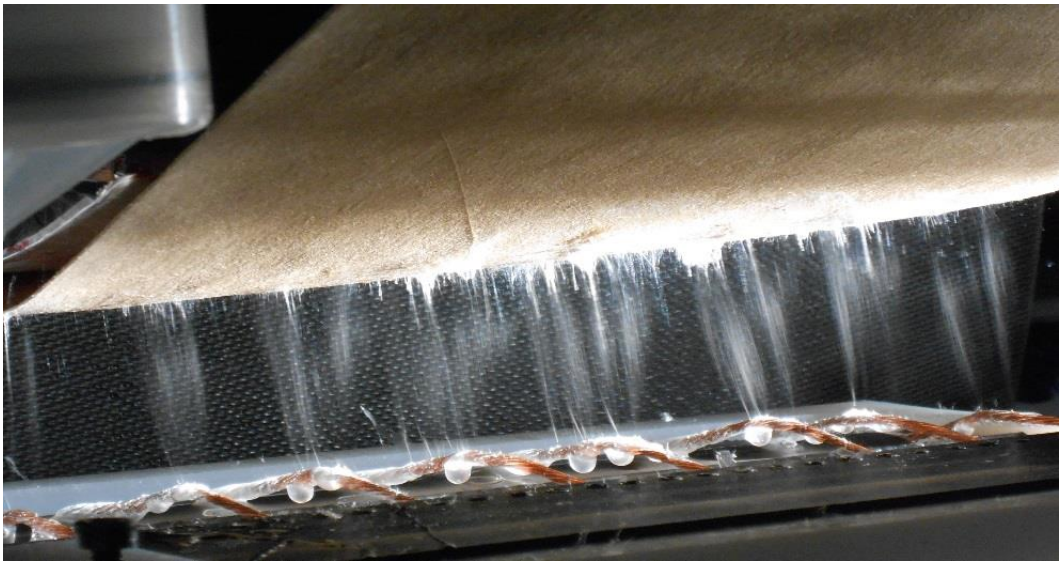

Figure 6-7: Mass production of soy based nanofibers using needleless electrospinning

To verify the formation of nanofibers, SEM analysis was used to observe the morphology of the fibers. Two images captured are shown in Figure 6-8, which displays 30 wt.% SPI/ 70 wt.% PVA nanofibers, image (A) represents 25,000x magnification while image (A') shows a magnification of 40,000x. Conditions for the needleless electrospinning included a positive potential voltage of 35,000 volts being applied to the rotating drum, a negative potential voltage of 2,000 volts being applied to the conductive foil on the collecting plate. The drum rotated at a speed of 75 rpms, while the automated substrate collection system moved the substrate at a rate of 3 mm/second. The nanofibers produced from the needleless electrospinning were not as uniform as the nanofibers formed from the classical electrospinning technique. The primary reason for this is suggested to be the small gap (8 cm) that was used when compared to the 30 cm gap used in the classical set up. Due to the small gap, the fibers were not allowed to elongate to their full potential. The limiting factor for the gap in the fabricated electrospinning machine is due to the low cost of the machine. Due to the budget restraints, certain components of the

machine were fabricated from left over steel material; this in turn resulted in limitation of the voltage that could be applied; finally resulting in limitation of gap distance.

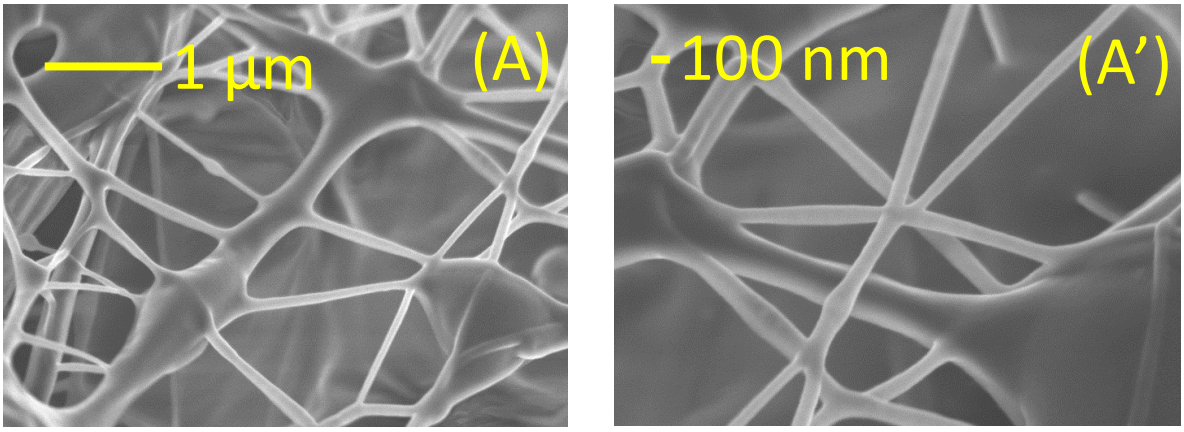

Figure 6-8: SEM images of needleless electrospun soy based nanofibers, (A) and (A') represent 25,000x and 40,000x magnification, respectively

From a fiber production standpoint, the needleless electrospinning design used in this study showed the formation of approximately 20 jets of solution protruding from the drum. When this is compared to the single jet seen in classical electrospinning, fiber production is increased substantially. Since design and fabrication were the main components addressed in this research, overall production rate was left for a future study. For a simple approximation, the 20 jets formed in the needleless process compared to the single jet used in classical electrospinning suggests an increase of 2000% in fiber volume. In addressing the nanofibers characteristics mentioned previously, to improve morphology of fibers the parameters of needleless electrospinning could be further optimized for spinning the soy based solution. As well as constructing the complete machine from low electrical conductive materials to allow a broader range of applied voltage. An overall completed image of the needleless electrospinning machine is shown in Figure 6-9. All of the design constraints proposed were successfully accomplished in the design and fabrication of this machine.

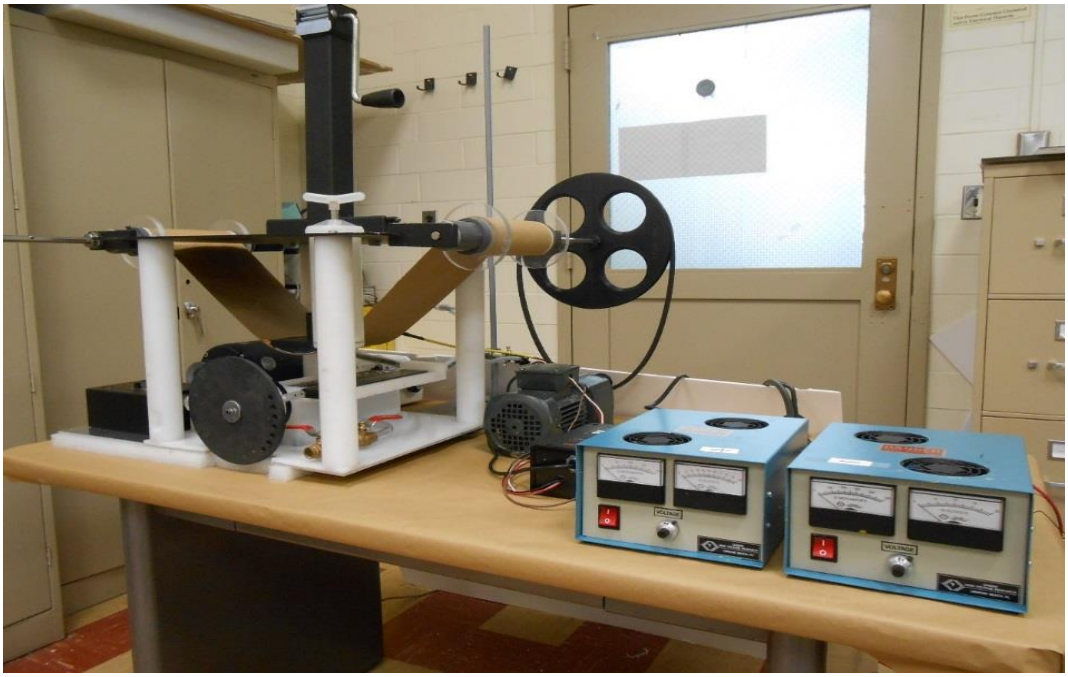

Figure 6-9: Image of completed needleless electrospinning machine

The most challenging obstacle overcome was the design and implementation of the automated substrate collection system. However, this was successfully accomplished along with making the machine fully adjustable to accommodate a variety of soy based solutions. The key adjustable components include a rack a pinion device to move the collecting plate vertically to accommodate the different gap distances required based on the solution. Both power sources allowed complete control of voltages applied (both positive and negative). The rotating drum was driven by an electric motor controlled by a variable speed controller much like the automated collection system to allow for full adjustability. The adjustable parameters along with the previously discussed automated substrate collection system allow for a fully adjustable needleless electrospinning machine capable of spinning a variety of soy based solutions.

7. CONCLUSIONS AND FUTURE WORK

7.1. Conclusions

The scope of this study ultimately centered on utilizing soy based material for a purpose that benefits the economy, local market, and material development. Four objectives were defined at the beginning of this research and are listed as follows:

1. Optimize the soy protein isolate content in nanofibers, then in turn use these nanofibers for successful delivery of a pharmaceutical product
2. Introduce a method of loading a nanoparticle for further controlled and sustained release
3. Develop the incorporation of silver acetate into nanofibers for antibacterial effects
4. Investigate and produce means for mass production of soy based nanofibers

The optimization of soy content consisted of trying various weight percentages of SPI and PVA to determine what resulted in the most desirable mechanical properties. While 30wt% SPI resulted in the best mechanical properties, 50wt% SPI was chosen for the controlled drug delivery studies due to the incorporation of more SPI as well as the ability to closely match the mechanical properties of pure PVA nanofibers. Based on the mechanical testing results, nanofibers for drug delivery were formed at a 1:1 weight ratio of SPI to PVA. These SPI based nanofibers were then exposed to in-vitro testing for measurement of their release profiles. The drug chosen for the study was ketoprofen due to its UV characteristics as well as its stability in basic solutions.

For further control of the release profile of said drug, the nanoparticle sepiolite was introduced and loaded with the drug prior to electrospinning. The loading technique used in this study resulted in a loading efficiency of 49%, 49% of the drug initially combined with the nanoparticle sepiolite became “loaded” onto the drug. This was determined from TGA analysis

that showed samples of ketoprofen loaded sepiolite were 33wt% ketoprofen after the loading process (initially combined at a 1:1 weight ratio). The effect of this loading was seen in the release profiles of three different formulations of nanofibers. The nanofibers containing the loaded sepiolite showed the most sustained release profile; at a time of 70 hours, the nanofibers containing loaded sepiolite only showed ~67% of the drug released, while the two other formulations both displayed release percentages of over 90%. By the observed experimental data, the loaded sepiolite had a substantial effect on delivery rate; and the potential to be used as a tool to tailor release rate to accommodate specific situations. Mathematical models for both erosion and diffusion were applied to the observed release data, both models calculated their respective release constants smallest for the formulation containing the loaded sepiolite.

The incorporation of silver acetate into the soy based nanofibers for antibacterial activity was also successful. For this application, 30wt% SPI / 70wt% PVA solution was chosen due to its higher mechanical properties and ease of electrospinning. Nanofibers contained varying amounts of Ag acetate powder, (0%, 0.5%, 1%, and 1.5%) to determine their corresponding effects on killing the DH5-alpha E. Coli. The Ag containing soy based nanofibers were successful in showing antibacterial behavior and as concentration increased so did the width of the zone of inhibition.

The design and testing of the needleless electrospinning machine was key to bringing this lab developed technology into a potentially industrial setting. Design of a fully adjustable machine with automated substrate collection was accomplished. Testing of the machine was conducted with 30 wt. % SPI / 70 wt. % PVA solution. Not only was the mass production of soy-based nanofibers accomplished, the design of the machine allowed for electrospinning of a variety of solutions due to the large amount of adjustment. Overall, all major goals of the

research were accomplished and new technology for using soy based material was investigated and developed.

7.2. Future work

To continue this research, further testing can be conducted of the release of silver acetate from the soy based nanofibers to establish a release profile. As done for the drug release process, a nanoparticle could again be implemented to further control the release rate and tailor it to a desired value. While the drug release profiles in this previous work were from classical electrospinning techniques, in future work progress should be made towards implementing the needleless electrospinning techniques for mass producing these nanofibers. The research accomplished provides a solid base for expansion or research in a variety of directions for investigating the use of soy based nanofibers.

8. BIBLIOGRAPHY

Effect of pH on properties of wheat gluten and soy protein isolate films [Journal] / auth. Gennadios A. [et al.]. - [s.l.] : Journal of Agricultural and Food Chemistry,, 1993. - 11 : Vol. 41.

Electrospun hybrid soy protein/PVA fibers [Journal] / auth. Cho D [et al.]. - [s.l.] : Macromolecular Materials and Engineering, 2010. - 8 : Vol. 295.

Functional properties of soy proteins [Journal] / auth. Kinsella J. E.. - [s.l.] : Journal of the American Oil Chemists' Society, 1979. - 3 : Vol. 56.

Morphology and properties of soy protein isolate thermoplastics reinforced with chitin whiskers [Journal] / auth. Lu Y, Weng L and Zhang L. - [s.l.] : Biomacromolecules, 2004. - 3 : Vol. 5.

Preparation and properties of electrospun soy protein isolate/polyethylene oxide nanofiber membranes [Journal] / auth. Xu X [et al.]. - [s.l.] : ACS applied materials & interfaces, 2012. - 8 : Vol. 4.

Soy protein products: processing and use [Journal] / auth. Lusas E. W. and Riaz M. N.. - [s.l.] : The Journal of nutrition, 1995. - 3 : Vol. 125.

Sustained release of dexamethasone from hydrophilic matrices using PLGA nanoparticles for neural drug delivery [Journal] / auth. Kim D. H and Martin D. C. - [s.l.] : Biomaterials, 2006. - 15 : Vol. 27.

"Adsorption of chloridazon from aqueous solution on heat and acid treated sepiolites [Journal] / auth. González-Pradas E. - [s.l.] : Water research, 2005. - 9 : Vol. 39.

Adhesives and plastics based on soy protein products [Journal] / auth. Kumar Rakesh. - [s.l.] : Industrial crops and products, 2002. - 3 : Vol. 16.

Adsorption of diquat, paraquat and methyl green on sepiolite: experimental results and model calculations [Journal] / auth. Rytwo Giora, Tropp Dvora and Serban Carina. - [s.l.] : Applied Clay Science, 2002. - 6 : Vol. 20.

Advances in Biomaterials Science and Biomedical Applications [Book] / auth. Ning Zhu and Xiongbiao Chen. - Biofabrication of Tissue Scaffolds in book entitled : InTech, 2013. - Vol. 1.

Antibacterial properties of novel poly (methyl methacrylate) nanofiber containing silver nanoparticles [Journal] / auth. Kong H and Jang J. - [s.l.] : Langmuir, 2008. - 5 : Vol. 24.

Antimicrobial wound dressing nanofiber mats from multicomponent (chitosan/silver-NPs/polyvinyl alcohol) systems [Journal] / auth. Abdelgawad A. M, Hudson S. M and Rojas O. J.. - [s.l.] : Carbohydrate polymers, 2014. - Vol. 100.

Biodegradable electrospun fibers for drug delivery. [Journal] / auth. Zeng J [et al.]. - [s.l.] : Journal of Controlled Release, 2003. - 3 : Vol. 92.

Biodegradable plastic made from soybean products. 1. Effect of preparation and processing on mechanical properties and water absorption [Journal] / auth. Paetau I, Chen C. Z and Jane J. L. - [s.l.] : Industrial & engineering chemistry research, 1994. - 7 : Vol. 33.

Biodegradable soy-based plastics: opportunities and challenges [Journal] / auth. Swain S. N [et al.]. - [s.l.] : Journal of Polymers and the Environment, 2004. - 1 : Vol. 12.

Characterization and properties of sepiolite/polyurethane nanocomposites [Journal] / auth. Chen Hongxiang. - [s.l.] : Materials Science and Engineering, 2007. - Vol. A445.

Characterization of flax fiber reinforced soy protein resin based green composites modified with nano-clay particles [Journal] / auth. Huang Xiaosong and Netravali Anil. - [s.l.] : Composites science and technology, 2007. - 10 : Vol. 67.

Composite nanofibers produced by modified needleless electrospinning [Journal] / auth. Kostakova E, Meszaros L and Gregr J.. - [s.l.] : Materials Letters, 2009. - 28 : Vol. 63.

Controlled drug release from biodegradable thermoresponsive physical hydrogel nanofibers [Journal] / auth. Loh X. J [et al.]. - [s.l.] : Journal of Controlled Release, 2010. - 2 : Vol. 143.

Controlled release from erodible slabs, cylinders, and spheres [Journal] / auth. Hopfenberg H. B.. - [s.l.] : Controlled release polymeric formulations, 1976. - Vol. 33.

Development of ecofriendly/biodegradable lubricants: An overview [Journal] / auth. Nagendramma P and Kaul S. - [s.l.] : Renewable and Sustainable Energy Reviews, 2012. - 1 : Vol. 16.

Drug delivery and nanoparticles: applications and hazards [Journal] / auth. De Jong Wim H and Paul JA Borm // International journal of nanomedicine. - [s.l.] : International journal of nanomedicine, 2008. - 2 : Vol. 3. - p. 133.

Drug delivery and targeting. Nature, 392(6679 Suppl), 5-10. [Journal] / auth. Langer R. - [s.l.] : Nature, 1998. - 6679 : Vol. 392.

Drug delivery system [Book] / auth. Jain K. K. (Ed.). - [s.l.] : Humana Press/Springer, 2014.

Drug release from submicronized o/w emulsion: a new in vitro kinetic evaluation model [Journal] / auth. Levy M. Y and Benita S.. - [s.l.] : International journal of pharmaceutics, 1990. - 1 : Vol. 66.

Effect of halloysite nanotubes on mechanical properties and flammability of soy protein based green composites [Journal] / auth. Nakamura R. - [s.l.] : Fire and Materials, 2013. - 1 : Vol. 37.

Effect of the size of biodegradable microparticles on drug release: experiment and theory [Journal] / auth. Siepmann J [et al.]. - [s.l.] : Journal of Controlled Release, 2004. - 1 : Vol. 96.

Effects of polyhydric alcohols on the mechanical properties of soy protein plastics [Journal] / auth. Wang S, Sue H. J and Jane J. - [s.l.] : Journal of Macromolecular Science, Part A: Pure and Applied Chemistry, 1996. - 5 : Vol. 33.

Electrospinning of soy protein isolate nanofibers [Journal] / auth. Vega-Lugo A. C and Lim L. T.. - [s.l.] : Journal of Biobased Materials and Bioenergy, 2008. - 3 : Vol. 2.

Electrospinning process and applications of electrospun fibers. [Conference] / auth. Doshi J. and Reneker D. H. // Conference Record of the 1993 IEEE . - 1993.

Electrospun cellulose nanofiber reinforced soybean protein isolate composite film [Journal] / auth. Chen G and Liu H.. - [s.l.] : Journal of applied polymer science, 2008. - 2 : Vol. 110.

Electrospun nanofibrous polymeric scaffold with targeted drug release profiles for potential application as wound dressing [Journal] / auth. Thakur R. A [et al.]. - [s.l.] : International journal of pharmaceutics, 2008. - 1 : Vol. 364.

Encapsulation of amoxicillin within laponite-doped poly (lactic-co-glycolic acid) nanofibers: preparation, characterization, and antibacterial activity [Journal] / auth. Wang S [et al.]. - [s.l.] : ACS applied materials & interfaces, 2012. - 11 : Vol. 4.

Hydrogels in pharmaceutical formulations [Journal] / auth. Peppas N. A [et al.]. - [s.l.] : European journal of pharmaceutics and biopharmaceutics, 2000. - 1 : Vol. 50.

In vitro antimicrobial activity of solution blow spun poly (lactic acid)/polyvinylpyrrolidone nanofibers loaded with Copaiba (Copaifera sp.) oil [Journal] / auth. Bonan R. F [et al.]. - [s.l.] : Materials Science and Engineering, 2015. - 48 : Vol. C.

Inclusion polymerization of isoprene in the channels of sepiolite [Journal] / auth. Inagaki S, Fukushima Y and Miyata M. - [s.l.] : Research on chemical intermediates, 1995. - 2 : Vol. 21.

Kinetics, isotherm and thermodynamic studies of adsorption of Acid Blue 193 from aqueous solutions onto natural sepiolite [Journal] / auth. Özcan Adnan, Öncü E and Özcan A. Safa. - [s.l.] : Colloids and Surfaces A: Physicochemical and Engineering Aspects, 2006. - 1 : Vol. 277.

Mechanical and physical properties of epoxy composites reinforced by vapor grown carbon nanofibers [Journal] / auth. Choi Y. K [et al.]. - [s.l.] : Carbon, 2005. - 10 : Vol. 43.

Mechanical properties and biodegradability of electrospun soy protein Isolate/PVA hybrid nanofibers [Journal] / auth. Cho Daehwan, Netravali Anil N and Joo Yong Lak. - [s.l.] : Polymer Degradation and Stability, 2012. - 5 : Vol. 97.

Modeling of drug release from delivery systems based on hydroxypropyl methylcellulose (HPMC) [Journal] / auth. Siepmann J and Peppas N. A. - [s.l.] : Advanced drug delivery reviews, 2012. - Vol. 64.

Morphology and properties of soy protein and polylactide blends [Journal] / auth. Zhang Jinwen [et al.]. - [s.l.] : Biomacromolecules, 2006. - 5 : Vol. 7.

Nanoparticle-based targeted drug delivery [Journal] / auth. Singh R and Lillard J. W.. - [s.l.] : Experimental and molecular pathology, , 2009. - 3 : Vol. 86.

Needleless electrospinning of nanofibers with a conical wire coil [Journal] / auth. Wang X [et al.]. - [s.l.] : Polymer Engineering & Science, 2009. - 8 : Vol. 49.

Physical and Biophysical Characteristics of Nanoparticles: Potential Impact on Targeted Drug Delivery. In Targeted Drug Delivery: Concepts and Design [Book] / auth. Peetla C and Labhasetwar V.. - [s.l.] : Springer International Publishing, 2015.

Preparation and characterization of electrospun PLGA/gelatin nanofibers as a potential drug delivery system [Journal] / auth. Meng Z. X [et al.]. - [s.l.] : Colloids and Surfaces B: Biointerfaces, 2011. - 1 : Vol. 84.

Preparation and properties of biodegradable multilayer films based on soy protein isolate and poly (lactide) [Journal] / auth. Rhim Jong-Whan. - [s.l.] : Industrial & engineering chemistry research, 2006. - 9 : Vol. 45.

Preparation and Properties of Electrospun Soy Protein Isolate/Polyethylene Oxide Nanofiber Membranes [Journal] / auth. Xu Xuezhu [et al.]. - [s.l.] : ACS Applied Materials & Interfaces, 2012. - 8 : Vol. 4.

Preparation of antimicrobial poly (vinyl alcohol) nanofibers containing silver nanoparticles [Journal] / auth. Hong K. H [et al.]. - [s.l.] : Journal of Polymer Science Part B: Polymer Physics, 2006. - 17 : Vol. 44.

Recent advances on the use of biodegradable microparticles and nanoparticles in controlled drug delivery [Journal] / auth. Brannon-Peppas L.. - [s.l.] : International Journal of Pharmaceutics, 1995. - 1 : Vol. 116.

Silk-Based Biomaterials for Sustained Drug Delivery [Journal] / auth. Yucel Tuna, Lovett Michael L and Kaplan David L. - [s.l.] : Journal of Controlled Release, 2014.

Structural and emulsifying properties of soy protein isolate subjected to acid and alkaline pH-shifting processes [Journal] / auth. Jiang J., Chen J. and Xiong Y. L.. - [s.l.] : Journal of agricultural and food chemistry, 2009. - 16 : Vol. 57.

Superabsorbent composite XXII: Effects of modified sepiolite on water absorbency and swelling behavior of chitosan-g-poly (acrylic acid)/sepiolite superabsorbent composite [Journal] / auth. Xie Y, Wang A and Liu G.. - [s.l.] : Polymer Composites, 2010. - 1 : Vol. 31.

Surface-functionalized electrospun nanofibers for tissue engineering and drug delivery [Journal] / auth. Yoo H. S, Kim T. G and Park T. G.. - [s.l.] : Advanced drug delivery reviews, 2009. - 12 : Vol. 61.

The effect of pH on heat denaturation and gel forming properties of soy proteins [Journal] / auth. Renkema J. M. [et al.]. - [s.l.] : Journal of Biotechnology,, 2000. - 3 : Vol. 79.

Thermal and mechanical properties of environment-friendly 'green'plastics from stearic acid modified-soy protein isolate [Journal] / auth. Lodha P and Netravali A. N. - [s.l.] : Industrial Crops and Products, 2005. - 1 : Vol. 21.

Thermal and morphological characterisation of organically modified sepiolite [Journal] / auth. Tartaglione G, Tabuani D and Camino G. - [s.l.] : Microporous and Mesoporous Materials, 2008. - 1 : Vol. 107.

Thermo-responsive drug delivery from polymeric micelles constructed using block copolymers of poly (N-isopropylacrylamide) and poly (butylmethacrylate) [Journal] / auth. Chung J. E [et al.]. - [s.l.] : Journal of Controlled Release, 1999. - 1 : Vol. 62.

Towards a definition of inorganic nanoparticles from an environmental, health and safety perspective [Journal] / auth. Auffan M [et al.]. - [s.l.] : Nature nanotechnology, 2009. - 10 : Vol. 4.

Upward needleless electrospinning of multiple nanofibers [Journal] / auth. Yarin A. L and Zussman E.. - [s.l.] : Polymer, 2004. - 9 : Vol. 45.

Vegetable oil-based lubricants—a review of oxidation [Journal] / auth. Fox N. J and Stachowiak G. W. - [s.l.] : Tribology international, 2007. - 7 : Vol. 40.

APPENDIX

FEM verification for needleless electrospinning machine design

In the design for the needleless electrospinning machine, Finite Element Analysis (FEA) was utilized to ensure that the weight demonstrated by the adjustable collecting plate would not cause any substantial deflection or yielding. Material used for the analysis was aluminum with the following properties; Elastic modulus of 10,000 ksi, yield strength of 8,000 psi a poisson's ratio of 0.33. Aluminum was chosen as the material because it was readily available, left over from another project which helped minimize cost.

The FEM analysis of this project was conducted on the structure used to support the collecting plate on the needleless electrospinning machine to which a negative potential voltage would be applied. The crucial aspect focused on was the weight of the collecting plate that would be supported so that the structure did not experience any deformation greater than 0.01 inches. The reason that no deformation is important is due to the nature of the gap distance in electrospinning. This gap distance is very crucial, and any deformation would change the gap distance, ultimately affecting the results. In Figure A-1 is a diagram of the geometry.

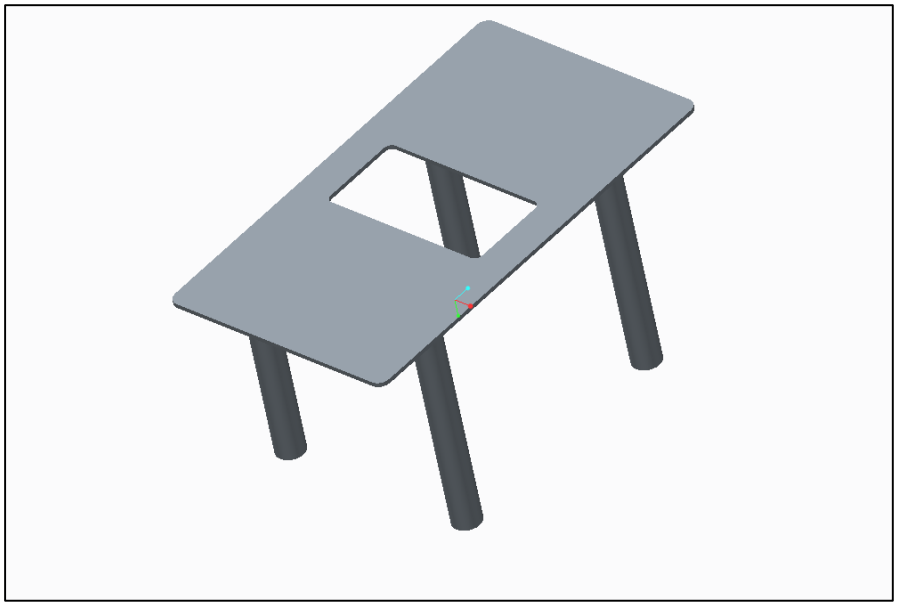

Figure A-1: Geometry of needleless electrospinning structure

Due to the geometry of the structure, symmetry was implemented to provide a denser mesh for the provided computing power. The goal of this analysis was to determine the largest force that could be applied to the top of the structure so that deformation did not exceed 0.01 inches and no yielding of the material occurred.

The physical preference was set to mechanical with the relevance center defined as coarse. The smoothing rate was set to medium, with the transition speed as fast. For the FEM analysis of the structure, a static-structural model was used. Static-structural is the model that was appropriate based on the boundary conditions and function of the structure. During this analysis, three different meshes were used. First was a coarse mesh with an element spacing of 0.500 inches, the second was an intermediate mesh with an element spacing of 0.130 inches, finally a fine mesh was used with an element spacing of 0.100 inches. The coarse mesh resulted in 6,945 nodes and 3,263 elements. The intermediate mesh contained 106,917 nodes and 59,728 elements, while the fine mesh had 178,231 nodes and 100,712 elements. Table A-1 shows an overview of element spacing and meshing characteristics.

Table A-1: Element spacing and mesh characteristics

	Element Spacing	Number of Nodes	Number of Elements
Coarse Mesh	0.500 in	6945	3263
Intermediate Mesh	0.130 in	106,917	59,728
Fine Mesh	0.100 in	178,231	100,712

The boundary conditions for this structure were defined as follows, first symmetry was implemented on the two surfaces where the symmetry cut was made, and this constrained translation in the y direction. Next, both bases of the supports were fixed, not allowing translation in any direction. Finally, a force was applied at each location where the collecting plate would be attached to the structure. Figure A-2 shows an overview of the initial conditions.

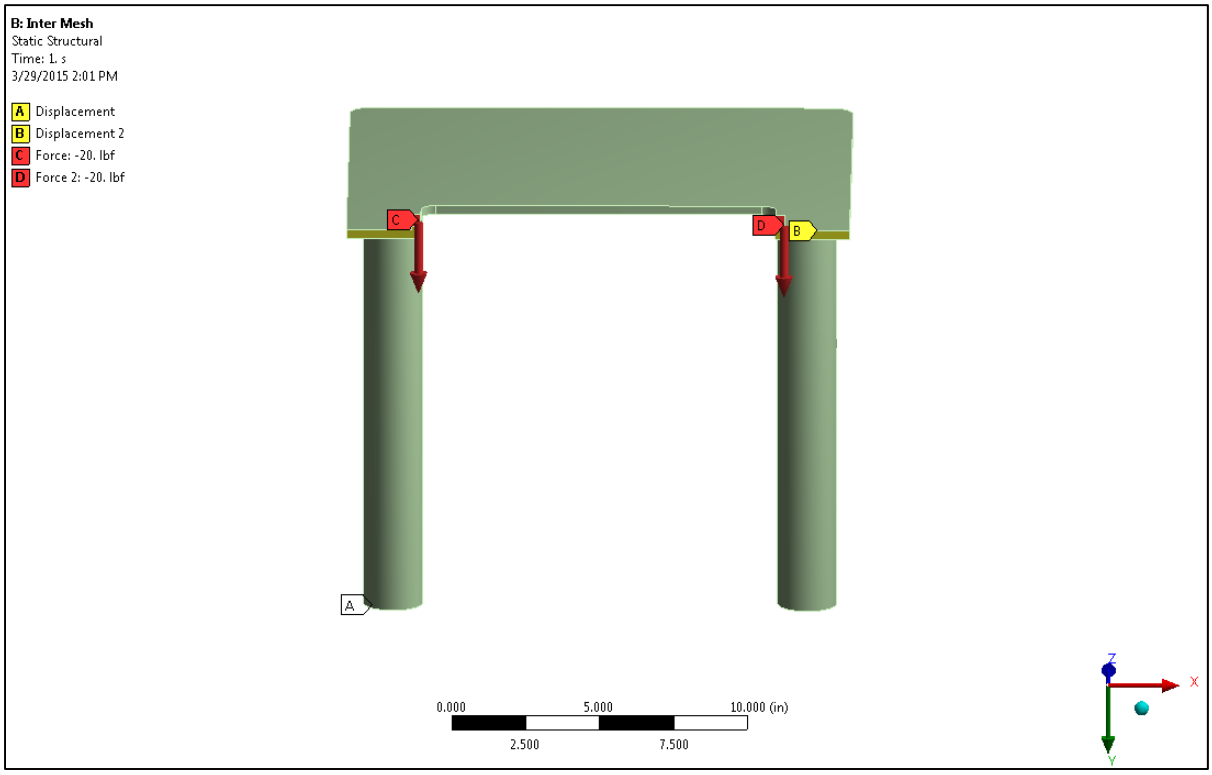

Figure A-2: Overview of boundary conditions

The meshing characteristics are described in the following three figures. Figure A-3 shows the coarse mesh which demonstrates an elements spacing of 0.5 inches. Figure A-4 shows the intermediate mesh which has an element spacing of 0.13 inches. Finally, Figure A-5 shows

the fine mesh with a spacing of 0.1 inches. Different mesh densitys are used in FEM analysis to verify results, ideally values will begin to converge.

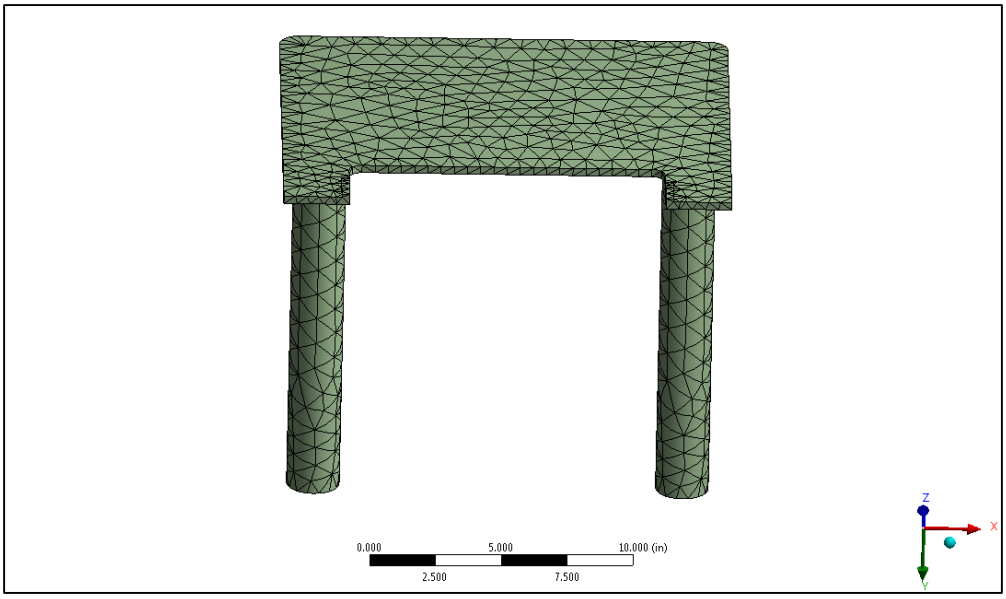

Figure A-3: Coarse mesh, elements size of 0.5 inches

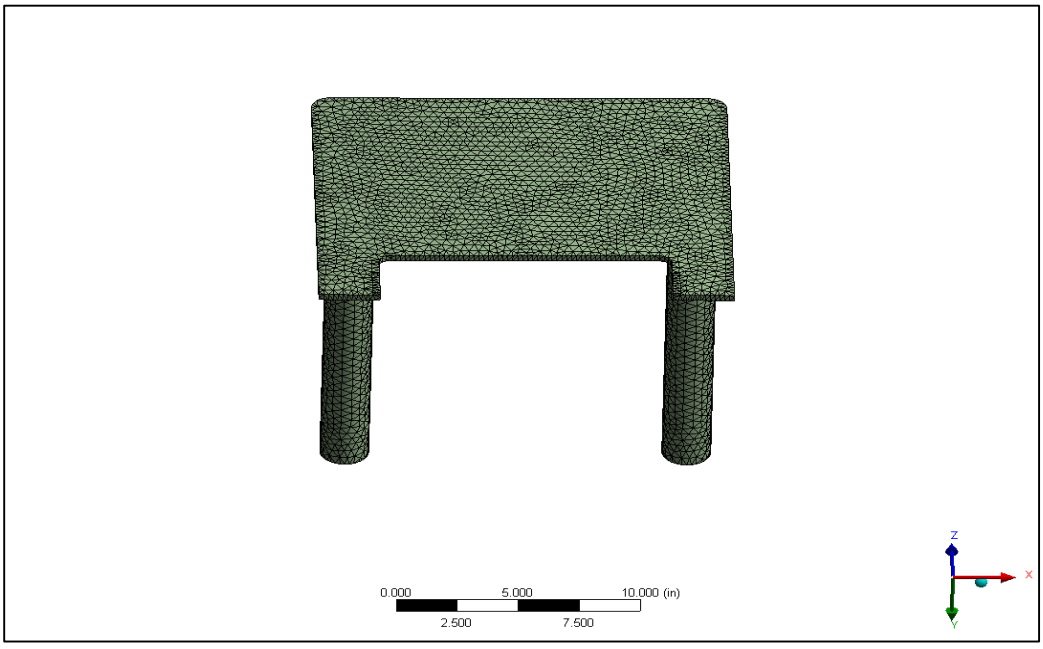

Figure A-4: Intermediate mesh, elements size of 0.13 inches

Figure A-5: Fine mesh, elements size of 0.1 inches

In order to find the maximum force required the structure could support, the force (F) that was applied at each end of the structure was varied. This was done using trial and error until a force was found that resulted in the deformation to be less than 0.01 inches. Also considered in the analysis was material yielding based on the forces that were applied; as previously mentioned, symmetry was implemented on the geometry to allow use of a denser mesh.

In the following figures are the results for the deformation plot for the coarse, intermediate, and fine meshes. Take note that the maximum deformation occurs right where the forces are applied. The force used for the analysis was found to be 40 pounds force (or 20 pounds force at each of the two points). This was found by using trial and error to achieve a value near 0.01 inches deformation, however it could not surpass it as this was one of the constraints. The deformation plots are as follow: Figure A-6 shows the coarse mesh, Figure A-7 shows the intermediate mesh, and finally, Figure A-8 shows the fine mesh.

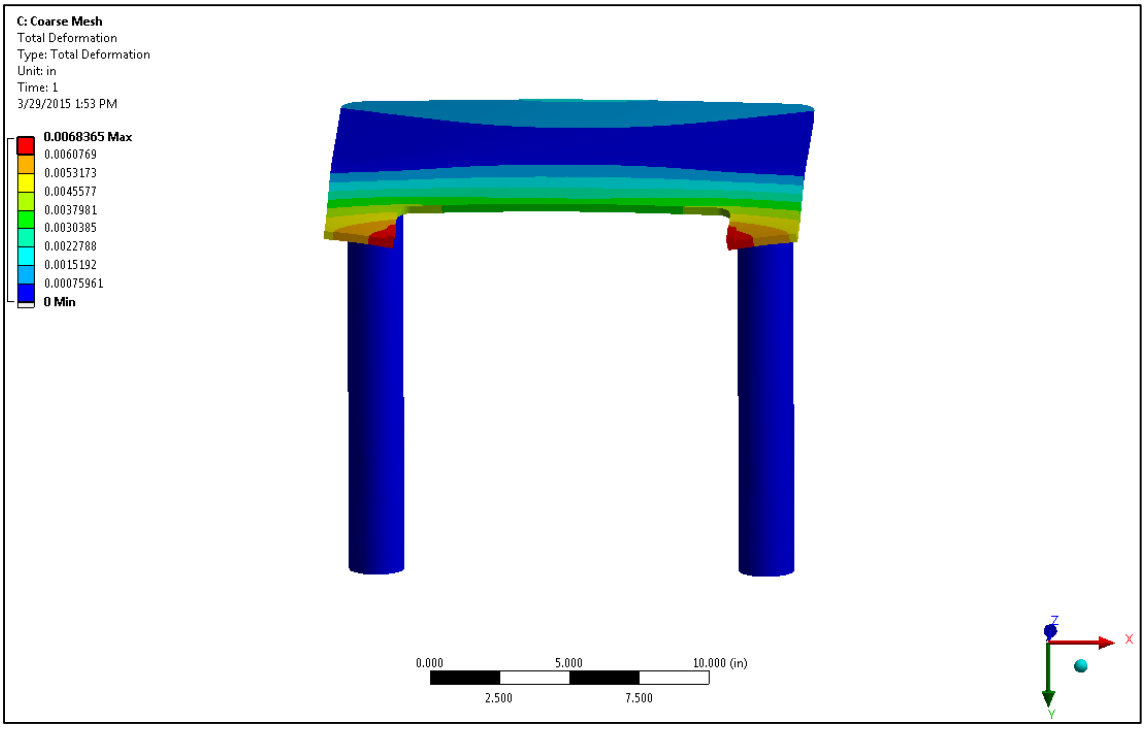

Figure A-6: Deformation plot for coarse mesh

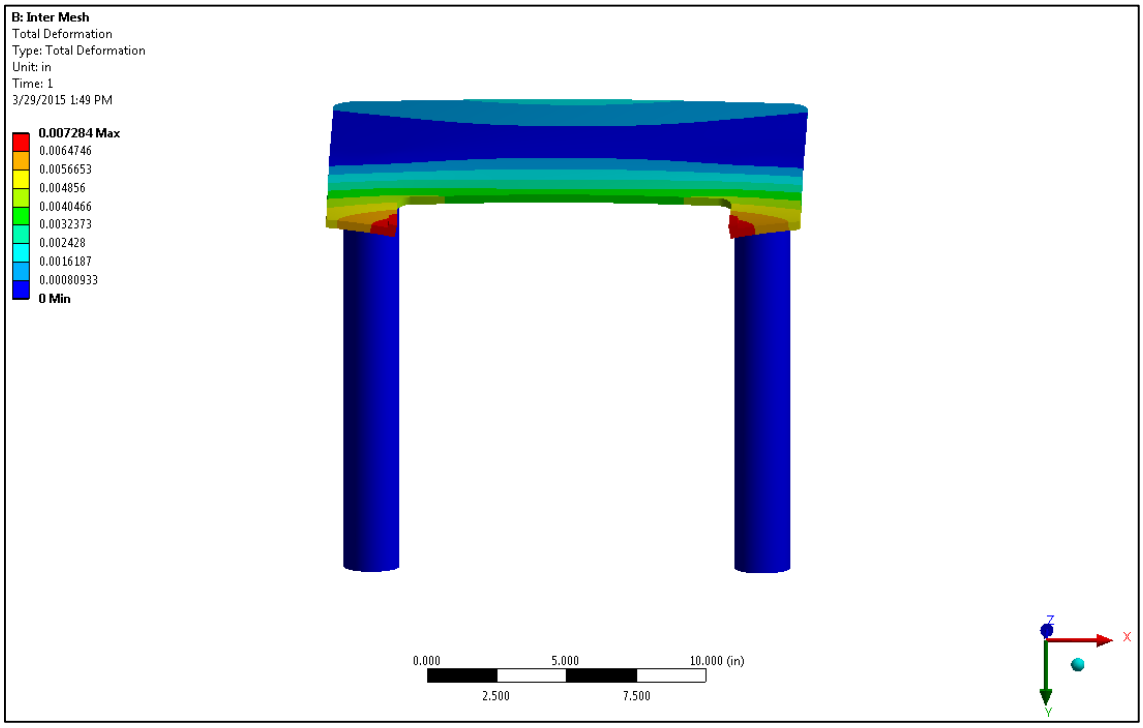

Figure A-7: Deformation plot for intermediate mesh

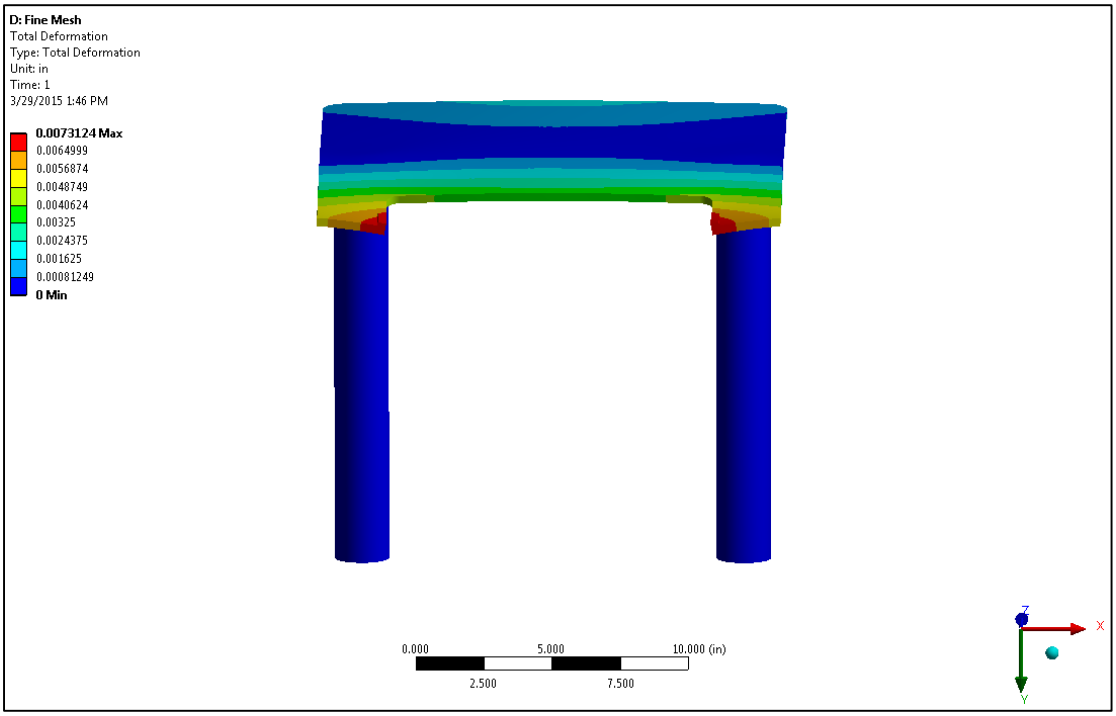

Figure A-8: Deformation plot for fine mesh

In Table A-2 is summary of the deformation results along with the corresponding mesh characteristics. As the mesh size decreased, the max deformation increased.

Table A-2: Summary of deformation results

	Element Size	Total Force Applied	Max Deformation
Coarse Mesh	0.5 in	40 lbf	0.006836 in
Intermediate Mesh	0.130 in	40 lbf	0.007284 in
Fine Mesh	0.100 in	40 lbf	0.007312 in

Also conducted in this analysis was verification that yielding of the material didn't occur under the conditions present. To do this, the Von-Mises stresses were plotted and verified that they did not surpass the yield strength of the material. In Figure A-9, Figure A-10 and Figure A-11 are the plots of the Von-Mises stresses for the coarse, intermediate, and fine meshes; respectively. Table shows the Von-Mises stresses results for the respective meshes.

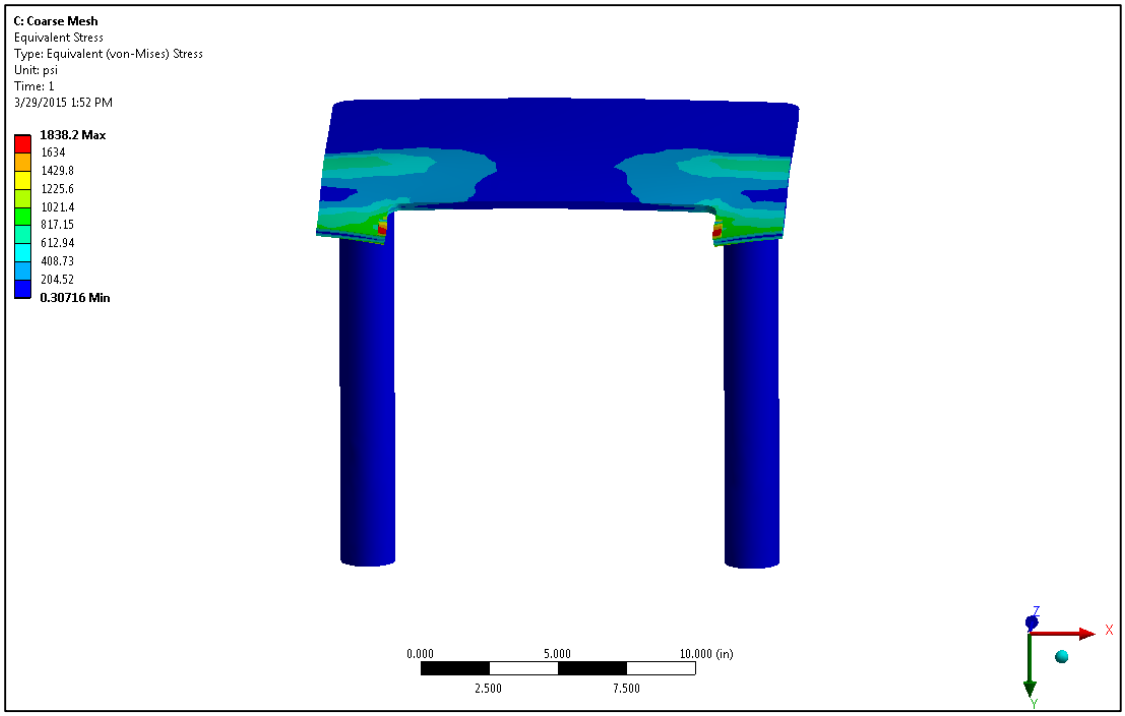

Figure A-9: Von-Mises stress plot for coarse mesh

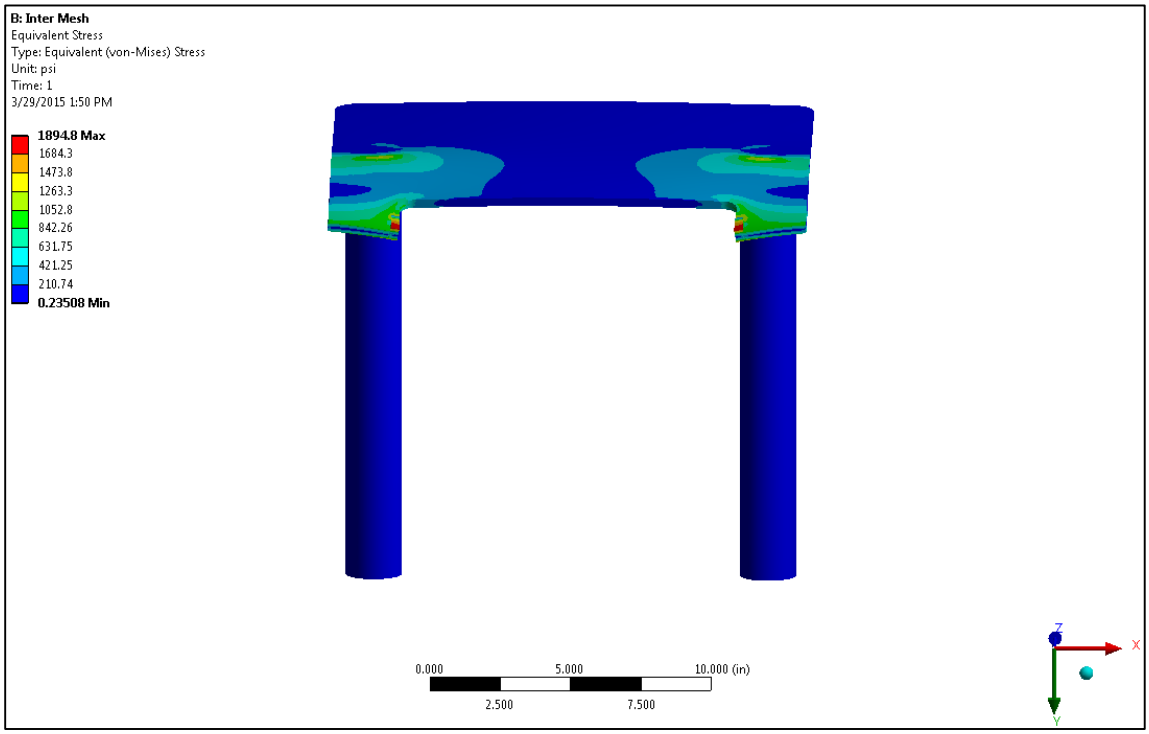

Figure A-10: Von-Mises stress plot for intermediate mesh

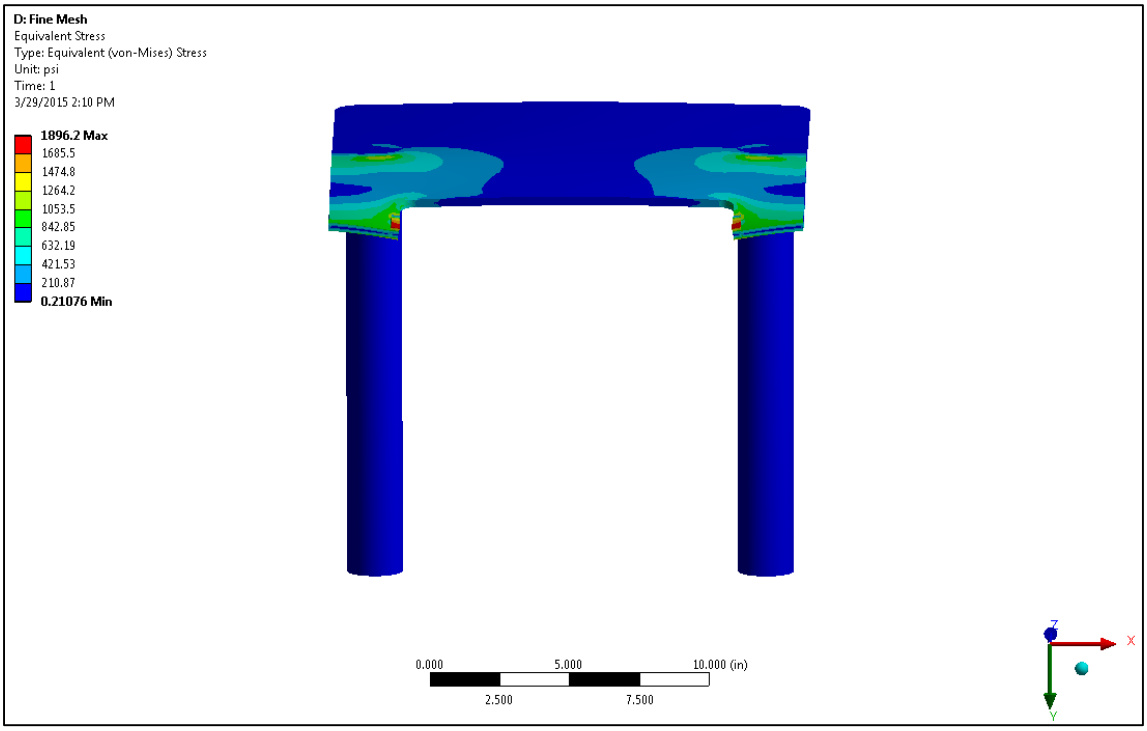

Figure A-11: Von-Mises stress plot for fine mesh

Table A-3: Von-Mises stress results for coarse, intermediate, and fine mesh

	Element Size	Total Force Applied	Max Stress
Coarse Mesh	0.5 in	40 lbf	1838.2 psi
Intermediate Mesh	0.130 in	40 lbf	1894.8 psi
Fine Mesh	0.100 in	40 lbf	1896.2 psi

The maximum stress found from the analysis was 1896.2 psi. This value was obtained from the fine mesh, where the stress value was the highest. As can be seen from the results shown in Table , the max deformation experienced was 0.007312 inches. This deformation occurred when a total 40 pounds force was applied to the structure. The requirements for the analysis included no more than 0.01 inches deflection and no yielding to occur. So for the deformation criteria, the structure successfully passed with a factor of safety of 13.7. These results were verified by the use of three different meshes, a coarse, an intermediate, and finally a fine mesh, respectively. Notice that as the mesh size decreased, the deformation increased

slightly. This is logical since as element size becomes smaller and smaller, there will be elements closer to the very edge where deformation is maximum. The yield strength of aluminum is typically given in range of 8,000 psi. As can be seen in the analysis Figure A-11, the maximum stress was found to be 1896.2 psi**,** significantly lower than the 8000 psi value. This produced a factor of safety for yielding of 4.22. This analysis was again conducted with all three meshes, however the value from the fine mesh was used as it produced highest stress value. Confidence was instilled with the use of all three meshes as results were very close (within 4%). With the use of the aluminum plate, the collection device could have a weight of 40 pounds and still be supported exercising a factor of safety of over 4.2.